ResCon'10

3rd Annual Research Student Conference

School of Engineering and Design

Research Conference Abstracts

21st – 23rd June 2010

Brunel UNIVERSITY WEST LONDON

RESCON'10

3rd Annual Research Students Conference

Welcome note from the Committee

Dear Reader,

On behalf of this year's ResCon Committee, it is our great pleasure to welcome you to the 3rd Annual Research Students Conference.

This year's conference boasts 3 days of oral and poster presentations which all showcase the high quality and diversity of the research being conducted within the school of Engineering and Design and its affiliates. We hope that this year's conference will be of great interest to you and that you find it very rewarding both professionally and personally.

We would like to express our grateful thanks to Professor Luiz Wrobel and Dr Jo Cole, whose experience and expertise in research has proved an invaluable asset to this year's committee. Also, we would like to thank Carole Carr, the Research Office Manager and her team, Janet Wheeler and Becca Byrne, whose hard work and guidance has been the foundation for this and previous conferences success. With a team like this contributing to future conferences, I have every confidence that ResCon will continue its tradition of high quality.

We would also like to thank Vice Chancellor Prof Chris Jenks for opening this conference, along with this year's other speakers. A special thanks to all the academic staff who have donated their time and support to judge the presentations this year.

Finally, we would like to thank the Heads of the School of Engineering and Design and the Graduate school for sponsoring ResCon '10 and providing the presentation prizes.

Thank you for attending the 3rd Annual Research Students Conference. We hope you thoroughly enjoy the three days and we look forward to welcoming you.

Matthew Littlefield
Committee Chair
on behalf of ResCon '10 Committee

ResCon'10
3rd Annual Research Students Conference
School of Engineering & design / Brunel University
21st – 23rd June 2010
Venue: Newton Room (Hamilton Centre)

Day 1 Monday 21st June Registration 8:30 – 9:00 (Thomas Walker AV)			
Welcome/ Opening Speech	***9:00 – 9:15***	***Prof Chris Jenks VC and Principal of Brunel University***	
		Prof Geoff Rodgers Pro VC (Research)	
Conference Chair	***9:15 -9:20***	***Matt Littlefield Session Chair***	***Dr Ian Stone / Prof John Cosmas (Session Judges)***
Session 1	*9:20 – 10:40*	***Electronic & Computer Engineering***	
		Abu Tarboush, Hattan	A Novel Reconfigurable CPW Antenna for Compact Wireless Devices
		Katsioulis, Vasileios	Design and Development of a Wireless Monitoring and Remote Controlling System Based on the ZigBee Protocol for Photovoltaic Systems
		Al-Dulaimi, Anwer	Cognitive Radio over Fibre Subnet
		Muhammad, Sanusi	SVC Concept and its Performance Evaluation over Conventional and Single Layer Coding
Break	***10:40 – 11:00***	***Tea /Coffee***	
Introduction	***11:00 – 11:05***		
Session 2	*11:05 – 12:25*	***Zen Cassinath Session Chair***	***Dr Brian McKay / Dr Mark Young (Session Judges)***
		Mechanical Engineering	
		Bromfield, Michael	Investigating factors affecting In Flights Loss of Control of general Aviation Aircraft
		Littlefield, Matthew	A Simulation of the Muon Ionisation Cooling Experiment (MICE)
		Lee, Cho-Yu	RegenEBD: A Cost-effective Pneumatic Regenerative Stop-start Hybrid System for Buses and Commercial Vehicles
		Al-Haifi, Nawaf	Human Hip Joint Simulator with Feedback Control System
Break	***12:25 – 13:50***	***Lunch***	
Introduction	***13:50– 13:55***		
Session 3	*13:55 – 15:35*	***Patrick Aigbomian Session Chair***	***Dr Kate Hone / Dr Hussam (Sam) Jouhara (Session Judges)***
		Electronic & Computer Engineering	
		Askar, Shanar	Fading Channels For Fixed IEEE802.16 Wimax System
		Ghaidaa Al-Sultany	Facilitating Mobile Communication with Annotated Messages
		Baharin, Ruzalina	Electron-sample interactions in gamma irradiated glass by CASINO and PENELOPE simulations
		Kurdi, Heba	A Personal Mobile Grid
		Abdollahi, Seyed Reza	Digital Radio over Fibre for Wireless Access Network Application
Break	***15:35 – 16:00***	***Tea/Coffee***	
Introduction	***16:00– 16:05***		
Session 4	*16:05 – 17:05*	***Irma Aleknaviciute Session Chair***	***Dr Jo Cole (Session Judge)***
		Advanced Manufacturing Engineering	
		Ahmad, Afandi	Rapid Prototyping of Finite Radon Transform (FRAT) for Medical Imaging Applications
		Chuddher, Bilal	Risk Analysis in Supplier Selection and Behaviour Model of supplier in supply chain linked to SCOR Model
		Basahl, Faisal	The Strategic Role of Human Resources Management: A Case of Health Care Management in Saudi Arabia
Social Evening Cavendish Room (Hamilton Centre) - 17:30 – 19:30			

Day 2 Tuesday 22nd June Registration 9:00 – 9:30 (Zen Cassinath AV)			
Welcome/Opening Speech	***9:30 – 9:35***	***Prof Savvas Tassou Head of the School of Engineering and Design***	
Session 5	*9:40 – 11:00*	***Anwer Al-Dulaimi Session Chair***	***Dr Ashraf Khir (Session Judge)***
		Mechanical Engineering / Bioengineering	
		Madani, Hossein	Analysis of Fluid-Structure Interaction (FSI) by Numerical Simulation for a cylinder-A literature review
		Dai, Dasong	Investigation of the dislocation of hemp fibres by FTIR
		Cifter, Abdusselam	How Users Differ in Using Instruction Manuals?
		Raza, Syed	On Demand Electrochemical Production of Hydrogen for Mobile Applications
Break	***11:00 – 11:20***	***Tea /Coffee***	
Introduction	***11:20 – 11:25***		
Session 6	*11:25 – 12:45*	***Feng (Joe) Yan Session Chair***	***Dr David Smith/ Dr Rebecca De Coster (Session Judges)***
		Environmental Studies	
		Anopa, Yulia	SchoolAir: Air Quality in Primary Schools and hildren's Health (a pilot study)
		Panchadcharan, Siva	Design and Implementation of Roof-top Wind Turbine Monitoring System
		Plant, Alexander	Economic Benefits of Sustainable Design Standards in Industry
		Janna, Hussein	Occurrence, Fate, and Removal of Emerging Contaminants from Wastewater Plants
Break	***12:45 – 13:45***	***Lunch***	
Introduction	***13:45 – 13:50***		
Session 7	*13:50 – 15:10*	***Emil Gegov Session Chair***	***Dr Maozhen Li/ Dr Jeff Scamens (Session Judges)***
		Electronic & Computer Engineering	
		Sadiq, Abubakar Umar	DIBR Algorithm for 3D Video Services
		Alzu'bi, Shadi	3D Multiresoultion Analysis for Segmenting Reduced Feature Medical Volumes using PCA
		Sharif, Mhd Saeed	Medical Volume Analysis using Artificial Neural Network
		Othman, Saharuddin	Discrete Time Simulation of Electrical Power Network with Intermittent Generation
Break	***15:10 – 15:30***	***Tea/Coffee***	
Introduction	***15:30 – 15:35***		
Session 8	*15:35 – 17:00*	***Ghaidaa Al-Sultany Session Chair***	***Prof Peter Hobson (Session Judge)***
		Advanced Manufacturing Engineering	
		Bin-Che-Ghani, Saiful	A critical review of the experimental, analytical and simulation techniques for the measurement of heat generation and temperature distribution in the cutting process
		Nusrat, Nazia	Novel State Estimation for Distribution Systems
		Nowak, Magdalena	Novel Grain Refiner for Aluminum Alloys
		Issakov, Nikolai	Growth and Tuning of many –layered grapheme on the 4H-SiC (0001) - $\sqrt{3}$ x $\sqrt{3}$ R30^{o} surface
End of The Second Day/ By Session Chair			

Day 3 Wednesday 23rd June Registration 8:50 – 9:10 (Matt Littlefield AV)			
Welcome/Opening Speech	***9:10 – 9:15***	***Dr Kate Hone Director of the Graduate School***	
Session 9	*9:15 – 10:55*	***Siva Panchadcharam Session Chair***	***Dr Paul Kyberd / Dr Hua Dong (Session Judges)***
		Electronic & Computer Engineering	
		Peter, Thomas	A Novel High Gain Semi-Planar UWB Antenna
		Walker, Thomas	The effects of radiation damage on the spectral resolution of the Chandrayaan-1 X-ray Spectrometer
		Nickpour, Farnaz	Representing Unstructured User Data for Inclusive Design
		Zarakovitis, Charilaos	Novel Game-Theoretic Cross-Layer Scheduling for Single-Cell OFDMA Systems with Heterogeneous QoS and Partial CSIT
		Aigbomian, Eboziegbe	The Use of Sustainable Materials and Designs to achieve Affordable Housing in Developing Countries. (A case study of Nigeria)
Break	***10:55 – 11:10***	***Tea /Coffee***	
Introduction	***11:10 – 11:15***		
Session 10	*11:15 – 12:35*	***Amal Mehanna Session Chair***	***Dr* Malcolm Ellis */ Dr Hua Dong (Session Judges)***
		Material Processing	
		Thornicroft, Keith	Long Range Ultrasonic Testing Using Chirp and Broadband Excitation Techniques
		Ghataore, Balraj	Inspection of Defects in Storage Tanks using Ultrasonic Guided Wave Inspection
		Cassinath, Zen	Parameter Investigation of Rheo-Extrusion Using AZ91D Alloy
		Aleknaviciute, Irma	Cracking of large hydrocarbon molecules using non-thermal plasma
Closing Cermony	***12:35 – 12:45***	***Prof Luiz Wrobel Deputy Head of the School (Research), School of Engineering & Design***	

RESCON'10

Table of Contents

Day One Sessions

Day Two Sessions

Day Three Sessions

Day One
Proceedings

SED Research Student Conference
Brunel University
21-23rd June 2010

A Novel Reconfigurable CPW Antenna for Compact Wireless Devices

Hattan F. AbuTarboush[1] and R. Nilavalan[2]

[1,2]Wireless Networks and Communications Centre (WNCC), School of Engineering and Design, Brunel University, Uxbridge, Middlesex, UK.
Hattan.AbuTarboush@brunel.ac.uk
Rajagopal.Nilavalan@brunel.ac.uk

Keywords: Small Antenna, Tir-Band Antenna, Reconfigurable Antenna

This paper presents a novel H-Shaped reconfigurable antenna fed by a Coplanar Waveguide (CPW) for wireless applications. The uniqueness of this antenna design relies in the ability to select the number of operating frequencies electronically by using a varactor diode switch. By electronically varying the value of the diode capacitance, the antenna can operate in a single band mode to cover GPS, a dual band mode to cover GPS and GSM1900 or a three-band mode to cover GPS, GSM1900 and Bluetooth or WLAN. Detailed simulations and experimental investigations are conducted to study and validate the behaviour of the antenna at each resonant frequency.

Introduction

There has been a significant interest in the field of reconfigurable multiband antennas during the last few years. Due to the demand for thinner devices, the requirement for multifunctional smaller antennas has increased. There has been much reported work on multiband antennas for different wireless applications using the H-Shape [1]-[2]. Although the fixed multiband antennas can widely be used in many different systems or devices, they lack the flexibility to accommodate new services compared with reconfigurable antenna. Different approaches to design an independent multiband antenna are reported recently to control three resonant frequencies by employing additional parts to the main radiating elements [3]-[4]. Independent operations were achieved in the reported designs [3]-[4] by incorporating additional parts or by changing the physical size of the antenna.

In this paper, a novel technique to electrically introduce independent resonant frequencies by using a varactor diode is presented. Up to three resonant frequencies can be generated and controlled to be used for GPS, GSM and Bluetooth or WLAN applications.

Design procedure and practical results

Fig.1 (a) shows the structure of the proposed reconfigurable antenna. The antenna is designed with an area of 43.6 x 50 mm^2 to make it better suited for compact wireless applications. The antenna consists of an H-shape CPW feed line and a varactor diode. A prototype has been fabricated to test the antenna as shown in Fig 1(b). It is designed on a 1.57 mm-thick FR-4 substrate with a dielectric constant of 4.4. The simulated and measured input S_{11} in dB of the proposed antenna for different varactor bias voltages are presented in Fig.2 (a)-(c). The antenna generates three independent resonant frequencies depending on the voltage applied to

the varactor diode switch. The first resonance occurs at 1.88 GHz while the second and third resonances occur at 2.4 GHz and 1.57 GHz respectively. Fig.2 (a) shows the simulated and measured single band response generated from the antenna when the varactor diode is set to be 2 pF, the antenna generates a single band at 1.88 GHz serving GSM1900 (1850–1910 MHz) applications. If the capacitance of the diode further increases to 4 pF, the antenna can resonate at an additional band at 2.4 GHz serving WLAN and Bluetooth applications while the resonant frequency of GSM1900 band is still supported as shown in Fig.2 (b). In a similar way, if the capacitance is further increased to 6 pF, a third band can be obtained at 1.57 GHz for Global Position Systems (GPS) (1575 MHz) applications, while the GSM1900 and the WLAN/Bluetooth bands are still supported as shown in Fig. 2 (c). The measured and simulated S_{11} results are in good agreement

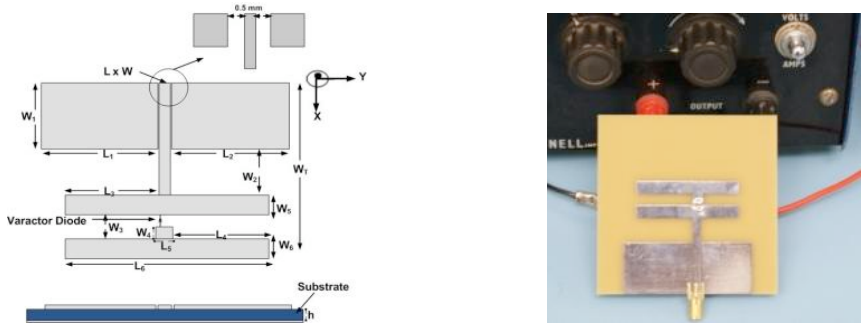

(a) (b)

Fig1. (a) Layout of the proposed antenna (b) Fabricated prototype of the proposed antenna

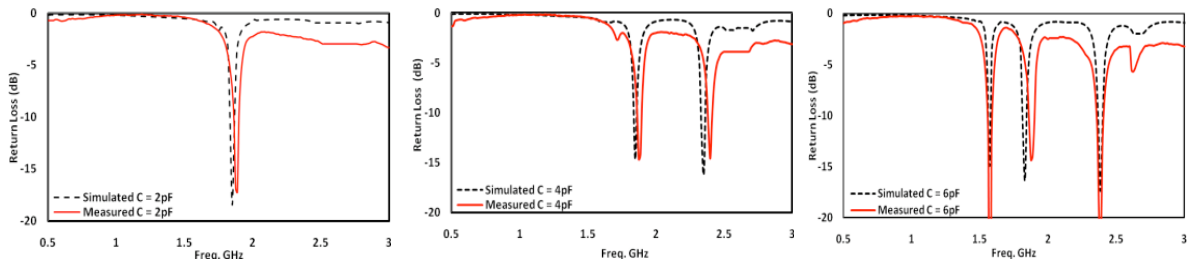

(a) (b) (c)

Fig. 2 Simulated and measured return loss for the three resonant frequencies at (a) Single band at 1.88GHz (b) Dual band at 1.88 GHz and 2.4 GHz (c) Tri-band at 1.57 GHz, 1.88 GHz and 2.4 GHz

Current Distribution and Radiation patterns

Further understanding of the antenna behavior can be observed from current distribution plots for the three resonant frequencies at 1.88 GHz, 2.4 GHz and 1.57 GHz. In Fig.3 (a) the current distributions are created all over the H-shape to generate the resonant mode of the GSM1900 (1.88 GHz) band. Fig. 3 (b) identifying the current distribution at 2.4 GHz where the current distribution are formed in the left hand side of the H-Shape to generate this band. Fig. 3 (c) shows the current distribution at 1.57 GHz where the currents are more concentrated in the right hand side of the H-Shape. The measured 3D radiation patterns for the three frequencies are shown in Fig. 4(a)-(c) which shows that the three bands have omni-directional pat

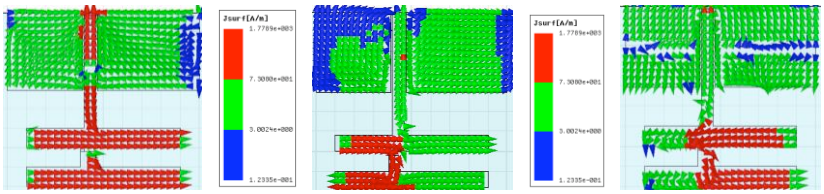

(a) (b) (c)

Fig. 3 Simulated surface current distributions of the proposed antenna at (a) 1.88 GHz (GSM1900) (b) 2.4 GHz (WLAN/Bluetooth) (c) 1.57 GHz (GPS) when the varactor diode is at 6pF

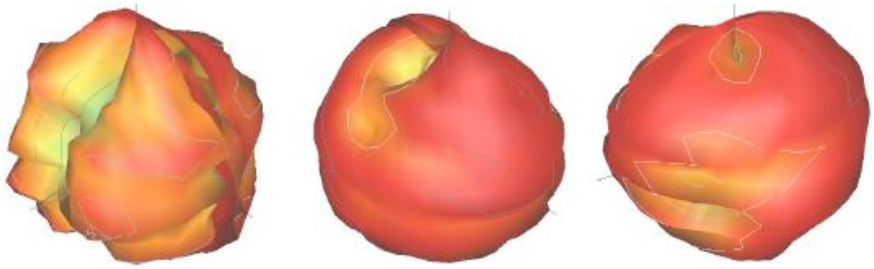

(a) 1.57GHz (b) 1.88 GHz (c) 2.4 GHz

Fig.4 Measured 3D patterns at the frequencies of interest

Parametric Study

A. Other combinations of frequencies

Other combinations of frequencies can also be achieved by modifying some parameters. In this section some example will be given to see how this method can be used with other frequencies such as Worldwide Interoperability for Microwave Access (WiMAX), Wireless Local area Network (WLAN), Bluetooth, Universal Mobile Telecommunications System (UMTS), the South Korean Wireless Broadband (WiBro), Digital Communication System (DCS) and Global System for Mobile Communications (GSM1800), (GSM1900), Global Positioning System (GPS), Personal Communication System (PCS) and many more. Figure 5 (a) shows the response of the return loss S_{11} when changing the widths of the H-shape namely W_5 and W_6. It is clear from Fig. 5 (a) that when the widths of both arms were decreased simultaneously, the generated bands can shifts to the higher bands. When increasing the widths simultaneously, the three bands can be shifted to lower bands. Therefore, the proposed method can be used with any other combination of frequencies.

B. Variation of the Varactor Capacitance

Compared to fixed multiband antennas, reconfigurable antennas can offer additional advantages of frequency reuse for doubling the system capability. The resonant frequencies can be further shifted to lower bands by applying different voltages (different capacitance) on the control line. The varactor diode used in this study has a capacitance range from 2pF to 14pF. When the capacitance of the varactor diode is varied from 7pF to 14pF, the tuning range for the first resonant frequency is found to be 11.44 % (from 1.57 GHz to 1.4 GHz) and that of the other resonant frequency 2.4 GHz is 6.46 % (from 2.4 GHz to 2.25 GHz) as shown

in Fig.5 (b). As expected, it has been noted that the 1.88 GHz band has shown no effect when changing the capacitance of the varactor diode. This is due to the current distribution of the 1.88 GHz. The same effect has been seen on those other frequencies in band 2 when varying the capacitance from 2pF to 14pF. Thus, the proposed antenna can offer more advantages to the communication systems by adapting to system requirements or environmental conditions.

The varactor diode could be varied when different capacitance are required to introduce a varied range of frequencies for the desired applications unlike fixed antennas which need to be re-fabricated and re-optimized for such requirements. Besides, for low frequency applications, fixed antennas normally require larger dimensions; the varactor diode can easily overcome this by varying the capacitance.

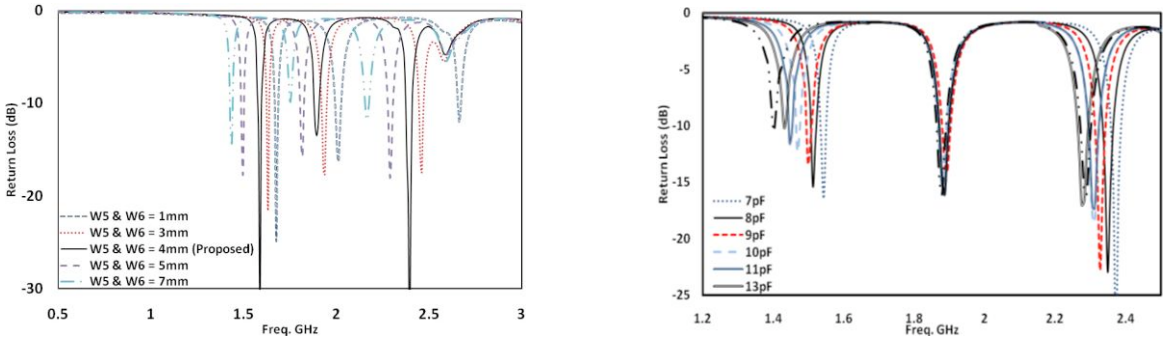

(a) (b)

Fig. 5 (a) The effect of changing W_5 and W_6 on the antenna performance to obtain other combination of frequencies (b) The effect of increasing the capacitance of the varactor diode on the three bands

Conclusion

A novel reconfigurable H-Shaped antenna is presented to electrically introduce multiple bands. The proposed antenna is fed by CPW and it is designed to be used in single, dual and three band communication systems. The generated bands can be easily controlled by varying the capacitance of the varactor diode. The simulated and measured result were in a good agreements.

References

[1] D. Singh, C. Kalialakis, P. Gardner, and P. S. Hall, “Small H-shaped antennas for MMIC applications,” IEEE Transactions Antennas Propagation., vol. 48, pp. 1134–1141, July 2000.

[2] Tsz Ym Yum, "A novel H-shaped active integrated antenna," Antennas and Propagation Society International Symposium, 2003. IEEE, vol. 2, pp. 708-711 vol.2, 2003.

[3] R. K. Raj, M. Joseph, C. K. Aanandan, K. Vasudevan and P. Mohanan, "A New Compact Microstrip-Fed Dual-Band Coplanar Antenna for WLAN Applications,” IEEE Transactions on Antennas and Propagation, vol. 54, pp. 3755-3762, 2006.

[4] D. Kim, J. Lee, C. Sik Cho and T. K. Lee, "Design of a Compact Tri-Band PIFA Based on Independent Control of the Resonant Frequencies," IEEE Transactions on Antennas and Propagation, vol. 56, pp. 1428-1436, 2008.

SED Research Student Conference
Brunel University
21-23rd June 2010

Design and Development of a Wireless Monitoring and Remote Controlling System Based on the ZigBee Protocol for Photovoltaic Systems

[2] Vasileios Katsioulis, [1] Emmanuel Karapidakis, [2]Marios Hadjinicolaou.

[1]TEI Chania – Crete, Greece

[2]School of Engineering and Design, Brunel University, Uxbridge, UK, UB8 3PH

Introduction

Systems that convert solar energy into electrical energy like photovoltaic (PV) have become widespread worldwide. This work deals with the prospect of using the promising technology of wireless sensor networks (WSN) in the field of photovoltaic (PV) plant supervising and monitoring. The knowledge of the status and good working condition of each PV module individually as well as of any PV system component will lead to a more efficient way of power management. This work concentrates in monitoring (in real time) as well as healthy operation control of separate PV modules.

This work focuses on the ZigBee technology. The versatility, ease of use and reliability of a mesh network topology offered by the ZigBee technology that is based on the IEEE 802.15.4 standard, is used here to offer its maximum advantages to a system that is capable of real time measurements and event alerts.

PV cells during their operation give off no atmospheric or water pollutants, need no fuel and require no cooling water (except some water cooled PV module types) [1, 2, 3]. Research led to new PV cell technologies and fabrication procedures reducing significantly the cost of a PV system. Studies on photovoltaic phenomena have drawn the attention to the problem of PV behavior under varying environmental conditions. The major problem is the strong dependence of a PV system response on many extrinsic factors such as temperature, insolation, cloudiness and pollution [5]. Another problem to be solved is to find an efficient and also cost-effective monitoring and supervising method of a PV plant even for small PV systems.

Regular performance checks on the functioning of PV systems are necessary for reliable use and successful integration of a PV. Monitoring for large PV systems is performed by specially designed hardware and software that might be expensive and is mainly operated by specially trained personnel. For small PV systems up to 5KW, these checks are not performed due to monitoring system costs [4]. Therefore small systems are often not checked on a regular basis. This situation can lead to partial energy losses that usually originate from partial system faults or decreasing performance that can go unnoticed for a long time. Thus, in order to achieve the maximum energy out of a PV plant, a low-cost, easy to use monitoring system is needed. Wireless sensor networks is a very promising technology in this field. A wireless sensor network is a system comprised of radio frequency (RF) transceivers, sensors, microcontrollers and power sources. Wireless sensor networks with self-organizing, self-configuring, self-diagnosing and self-healing capabilities have been developed to solve problems or to enable applications that traditional technologies could not address [6]. In the field of WSN, the ZigBee technology has met wide acceptance because of its capability to operate in a large number of applications. In this work, the main objective is to study the functionality of a ZigBee based monitoring and supervising system. The under test PV system is located on the roof of the Technological and Educational Institute of Crete (Chania-Greece). It consists of 6 polycrystalline-Si technology PV modules and rated power 100 Wpeak each connected in parallel.

Methodology/Approach

The PV monitoring system architecture consists of two basic blocks; the PV area sector (PVAS) and the central station sector (CSS) (Fig 1). The description of each building block is described below:

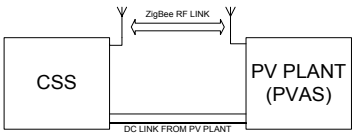

Figure 1: System architecture.

PV area sector: This is actually the PV plant area where basic monitoring parameters are observed. An alternative title instead of PVAS could be the 'ZigBee modules area', because each PV module in the plant is equipped with a ZigBee module and a set of sensors. The PVAS is part of ZigBee end devices (ZED) and a ZigBee router node (ROUT) that serves all ZED's devices as a data sink to the ZigBee coordinator board (COO).

Central Station sector: It can be assumed that CSS is the control station of a PV system. In such a station, various components of a PV system like the inverter, the batteries and the battery charger can be found. In the CSS the ZigBee coordinator module, the host PC and the remote measurement board (REMB) are located.

Remote Measurement Board: For safety reasons, all high voltages and currents of the PV plant are monitored in a separate PC board that is connected to the coordinator board.

The monitoring system operates as follows:
The attached ZigBee devices, in each PV module, send data corresponding to the voltage, current and temperature of the respective PV module. Data from ZEDs are sent to the router which is also an attached mote to a PV module. The router has the same functionality as with any ZED but is additionally capable of PV array angle reading (when a sun tracking system is used) and has also a dust sensor. All collected data from ZEDs and the router itself are sent to the coordinator board.

The coordinator board collects data from ZEDs via the router and supplies the host PC. The host PC runs suitable Graphic User Interface (GUI) software where monitoring and data logging are implemented.

Finally, the coordinator board monitors the total current and voltage originating from the PV plant and inverter as well. Extra functionality such as inverter and battery temperature as well as relative humidity is available. Below is a list of all parameters that can be measured by the PV monitoring system:

PV module output voltage, PV module output current, PV module temperature, Ambient temperature, The total output voltage of all PV modules (array) of the PV system, The total output current of all PV modules (array) of the PV system, Inverter output voltage, Inverter output current, Inverter temperature, Battery voltage, Battery charging current, Battery temperature, Relative humidity and Dust air concentration.

Figure 2: Monitoring system hardware.

Results and discussion

Two different experiments were conducted in order to verify the performance and reliability of the ZigBee PV monitoring system.

i) Bad connection experiment.

In the first experiment, the case of a bad or corrupted connection has been simulated. In case No1, we disconnect the positive terminal of a PV module. This disconnection led to a zero current reading of the respective PV module (PV module no3) in the GUI application. The absence of current measurement but the presence of a 17V voltage reading leads to the conclusion that the PV module is disconnected from the DC bus. Such a state can be easily managed by a software application in order to enable an alarm.

In case No2, we connected a PV module (PV module no4) in the DC bus but in that case corroded connectors were used. This situation led to fluctuations of current and voltage readings in the GUI for the specific PV module confirming the bad connection.

ii) Low performance of a PV module

In this experiment, the case of a low performance caused by dirt or dust in the transparent surface of the module had been investigated. A mixture of fine sand and water was sprayed onto the glass surface of PV module No4 simulating the red rain effect caused from the African dust, that is a very common phenomenon in the area of Crete. The PV monitor displayed a slightly lower current reading in comparison to the mean value of the rest PV modules. The dust sensor discussed previously can alert for high air dust concentration. Depending on the software extra reading can be extracted like power (W) and energy (Joules).

Measurements

Below, a number of graphs are shown representing the measurements corresponding to a specific day for each PV panel separately. The small differences between the graphs are mostly sensor errors. Another reason of these variations can be the fact that none of the PV modules output the same amount of energy for a specified sun illumination.

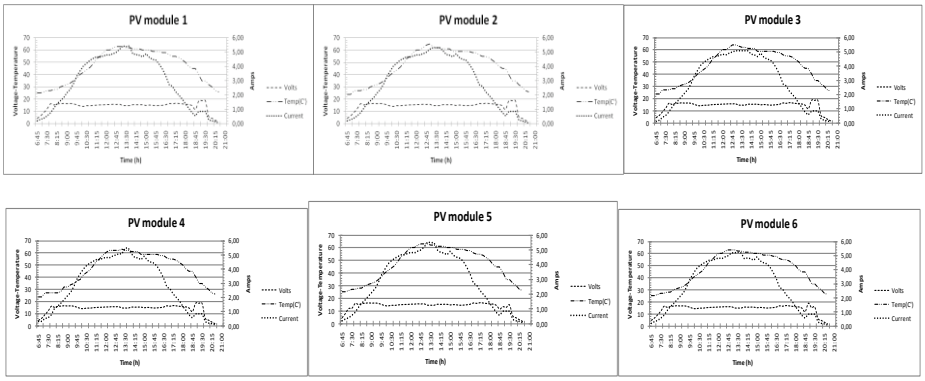

Figure 3: PV current, voltage and temperature measurements of a specific day.

Conclusion

In this work, the prospect of using the ZigBee wireless technology in the field of PV supervising and monitoring was experimentally assessed. This kind of system can be installed in any kind of PV generation system regardless of size, as the ZigBee standard allows for a very large volume of nodes (up to approximately 63,000) to be connected. The system presented here, provides accurate real time information about not only the overall PV plant behavior but also for any lone PV module. Failures as well as misoperation of any component comprising the PV system can be identified immediately. As described, the system estimates and monitors the state of the PV plant through a strain forward process contrary to other systems that base their operation on indirect methods, such as complicated statistical algorithms and comparisons of current performances with previous. The cost of the hardware for each ZED mote (fully assembled with set of sensors included) reaches the amount of 25Euros. Although it might look expensive, it must be kept in mind that this cost could be reduced significantly under the production of large quantities. Another important factor that can be characterized is the fact that there is no need for system inspection and testing, in the case of malfunctioning, by any technician. Thus, specially trained personnel costs and energy could be saved by the fact that the malfunctioning element is located very fast. Finally, the issue of integrating a ZigBee monitoring mote in each PV module in order to produce ready off-the-shelf ZigBee builds in PV modules must be seriously investigated by the PV module manufacturers.

References

[1]K. Zweibel, Harnessing Solar Power. The Photovoltaics Challenge, Plenum Publishing, New York, 1990.

[2] M. Brower, Cool Energy: The Renewable Solution to Global Warming, Union of Concerned Scientists, 1990.

[3] Horia Andrei , Valentin Dogaru-Ulieru , Gianfranco Chicco, Costin Cepisca, Filippo Spertino, 2007. Photovoltaic applications, Journal of materials processing technology 181: 267-273.

[4] A. Drews, A.C. de Keizer, H.G. Beyer, E. Lorenz,J . Betcke, W.G.J.H.M. van Sark, W. Heydenreich, E. Wiemken, S. Stettler, P. Toggweiler, S. Bofinger, M. Schneider, G. Heilscher, D. Heinemann. 2007. Monitoring and remote failure detection of grid connected PV systems based on satellite observations, Journal of solar energy 81: 548-564.

[5] Silvano Vergura, Giuseppe Acciani, Vitantonio Amoruso, Giuseppe E. Patrono, and Francesco Vacca. 2009. Descriptive and Inferential Statistics for Supervising and Monitoring the Operation of PV Plants, IEEE TRANSACTIONS ON INDUSTRIAL ELECTRONICS vol.56, NO.11

[6] Vehbi C. Gungor and Gerhard P. Hancke, 2009. Industrial Wireless Sensor Networks: Challenges, Design Principles, and Technical Approaches, IEEE TRANSACTIONS ON INDUSTRIAL ELECTRONICS, VOL. 56, NO. 10

[7] ZigBee Specification Document 053474r13, ZigBee Alliance, December 1, 006.

[8] H. LABIOD, H. AFIFI, C. DE SANTIS, WI-FI, Bluetooth, ZigBee and Wimax, Springer, The Netherlands, 2007.

[9] Abdellah Chehri, Paul Fortier, Pierre-Martin Tardif. 2009. Cross-layer link adaptation design for UWB-based sensor networks, Journal of computer communications 32: 1568-1575.

SED Research Student Conference
Brunel University
21-23rd June 2009

Developing Secondary Network Services using Cognitive Radio over Fibre Subnet

Anwer Al-Dulaimi and H. S. Al-Raweshidy
Electronic and Computer Engineering, School of Engineering and Design,
Brunel University, Uxbridge, Middlesex, United Kingdom
{anwer.al-dulaimi, hamed.al-raweshidy} @brunel.ac.uk

1.0 Keywords
Cognitive Network, Radio over Fibre, Spectrum Unavailability.

2.0 Abstract
Wireless mesh networks (WMNs) are known for their self configuration ability to form a network on power-up, for their easy installation and maintenance, and for their cost effectiveness [1]. The concept of cognitive radio can be applied to this wireless mesh network in which the mesh clients and routers can opportunistically access the channels which are licensed to a user [2]. The integration of optical and wireless systems is considered to be one of the most promising solutions for increasing the existing capacity and mobility as well as decreasing the costs in next-generation optical access networks [3]. This is where Radio over Fibre (RoF) technology comes in. It achieves the simplification of the Base Stations (BSs) and Remote Antenna Units (RAUs) through consolidation of radio system functionalities at a centralised headend, which are then shared by multiple RAUs [4]. The contribution of this proposal is to devise the Cognitive Radio over Fibre (CRoF) solution to overcome the interruption in the services of cognitive mesh networks as a result of spectrum unavailability and unsuitable links. The proposed solution is based on using the RoF as a long term alternative land line for the wireless links. The success of the suggested solution was examined through analyzing the end-to-end packet time delay and throughput.

2.0 Methodology
The CRoF system can be implemented only with an upgraded Cognitive Radio (CR). In this adjustment, the CRoF node will have the necessary awareness to communicate with other CRoF using fibre and wireless connections. The criteria to choose between these two options depend on the available free resources and the requested data downloads. Therefore, the CRoF system appears as a wireless-fibre access network. On the other hand, the CRoF nodes act also as similarly to the traditional CRs in achieving secondary wireless communications. Although, this modification in CR may increase the complexity of the CRoF developed nodes, it will improve the reliability of the secondary networks in server changeable wireless environments.

3.0 CRoF Application
3.1 Network Level

3.1.1 Scenario

The CRoF-BSs are positioned to coexist with other CMN-BSs as shown in Fig. 1. These positions may be chosen according to the free resources available at different geographical areas and the number of the expected end-users. It is important to remember that BSs of the primary networks are also working in the same space. The CRoF installation will not change the secondary working etiquettes of dynamically accessing holes on spectrum.

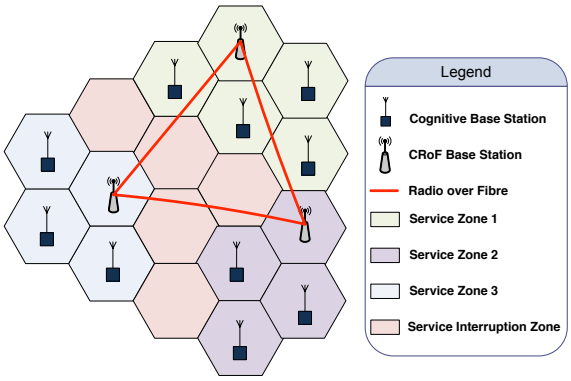

Figure 1. Multi zones of CR and CRoF.

The set of cognitive BSs send to a certain neighbour CRoF station which may form a zone of services. This splitting can happen all over the cognitive network. Clearly, the CRoF stations will act as seniors for other cognitive BSs in these zones. This is comparable to the cloud proposals for the future communication networks. Similarly, each service zone can be assumed as a cloud to provide necessary services to its clients individually. As the CRoF developed stations are a bit different from the traditional CMNs stations, they will be able to save huge amounts of data especially during the data transfers between wireless and fibre systems.

3.1.2 Simulation Results

Opnet software simulations were conducted to simulate the CRoF scenario shown in Fig. 1 in comparison to the traditional CMN arrangement. Primary and secondary base stations were created using the *manet_gtway_wlan_ethernet_slip4_adv* and *wlan_ethernet_router_adv* respectively. The IEEE 802.11e standards are the nodes used to simulate the CR behavior as in [5]. Ping traffic was used to create the dynamic wireless environment that a CR experiences in real life. The 1000BaseX connections were combined to the 802.11e nodes to act as RoF in the CRoF scenario.

Simulations carried out for three hours at a time. Hata propagation model (which is applicable to the radio propagation within urban areas) was set as the wireless default conditions for all simulated projects. Results show a key savings in the time delay accomplished with the CRoF scenario compared to the CMNs as shown in Fig. 2. The explanation for this is that link creation in the cognitive radios consumes more time than all the other wireless radio transmitters. This is a direct effect of the listen to

talk principle of the CR transmissions. Because, the CR can only transmit when the primary user goes off and the time required for CRs adaption. While, fibre links save more time and increase the reliability of the cognitive communications especially for online transmissions.

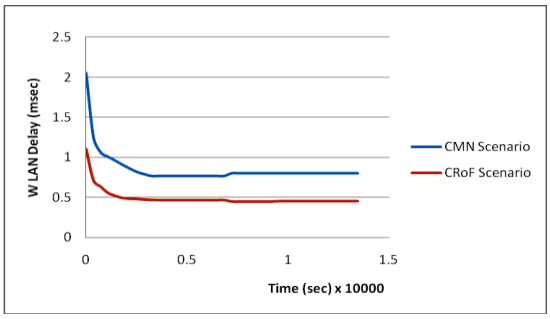

Fig. 2. Time delay for CMN and CRoF scenarios

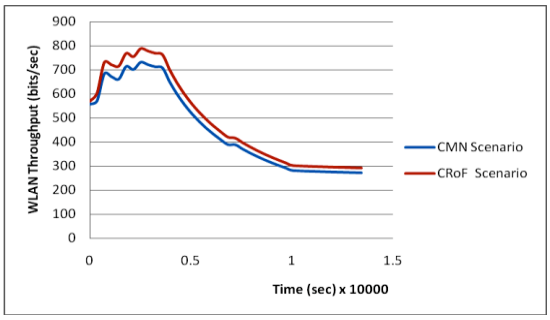

Fig. 3. Throughput for CMN and CRoF scenarios

Evidently, wide bandwidth provided by the RoF allows guaranteeing higher throughput for CMN equipped with the CRoF systems compared to the traditional CMN as shown in Fig. 3.

3.2 Microcell Level

3.2.1 Scenario

The CRoF subnet can be also applied at the microcells level. The same wireless environmental changes are likely to happen inside the macrocell itself. Therefore, the CRoF subnet can be used to deliver services locally for small enterprise services for example microcells. A CRoF core node is assumed as the main macrocell CRoF-BS. On the other hand, small range CRoF nodes can be installed at different microcells to perform secondary communications and local spectrum access as shown in Fig. 4. RoF is used also for connecting the CRoF stations in addition to wireless links.

The complexity of the CMNs equipped with the CRoF subnet are not increased by this major modification to the infrastructure and routing protocols. The reason for such this is that dealing with portioned networks will simplify the resources allocation and user detection. In fact, the complexity of the CRoF-BS is what really needs to be studied and analyzed to guarantee the successful of application in real environments. On the other hand, the cost of fibre installation should be considered, especially in urban and metropolitan areas.

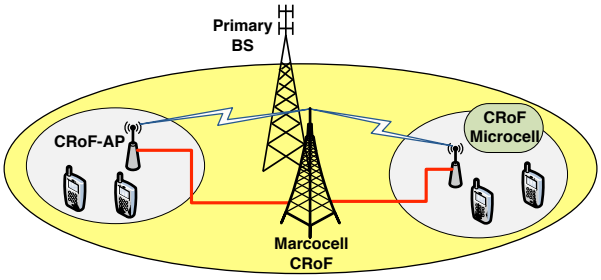

Fig. 4. CRoF and CR microcell scenario

3.2.2 Simulation Results

Simulations were conducted as in *3.1.2* to analyse the performance of the CRoF in comparison with the traditional CR-BS in coexistence with the macrocell primary BS. Results show major savings in time delay using CRoF subnet in as shown in Fig. 5.

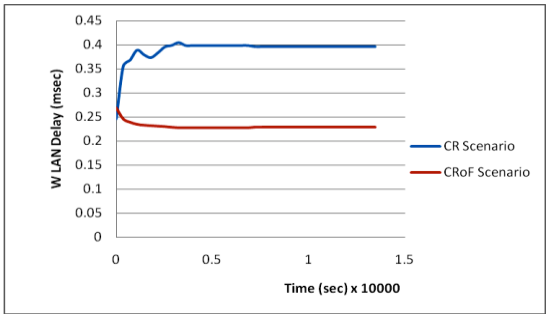

Fig. 5. Time delay for CR and CRoF scenarios

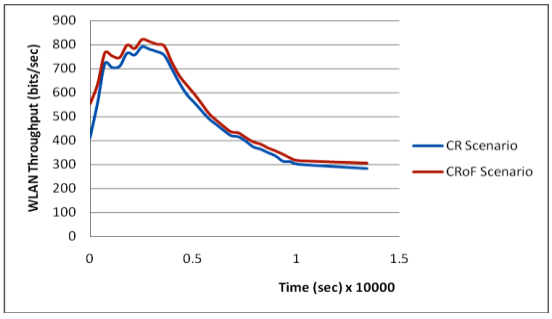

Fig. 6. Throughput for CR and CRoF scenarios

The throughput of the CRoF scenario is higher than the traditional CR simulations scenario as shown in Fig. 6. Obviously, simulations show the same performance for the network and microcell levels as compared to Fig. 3.

4.0 CONCLUSIONS

A new subnet developed to restore cognitive network services is proposed as Cognitive Radio over Fibre. The new subnet uses the radio over fibre as alternative connections for the wireless links. This will help to overcome the obstacles against online cognitive communications that resulted from spectrum unavailability and temporary links. Accordingly, the new CRoF base stations will have the opportunity to transmit to each other wirelessly and via RoF. The CRoF nodes can only transmit wirelessly to other CWN-BSs. The anticipated system is applicable to networks and microcells services. Opnet simulations proved the performance of the cognitive networks supported by CRoF in comparison with the traditional CMN. A permanent solution is being developed to ensure the reliability and continuity services for cognitive networks under severe wireless environmental changes.

1. REFERENCES

[1] C. Edmonds, D.Joiner, S. Springer, K. Stephen, and B. Hamdaoui, "Cognitive Wireless Mesh Network Testbed", *Proceedings of IEEE Conference on Wireless Communications and Mobile Computing (IWCMC2008)*, pp. 373-376.

[2] E. Hossain, D. Niyato, and Z. Han, *Dynamic Spectrum Access and Management in Cognitive Radio Networks*, Cambridge University Press, 2009, ISBN 978-0-521-89847-8.

[3] Z. Jia, J. Yu, G. Ellinas, and Gee_kung Chang, "Key Enabling Technologies for Optical-Wireless Networks: Optical Millimeter-Wave Generation, Wavelength Reuse, and Architecture", *Journal of Lightwave Technology*, Vol. 25, Issue 11, 2007, pp. 3452-3471.

[4] A. Ng'oma, "Radio-over-fiber technology for broad-band wireless communication systems," PhD Thesis, Dept. Telecommun. and Electronic Engineering, Eindhoven Univ. of Technology, Eindhoven, The Netherlands, 2005.

[5] L. Berlemann and S. Mangold, *Cognitive Radio and Dynamic Spectrum Access*, John Wiley & Sons Ltd, 2009, ISBN 978-0-470-51167-1.

SED Research Student Conference
Brunel University
21-23rd June 2010

SVC Concept and its Performance Evaluation over Single Layer Coding.

Sanusi Muhammad

School of Engineering and Design, Brunel University, Uxbridge, Middlesex, UK.

Sanusi.Muhammad@brunel.ac.uk

Abstract: Video delivery and consumption environments are often heterogeneous, due to the use of various types of physical electronic equipment and decoders with variable network conditions across different terminals. Scalable video coding (SVC) can be used to deal with the diverse variety of targeted receiving decoders and network conditions using a single video coder output. One good example of such an environment is the 3G wireless network delivering multimedia services to mobile, computer and TV Devices. Scalable video (SV) stream provides scalability which can serve some target decoders that have different restrictions on bandwidth, display resolution, power consumption and computational power. Scalability of a video stream provides graceful degradation; media bit rate as well as device capability, format and power adaptation functionalities. On the other hand a video stream which does not adapt to network constrained resources is regarded as non-scalable or conventional coding. H.264/AVC Extension provides efficient, standard-based temporal, spatial, and quality scalability of video streams. In this paper the technological concept of the H.264 Extension SVC in multimedia services is presented. Also comparative performance of SVC over conventional and single layer coding using H264 Extension JSVM 9.19.4 coder is evaluated and presented from experimental results.

Key Words- SVC, H.264 Extension, Single layer.

1. Introduction

In recent years, the number of video services has rapidly grown and gained popularity with the advancement in computer and electronic technologies. These services include high definition TV which requires high resolution, UMTS which offer lower data rates than broadcast channels and 3G video services. Each of these and other video services exhibit network resource constraints for the service to be efficiently provided. SVC encoder will encode a video stream which will adapt to the different network conditions and constrain features such as bit rate, resolution and network congestion. H.264/AVC Extension is the most recent video coding standard of the ITU-T Moving Picture Experts Group (MPEG) which offers scalable video with an enhanced coding performance and a network friendly video representation [1]. H.264 addresses conversational applications (video telephony, video conferencing) and non-conversational (streaming, storage) applications. SVC structure is characterised with a base layer and other embedded multiple layers meant for enhancement, or for servicing decoders with other limited requirements. This desirable feature of SVC enable bit rate adaptation, enhanced user Qos for networks and video applications.

2. Methodology

H.264 extension JSVM 9.19.4 codec using sequences of CIF, QCIF resolutions is adopted for characterising both scalable and single layer video streams. JSVM 9.19.4 has built in functions that allow many coding operational functionalities for a video data to be simulated and is the most recent used standard codec.

3. H.264 SVC concepts,

The H.264/AVC Extension was standardised as an extension of H.264/AVC. It is the recent standard scalable video coding [1] approved by ITU-T. ITU has recommended the adaptation of H.264 extension and ISO/IEC has approved it as a standard in multimedia video communications. The reader is referred to the standard [2] or other corresponding overview papers for more detailed description.

SVC is a highly attractive solution to the problems posed by the characteristics of modern video transmission. Efficient SVC such as H.264\AVC Extension provides a number of benefits. Consider a scenario of a video transmission service with heterogeneous clients where multiple bitstream of the same content differing in coded picture size, frame rate and bit rate should simultaneously be provided. With properly configured H.264\AVC SVC the source content has to be encoded only once. This encoded source will consists of a scalable stream represented with lower, higher resolutions and/or quality streams with variable bit rates. For instance, a client with limited resources – display resolution, processing or battery power needs to decode only a part of the delivered bitstream. Similarly terminals with different capabilities can be served by a single bitstream. SVC stream usually contains parts with different importance in terms of decoded video quality. This can serve different application Qos demand. SVC is also highly desirable for surveillance applications, in which video not need to be viewed on multiple devices ranging from high definition monitors to videophones or PDAs, but also need to be stored and archived [6]. Conceptually, the design of H.264/AVC covers a Video Coding Layer (VCL) and a Network Layer (NAL). The VCL creates coded representations of the source content, while the NAL encapsulates each slice generated by the VCL into typical NAL units [11]. This provides header information which enables effective customization of VCL data for a broad variety of systems [11].

Spatial, temporal and quality scalability

H.264 SVC supports spatial and temporal resolutions scalability in which subset of the bitstream represent the source content with a reduced (spatial) picture size or frame rate respectively(temporal) [6]. It also supports Quality scalability commonly known as signal to noise ratio (SNR) and is concern with the fidelity of the video signal [6]. The described scalability types can also be combined as in Figure 3.

4. Results

The result is obtained from simulation of H.264/AVC Extension codec as presented with Figure 2, Figure 3 and Figure 1. The same scene and configuration used for both SVC and single layer. Figure 2 demonstrated the bit and frame rate adaptability for SVC stream. Figure 3 demonstrated SVC capability for encoding two different streams of different resolutions

and temporal characteristics. Figure 1 shows the original QCIF CITY sequence used in this experiment and the decoded SVC and single layer of the same original scene. Subjectively these show no visual differences. This simulation used a standalone system with no wireless or distanced video transmission. There was no error detected within the codec.

Figure 1: (a) Decoded QCIF, CITY sequence from encoded base and 7 enhancement layers at 144kb/s and 38.10dB.

(b) Decoded QCIF, CITY sequence from encoded base layer at 107kb/s and 38.02dB . (c) Original sequence

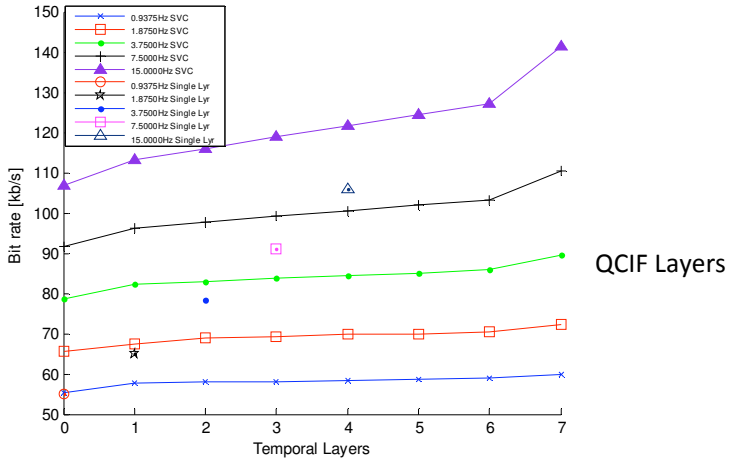

Figure 2 : Bit rate and temporal layers of SVC and single Layer

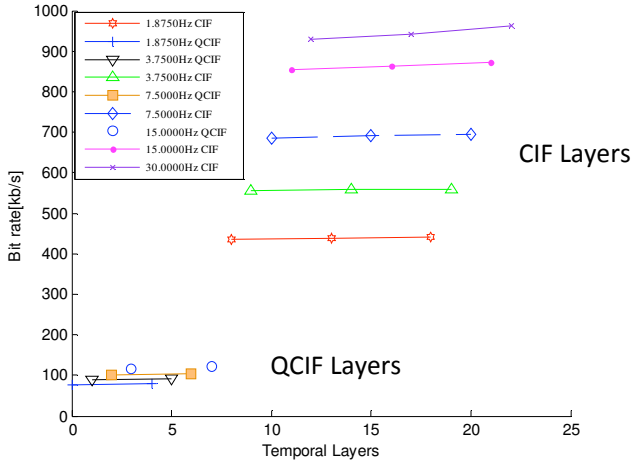

Figure 3: Combined spatial scalability QCIF and CIF

Conclusion

It can be concluded from the experimental results that

- SVC support bit rate adaptation. It is clear from Figure 2 and Figure 3 that the streams are encoded for different bit rate adaptation. The adaptation is made present within the temporal layers. Each of the temporal layer for SVC with 7 enhanced layers is generated with 8 levels of bit rate. For example the temporal layer 15Hz has 8 bit rate levels ranging from a minimum of 106.90kb/s to maximum of 141.40kb/s and 1.8750Hz layer from 65.50kb/s to 72.20kb/s.
- The above bit rate adaptation characteristic of JSVM 9.19.4 coder has made it desirable for network friendliness. This is not the case with single layer having only 1-bit rate level for each temporal layer.
- SVC stream can support applications with limited resources of bandwidth, spatial resolution and power capability. SVC shows wide range of bit rate adaptability and frame rate to couple with heterogeneous network service.
- Temporal scalability can be achieved without any rate distortion performance in SVC. Single layer can also achieve temporal scalability when run in a scalable mode with limited layers and bit rate adaptability output.
- SVC supports combined scalability with different spatial resolutions. High and low data rate is supported for higher and low resolution applications respectively.
- The visual quality between SVC and single layer is not distinguishable even with slight performance increase of <1% for the SVC stream for a fixed bit rate.

References:

[1] T.Wiegand, J. Gary Sullivan, G. Bjontegaad, and A. Luthra " Overview of the H.264/AVC Video Coding Standard" in IEEE Transactions on circuits and systems for video technology, pp. 1-5, July 2003.

[2] Advanced Video Coding for Generic Audiovisual Services, ITU-T Rec. H.264 and ISO/IEC 14496-10 (MPEG-4 AVC), ITU-T and ISO/IEC JTC 1, Version 1: May 2003, Version 2: May 2004, Version 3: Mar. 2005, Version 4: Sept. 2005, Version 5 and version 6: June 2006, Version 7: Apr. 2007, Version 8 (including SVC extension): Consented in July 2007.

[3] A.H.Sadka, "Compressed Video Communications" John Willey & Sons, Ltd Baffins Lane, Chichester, West Sussex PO19 1UD, England. pp 14-15, 75-82, 2002.

[4] Generic Coding of Moving Pictures and Associated Audio Information- Part 1: Systems, ITU-T Rec. H.222.0 and ISO/IEC 13818-1(MPEG-2 Systems), ITU-T and ISO/IEC JTC 1, Nov.1994.

[5] Narrow-Band Visual Telephone Systems and Terminal Equipment, ITU-T Rec. H.320, ITU, Mar.1993.

[6] H. Schwarz, D.Marpe and T. Wiegand, " Overview of the Scalable Video Coding Extension of the H.264/AVC Standard" in IEEE transactions on circuits and systems for video Technology, Vol.17,No 9, September 2007.

[7] JSVM Software Manual, ISO/IEC, MPEG and ITU-T (VCEG), November 2009.

[8] D. Peter, "Digital Video Compression", McGraw-Hill, New York 2004, pp 224-245.

[9] S. Chang., A. Vetro, " Video Adaptation: Concepts, Technologies and Open Issues", Published in Proc IEEE, vol. 93, no. 1, pp 148-158, Jan 2005.

[10] S. Wenger., Y. Wang, M. Miska Hannuksela, " RTP Payload format for H.264/SVC scalable video coding", Journal of Zhejiang University Science A, ISSN 1009-3095; ISSN 1862-1175(online), 2006.

[11] E.G. Richardson, "H.264 and MPEG-4 Video Compression ", John Wiley & Sons Inc., 111 River Street, Hoboken, NJ 07030, USA, pp 142, 2003.

SED Research Student Conference
Brunel University
21-23rd June 2010

Investigating Factors affecting In Flight Loss of Control of General Aviation Aircraft

M.A. Bromfield

Brunel Flight Safety Laboratory,
School of Engineering and Design,
Brunel University,
Uxbridge,
Middlesex, UK

Keywords: aviation, safety, control

Introduction

A quarter of all fatal General Aviation (GA) accidents in the UK during the period 1980 to 2006 involved Loss of Control (LoC) in Visual Meteorological Conditions (VMC) [1]. Loss of Control - effectively an inadvertent stall (occurs when the aircraft wing suddenly stops developing lift), has consistently appeared in accident statistics over this period, but at apparently different rates for different aircraft types. This raises a number of important and intriguing research questions:-

- Why does Loss of Control happen?
- Why do certain aircraft types appear to be more susceptible than others?
- How we can improve operational safety?
- Is it possible to make future GA designs "Loss of Control-proof"?

Figure 1 – Loss of Control Fatal Accident (Timesonline.com)

This programme of research aims to answer these questions and influence future light aircraft operations and design

Methodology/Approach

A case study approach was used to begin the research and assist in identifying relevant factors for consideration. A noticeable difference exists between the Cessna 150 and Cessna 152 aircraft, similar in appearance and highly popular in the pilot training environment. The Cessna 150 falls approximately on the average for inadvertent stall-related fatal accidents in the UK GA fleet, whereas the Cessna 152 exhibits a lower accident rate. Both a quantitative and qualitative review of fatal accidents involving Loss of Control for these aircraft was performed.

Key design differences affecting performance and handling qualities were thoroughly researched using available published material and informal interviews with type-experienced students, pilots and flying instructors.

A flight test programme was undertaken using several models of both aircraft types to gather additional research data in order to assess and compare the apparent performance and handling qualities (both qualitatively and quantitatively). The flight tests were performed at different centre of gravity conditions relevant to the key design differences, concentrating upon apparent longitudinal (static and dynamic) stability and control characteristics, stalling and low-speed handling characteristics, and cockpit ergonomics / pilot workload [2][3][4].

In parallel, a critical review of established theory was undertaken to better understand the contributory factors and compare them with actual flight test data.

Results and discussion

Flight test results showed marked differences in the Apparent Longitudinal Static Stability during power on/flaps down configurations for the different aircraft types. To the pilot, these differences manifest themselves as stick forces felt directly and immediately by the pilot. Stick force cues form a major part of the ‘pilot in the loop’ control feedback to the pilot. Steep stick force gradients (low gain) provide positive cues to the pilot of airspeed changes allowing more precise tracking of airspeed (point tracking). Moderate to high stick forces at the stall act a natural ‘barrier’ to the stall (boundary avoidance) by making the pilot work much harder to ‘get into trouble’.

Poor cockpit ergonomics contribute to increased pilot workload, widening the scan, reducing readability and diverting attention during safety critical manoeuvres such as the ‘go-around’ (aborted landing).

Conclusions

The combination of poor static stability with poor ergonomic design can considerably reduce safety margins therefore increasing the risk of an inadvertent stall, leading to LoC during safety critical manoeuvres

Further Work

Stick force theory will be extended using empirical flight test data and MatLab scripts to include the effects of flying control mechanical characteristics (FCMC), flap and power on longitudinal static stability and in turn, pilot stick force cues.

In parallel with this, a series of task-based and scenario-based simulation tests will be conducted with volunteer pilots of different experience levels (n=50), representative of the present day UK GA community. The tests will enable additional research data to be obtained with respect to airspeed tracking, stall boundary avoidance, pilot workload and pilot decision making during safety-critical manoeuvres with varying levels of aircraft stability to replicate real-world situations.

Acknowledgements

Thanks to both Dr Guy Gratton and Dr Mark Young for their support and encouragement during the course of the research to date. I also gratefully acknowledge the financial support of the Thomas Gerald Gray Charitable Trust Research Scholarship Scheme. The General Aviation Safety Council's 'Stall/Spin Working Group' provided initial accident data. The Civil Aviation Authority (UK) who provided accidents reports, on which quantitative and qualitative analysis was based.

References

[1] Thorpe, J., GASCo Flight Safety Seminar, RAF Uxbridge, 30th June, 2008.

[2] Gratton, G.B., Bromfield, M.A., Aspects of General Aviation Flight Safety Research, Proceedings of the Royal Aeronautical Society 2008 General Aviation Conference. Cambridge, 28 September 2008.
(http://bura.brunel.ac.uk/handle/2438/2847)

[3] Bromfield, M.A., Gratton, G.B., Factors Affecting Loss of Control in General Aviation Aircraft, 39th Symposium of the Society of Experimental Test Pilots, San Diego, California, USA, 19-20 March 2009.
(http://bura.brunel.ac.uk/handle/2438/3255)

[4] Bromfield, M.A., Gratton, G.B., Flight Test: Supporting the Investigation of Factors Affecting Loss of Control of Light Aircraft, Proceedings of the 40th Annual International Symposium - Society of Flight Test Engineers, Linköping and Stockholm, Sweden, 7 - 11 September 2009.
(http://bura.brunel.ac.uk/handle/2438/4026)

SED Research Student Conference
Brunel University
21-23rd June 2010

A Simulation of the Muon Ionisation Cooling Experiment (MICE)

Malcolm Ellis, Paul Kyberd, Matthew Littlefield
Centre for Sensors and Instrumentation, School of Engineering and Design, Brunel University, Uxbridge, Middlesex, UK

Keywords (3): Simulation, MICE, Beam Line

Introduction

The Muon Ionisation Cooling Experiment (MICE) based at the Rutherford Appleton Laboratory (RAL) near Didcot is an experiment which intends to examine the effects of reducing the temperature of the particle beam, which consists mainly of muons, to decrease the cross sectional area. This process is known as cooling. The reason for this is to discover the plausibility of cooling such a beam to a sufficient cross sectional size to enable it to be used in a colliding experiment or as the basis of a Neutrino Factory (NuFact). The experiment is still in its early stages of data taking and the downstream section of the beam line, where the particle detecting apparatus are, is not yet installed.

This paper will discuss the computer simulation of the experiment which is currently being constructed. The purpose of simulating the beam in the G4MICE program, devised especially for the MICE project, is to gain an insight into the beams behavior in the downstream section. The simulation will look to be as accurate as possible to the real set up and its components. This accuracy will include the dimensions and positions of the components within the MICE hall as well as the physics aspects of the beam and magnets themselves. The results which will be taken from the simulation will be the theoretical readings of the trackers, used to detect the path of the particles, and time of flight detectors, which are used to measure the particle's speed. The simulation will also have other advantages, these being that an 'invisible' detector plane can be placed in any position in the simulation's domain for the users to ascertain the beams characteristics at any arbitrary point. It is also possible to simulate the radiation levels around specific components in order to assess the level of danger to the users of the experiment while data is being taken. The results of this simulation will also be compared to actual data from the detectors. This will aid in the understanding of potential problems.

This paper will outline the steps taken thus far in the update and will also present the preliminary results.

Methodology/Approach

Firstly a Computer Aided Design (CAD) drawing, drawn by the engineers at RAL, was manipulated into technical drawings of the overall experiment's layout. The technical drawings include the dimensions of all the components and their position to a relative datum point called the 'MICE centre'. The MICE centre can be seen in Fig 2 .Fig 1 is a CAD drawing of the entire hall and Fig 2 depicts one of the technical drawings taken from the initial CAD file.

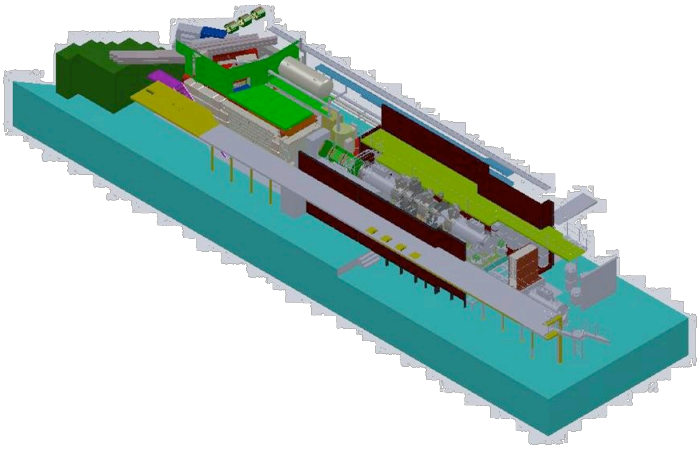

Figure 1: CAD drawing of MICE hall

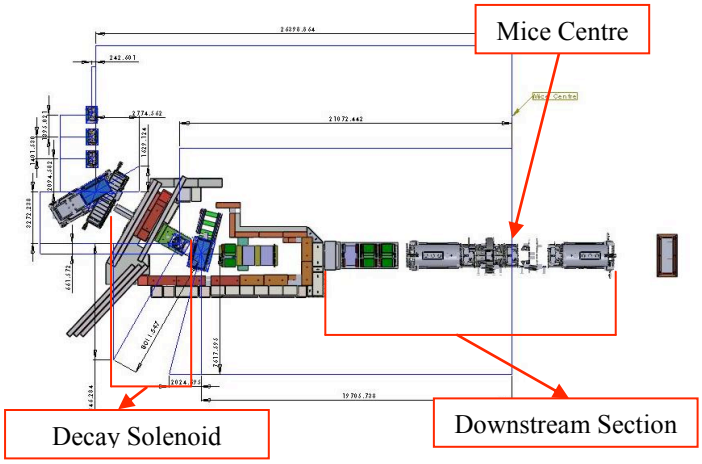

Figure 2: Technical drawing of MICE beam line

Various technical drawings were created in order to get accurate positions of all the components of the beam line.

The next stage of the simulation was to modify the G4MICE program to add any changes to the previous file, which is a legacy programme, which may not have been included. The G4MICE program is a program devised especially for use by the team working on the MICE project. This program uses three different visualization platforms to represent the geometry of the files inputted. The beginning stage of the update was to alter the positions of the components, which were already in the previous simulation, to the positions indicated by the technical drawings.

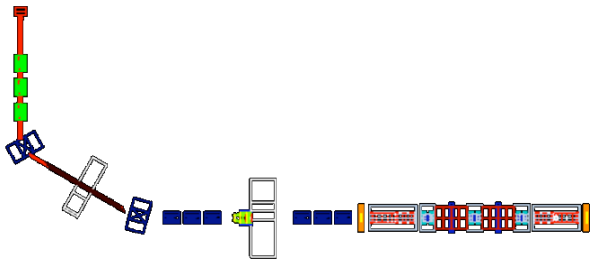

Figure 3a: Simulation of MICE before update

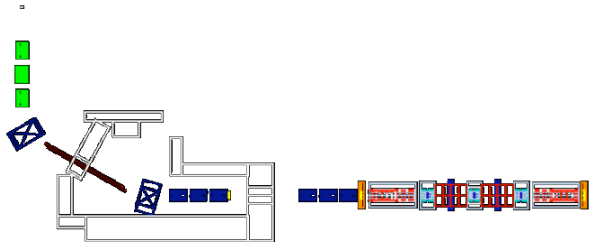

Figure 3b: Simulation of MICE after update

Fig 3a and Fig 3b show the previous geometry and the updated geometry of the MICE run. One can see that there were components within the beam line which were excess to

requirement and other components which were not included. The centre section, surrounded by the white blocks, is known as the Decay Solenoid Area (DSA). This is a solenoid coil where the decay of pions to muons takes place; this area is surrounded by concrete walls as there is a considerable amount of radiation within its vicinity. These walls can be seen in the updated G4 simulation (white blocks) this is so that the radiation levels can be calculated by the G4MICE program this can then be used in a comparison to actual data. Other updates of the beam line will include accurate physical and theoretical representations of the magnets within the hall. The magnets in use are two sets of dipoles, used to bend the beam, and nine sets of quadrupoles, used to focus the beam. These existing models will be studied and compared to the real dimensions and magnetic field properties taken from the actual magnets and any modifications needed will be undertaken to update the models thus making these much more accurate. The actual beam will also be examined to see whether it can be improved this will then be implemented to simulate its characteristics. These characteristics will include momentum, phase space/cross sectional area and particle composition to name a few. As well as altering and updating the geometries and physics of the magnets, the Decay Solenoid will also be updated as the current simulation model is assumed to be inaccurate.

Results and Discussion

Initial results have shown that the current simulation is not accurate in terms of the positions of the components. The first set of simulations which were undertaken, once the positions of the components had been corrected, was to investigate whether the beam would travel the length of the beam line. This simulation was carried out with only 10 particles starting at the target end of the beam line.

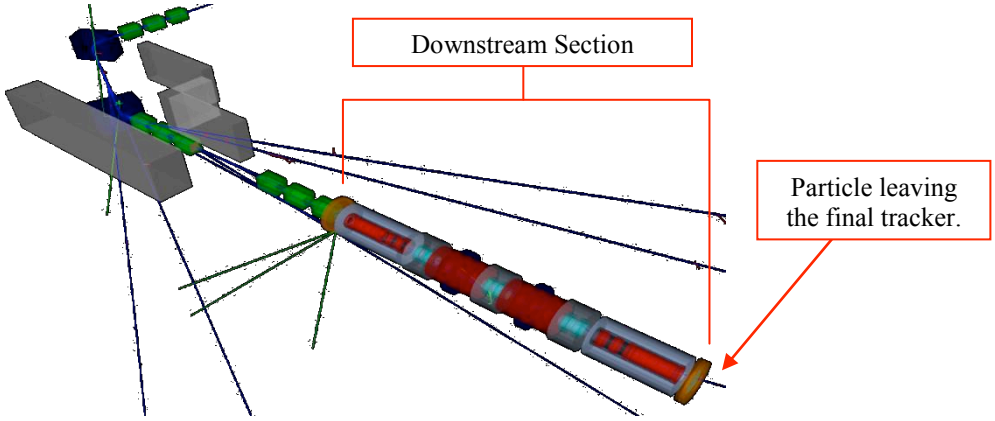

Figure 4: Simulation with a Beam Travelling the Length of the Beam Line

Fig 4 shows the results of this simulation and clearly shows one of the particle exiting the final tracker in the downstream section. This shows that there are no physical obstructions in the geometries. One might expect that all of the particles would travel the entire length of the beam line; however some reasons for this will be due to the scattering of the particles through the air and other components. This will need to be investigated as it appears that quite a large quantity of particles are being scattered. The bending dipoles had their magnetic field maps updated for this simulation and their currents were set to the actual currents taken from real data. However the beam was not bent correctly using

the actual magnet currents and had to be adjusted. Getting the field maps correct will be another point of focus for future work. The decay solenoid was then implemented into the simulation and the beam directed down this component. A point to note is that the decay solenoid is not simulated correctly in terms of its physical parameters and will be updated with its physical and magnetic parameters. However, for the purpose of this initial simulation the current decay solenoid model will suffice.

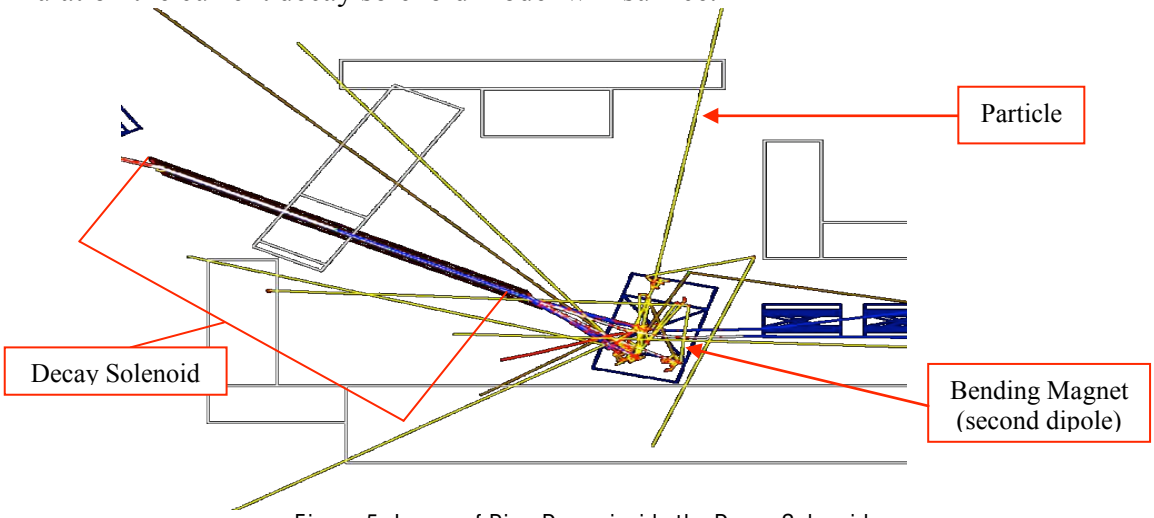

Figure 5: Image of Pion Decay inside the Decay Solenoid

Fig 5 shows the simulation of this section and shows the particles travelling down towards the second dipole. The particles are the coloured lines seen in Fig 5. The colour coding of the particles was also updated from the default colours. All the particles of interest have been altered so the decays of the pions to muons can be seen more clearly. In the centre of the decay solenoid the white lines changing to blue indicates this decay. This image also shows the particles after the decay solenoid; Fig 5 shows that the beam diverges a considerable amount and is not guided correctly by the second dipole and therefore towards the downstream detectors. Guiding the particles towards the detectors has proved to be tricky, in the simulation, which indicates that there may be more problems with the simulation. This is due to inaccuracies in either the physical or magnetic parameters of either the dipoles or the decay solenoid and this is currently being investigated.

Conclusion

In any project theoretical simulations prove to be an invaluable and cost effective way to investigate the experiment. Therefore an accurate simulation of the MICE beam line would aid in any future problems or queries which might occur. The simulation will also help in understanding any problems and can also be used in conjunction with any real data taken.

The simulation is still being updated and some of the problems which have occurred during the update are yet to be investigated and once completed this should provide accurate theoretical information for the members of the MICE project.

SED Research Student Conference
Brunel University
21-23rd June 2010

RegenEBD: A Cost-effective Pneumatic Regenerative Stop-start Hybrid System for Buses and Commercial Vehicles

Cho-Yu Lee1, Hua Zhao1, Tom Ma1, Jing Feng2, Jie Shen2, Zhiqiang Lin2
1. Mechanical Engineering, School of Engineering and Design, Brunel University, Uxbridge, Middlesex, UK
2. 88 Tianqiao West Road, Yulin, Guangxi 537005, People's Republic of China
Cho-Yu.Lee@brunel.ac.uk

Keywords (3): Pneumatic hybrid system, regenerative, stop-start

Introduction

Simulations made by Tai et al. [1] show round-trip efficiency of 36%, 38% reduction in fuel consumption and 64% fuel economy improvement. Through engine experiments, Trajkovic et al. [2] have shown that a regenerative efficiency of 40-48% can be achieved using a pneumatic actuated camless system. However, such complex camless systems are limited to research engines and they are unlikely to be suitable for production.

Calculations done by authors [3] have shown that 14-15% regenerative efficiency can be achieved in an air hybrid engine by adopting cam profile switching (CPS) system on both intake valves in a light duty diesel engine. Such an air hybrid engine utilizes all proven technologies and makes mass production possible at low cost.

In this paper, a novel cost-effective pneumatic regenerative stop-start hybrid system, Regenerative Engine Braking Device (RegenEBD), for buses and commercial vehicles is presented. RegenEBD is capable of converting kinetic energy into pneumatic energy in the compressed air, saved in an air tank using standard engine braking device and other production type automotive components and a proprietary intake system design. The compressed air is then used to drive an air starter to achieve regenerative stop-start operations. The proposed hybrid system can work with the existing vehicle transmission system and can be implemented with the retro-fitted valve actuation device and a sandwich block mounted between the cylinder head and the production intake manifold.

Methodology/Approach

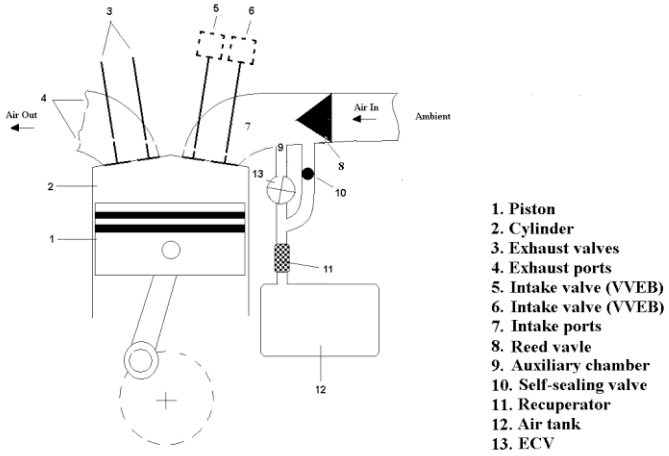

Figure 1: Schematic diagram of an air hybrid engine with an Energy Control Valve (ECV).

Figure 1 shows an air hybrid engine having a piston (1) reciprocating in a cylinder (2). Air flows through the intake valves (5 and 6) via a siamesed intake port (7) and leaves exhaust valves (3) via exhaust port (4). Intake valve 5 and Intake valve 6 can be actuated by the variable valve exhaust brake (VVEB) system when the compression mode (CM) operation is desired. A non-return Reed valve (8) is additionally provided in the intake port (7). While air pressure downstream of the Reed valve is lower than the pressure in the intake manifold, the reed valve pedals open and air is induced into Intake port 7. On the other hand, if air pressure inside the auxiliary chamber formed between the intake valves and the Reed valve is higher than the pressure in the intake manifold, reed valve pedals close and air will be kept within the intake port.

The energy control valve ECV (13) is a solenoid valve that controls air flow out of the air tank (12) for the cranking mode operation. In addition, a check valve has been adopted to be a self-sealing valve (SSV 10) that controls air flow into the air tank (12) for CM. The air tank is connected to intake port 7 through a recuperator (11).

The engine also includes five more cylinders, a fuel system and an ignition system which are not shown in Figure 1 for highlighting the main subject of the present study.

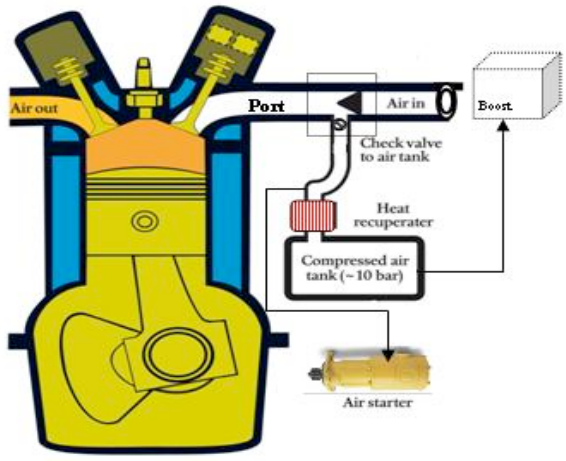

Figure 2: Schematic diagram of an air hybrid engine with an air starter

However, it will be simpler if an air starter can be used to achieve regenerative stop-start operation. As shown in Figure 2, a standard production type air starter, e.g. the SS175 by Ingersoll Rand, can be readily employed to crank start the engine using the compressed air produced during the compression mode operation. Assuming 1-second crank time, the air starter is able to provide 2 start-up operations with a 151 litres air tank at 6.2 bar [4]. Compared to the direct use of compressed air to crank start the engine, the employment of air starter is a much simpler system and easier to implement, by dispensing with the need of fast acting ECV valves and sophisticated controls.

Figure 3 shows the valve timing diagrams for the compression mode. During deceleration and braking, both intake valves remain slightly open (1.25 mm lift) by the action of the VVEB system during the normal compression stroke of the four-stroke cycle so that the air is compressed and stored in the auxiliary chamber formed by the one-way Reed Valve and the SSV. As a result, the engine will be operated as a compressor driven by the kinetic energy of the moving vehicle.

In order to start the engine using the compressed air, it would require 6 fast acting ECV and associated controls. And they have to be operated individually to release the compressed air into the cylinder and timed to synchronize with the firing order of the engine for the cranking mode.

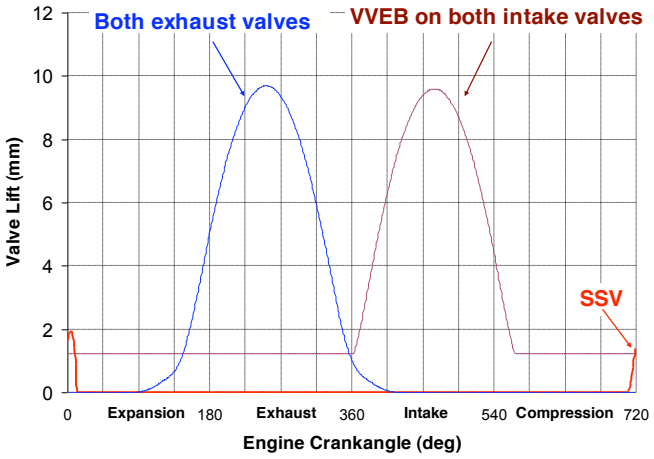

Figure 3: Valve timing diagram for compression mode

Results and discussion

Figure 4 shows air tank pressure against 120th, 240th and 360th engine revolutions at 1500rpm engine speed during the CM operation. The results show that the air tank can be charged from 1bar to 7.1bar within 9.6 seconds at 1500rpm engine speed.

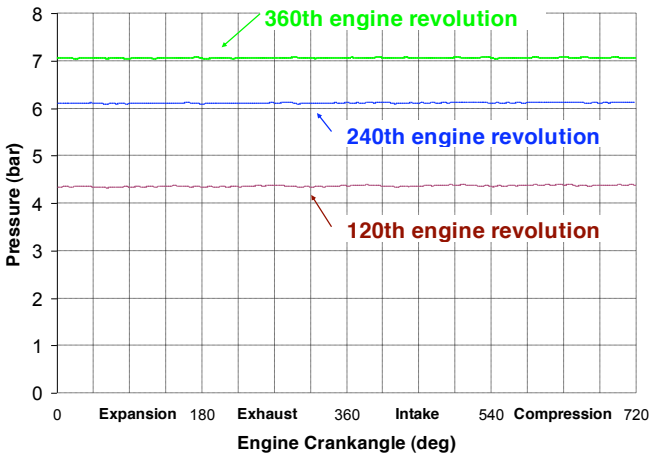

Figure 4: Air tank pressure against various engine revolutions for 1500 rpm engine speed

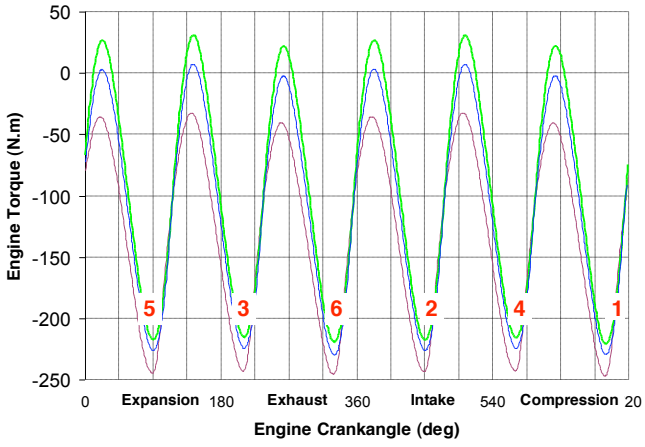

Figure 5: Braking torque for 1500 rpm engine speed

Figure 5 shows the corresponding engine braking torque values for the 6 individual cylinders at 120^{th}, 240^{th} and 360^{th} engine revolutions at 1500rpm engine speed. The cylinder number is included in the diagram to show the firing order of 6 cylinders. At 120^{th} engine revolution, according to Fig.5, the tank pressure has reached to 4.3 bar and the peak braking torque of cylinder 5 reaches 210 N.m. The tank pressure reaches 7.1bar after 360 engine revolutions, the peak braking torque from the cylinder 1 approaches 250 N.m.

The maximum air tank pressure is limited by the effective compression ratio defined by the auxiliary chamber volume. Before the air tank is fully charged, the compressed air is captured by the check valve (SSV) when the auxiliary chamber pressure is higher than the air tank pressure. As the air tank pressure increases, the check valve opening period decreases. As a result, the piston compression takes place against higher auxiliary chamber pressure over a longer period, resulting in higher braking torque seen.

Conclusion

A cost-effective pneumatic regenerative stop-star hybrid system for buses and commercial vehicles, named as RegenEBD, has been proposed and analysed. The concept can be realised with current production technologies and it does not require the use of camless technologies that other air hybrid engine concepts mandate.

In addition to the regenerative stop-start capability, Brunel RegenEBD can also lead to reduced fuel consumption by providing free energy for vehicle service air. The engine braking function will also reduce maintenance costs by minimizing the usage of or replacement of the engine driven compressor as well as reduced brake wear. It allows the bus operators and delivery companies to reduce operating cost through reduced fuel consumption by providing free energy for vehicle service air (~2%) and by engine stop/start (~6%) using free energy for every engine start.

Finally, Brunel RegenEBD is expected to be an order of magnitude cheaper than electric hybrid systems. Thus, with a fuel saving of half that of an electric system, it is expected to deliver ~5 times the economy benefit/cost ratio over electric hybrid systems. And it does not require the fundamental re-design of the powertrain and transmission system, making it a ready deployable and suitable for mass production.

References

[1] Tai, C. and Tsao, T., “Using Camless Valvetrain for Air Hybrid Optimization”, SAE paper 2003-01-0038, 2003.

[2] Trajkovic, S., Tunestal, P. and Johansson, B., “Investigation of Different Valve Geometries and Valve Timing Strategies and their Effect on Regenerative Efficiency for a Pneumatic Hybrid with Variable Valve Actuation”, SAE paper 2008-01-1715, 2008.

[3] Lee, C., Zhao, H. and Ma, T., “Analysis of a cost effective air hybrid concept”, SAE paper 2009-01-1111, 2009.

[4] “Vane Starters (Ingersoll Rand)”, obtained from http://www.ingersollrandproducts.com/IS/product.aspx-eu_en-4250 2009.

SED Research Student Conference
Brunel University
21-23rd June 2010

Human Hip Joint Simulator with Feedback Control System

Nawaf Alhaifi, Simon Poli, Ibrahim Esat, Khaled Alrashdan
Mechanical Engineering, School of Engineering and Design, Brunel University,
Uxbridge, Middlesex, UK
Nawaf.Al-haifi@brunel.ac.uk

Keywords: Stewart platform, human joint simulator, 6 DOF

Introduction

The work proposed in this paper involves the study of the human hip joint kinematics and load analysis. Such analyses are very useful to investigate the mobility and natural functionality as well as the motion variation due to replacement implant. Equally the simulator can be used in implant design. The simulator is developed to provide six degrees of mobility with an intention of using it for different joints loaded under different body activities. Modelling the human joint as six DOF is a challenge because of the complexity of linking the motion drivers of the simulator with the constrained joint motion of the joint to be simulated. This project involved designing a test rig for use on testing joint replacement designs with a view to optimise them in terms of prolonging their lifespan by mimicking the activities that they will perform and measuring the stresses exerted on the joint.

Stewart platform is originally designed by D. Stewart in 1965 [2]. Since then it has been widely used in flight simulators. The six DOF parallel mechanisms simulate the flight conditions by generating general motion in space. Fully actuated parallel mechanism is achieved by connecting six linear actuators via spherical joints to the top and bottom plates. When the extension of each actuator is controlled properly the upper platform is capable of performing six DOF motion within its working space. Although Stewart platform mechanism are available commercially and widely used in flight simulators, it has not been used in the medical field.

Many researchers have considered Stewart platform in their studies, for kinematics and dynamics analysis [3, 4], consideration of practical design [5], working space [6], controller synthesis [7, 8]. The designed Stewart platform in this paper is based on the proposed Azevedo et al. model where inverse and forward kinematics are considered [1]. There are

several current two dimensional hip joint simulators which each use different force track patterns during the gait cycle. Some of these are given here in Force Track Analysis of Contemporary Hip Simulators [9].

Methodology

The system uses a hexapod Stewart platform using six linear actuators to control the platform movement in all six degrees of freedom. The system works by fixing one bone of the joint to a location above the platform and fixing the other bone to the platform and controlling its movement according to the activity using data regarding kinematics and loading of the joint for the activity. The platform is designed to operate the actuators using position feedback in order to set the location of the moving bone for a stage in the activity movement and then change to torque feedback for applying the joint loading at that stage. Because of its layout and operation, the platform is configurable to simulate many different activities of several joints by implementing data collected for them. The kinematic and loading criteria for the motion of the platform were graphically simulated using Visual Basic. For the purposes of this paper the hip joint bones were used for the simulation. The rig is designed to take measurements using position feedback of the actuators and strain gauging, for which the readings are used for torque feedback. The rig is designed to incorporate the actuators and the bones in a configuration suitable for carrying out the simulation. The actuator amplifiers and all of their various connections are contained in a cabinet featuring full electrical protection. The external connections from the amplifiers to the servos, three phase power supply and host computer connections are attached via cables from a hole in the cabinet. The set of axes are connected in a network for control from a single host, only without the independent simultaneous control. The motion of the platform is programmable using the multiple axis cards using Motion Script software.

Results and discussion

The results for single actuator use on the platform show that the actuators assembled on the rig respond well, according well to the signals given, producing motion specified by user. The platform was too heavy to be fully lifted by a single actuator but the full six will have much more power.

Conclusion

The rig has been designed in a way that can simulate joint movement in a configurable way. Further development and modification to the presented platform may be introduced to achieve simpler design with mobile capabilities and lower cost. The hardware uses six actuators controlled using amplifiers from a host computer. The programming provides a simulation for several activities and kinematic and loading analysis framework for future use of the platform.

The platform could be implementing for desired joint simulation in biomedical research by configuration using programming of kinematic analysis. The development of this concept can be made to simulate the joint movement with only one configurable device in the place of several different machines.

References

[1] T. C. d. Azevedo, et al., "Report on the Stewart platform problem," 2008.

[2] D. Stewart, "A Platform with Six Degrees of Freedom," Proceedings of Mechanical Engineering, pp. 371-386, 1965.

[3] K. C. Cheok, et al., "Exact Methods for Determining the Kinematics of a Stewart Platform Using Additional Displacement Sensors," Journal of Robotic Systems, vol. 10, pp. 689-707, Jul 1993.

[4] W. Q. D. Do and D. C. H. Yang, "Inverse dynamic analysis and simulation of a platform type of robot," Journal of Robotic Systems, vol. 5, pp. 209-227, 1988.

[5] E. F. Fichter, "A Stewart Platform-Based Manipulator - General-Theory and Practical Construction," International Journal of Robotics Research, vol. 5, pp. 157-182, Sum 1986.

[6] K. Liu, et al., "The singularities and dynamics of a Stewart platform manipulator," Journal of Intelligent and Robotic Systems, vol. 8, pp. 287-308, 1993.

[7] C. N. Charles, et al., "Adaptive control of a stewart platform-based manipulator," Journal of Robotic Systems, vol. 10, pp. 657-687, 1993.

[8] K. T. K. Kosuge, T. Fukuda, H. Kitayama, N. Takeuchi "Force control of parallel link manipulator with hydraulic actuators," International Conference on Robotics and Automation, pp. 305–310, 1996.

[9] O. Calonius and V. Saikko, "Force track analysis of contemporary hip simulators," Journal of Biomechanics, vol. 36, pp. 1719-1726, 2003.

Fading Channels For Fixed IEEE802.16 Wimax System

Shanar H. Askar, Shahzad A. Memon, H S Al-Raweshidy

School of Engineering and Design
Brunel University
London

Shanar.askar@brunel.ac.uk

Keywords- WIMAX, OFDM, Fading Channel, SUI, Doppler Effect, LOS, NLOS.

1. Introduction

The biggest advantage of the broadband wireless application (BWA) over its wired competitors is increased capacity and ease of deployment. Worldwide Interoperability for Microwave Access (Wimax) is a broadband wireless access technology that provides very high data throughput over long distance in a point-to-multipoint and line of sight (LOS) or non-line of sight (NLOS) environment [1]. The Wimax is a promising technology which can offer high speed data, voice and video service to the customer end. Presently, it offers replacement of high speed wired services such as cable and digital subscriber line (DSL). In Wimax, physical layer is based on Orthogonal Frequency Division Multiplexing (OFDM) which is used to provide high rates of data transmission within fixed broadband applications. In terms of the coverage, it can provide services up to 20 or 30 miles away from the basestation.

Propagation models take into account the type of environment and the materials. According to Andrews, Jeffrey, Ghosh, Arunabha, Muhamed and Rias. "Fundamentals of Wimax" [2], Propagation models can be classified into theoretical and empirical categories. The theoretical models could be divided into two types, one is deterministic and other is statistical. Both models have an advantage that their results are valid independently of the range of input parameters. Moreover, deterministic models can have high computational requirements and their complexity makes it difficult to establish a clear relationship between technical parameters and results, for example the relationship between the height of an aerial and obtained signal to noise ratio (SNR). Statistical models were developed to cope with this issue, but their predictions can become less reliable; However, their computational cost and complexity are notably lower. In the second category are the empirical models which are based on experimental data. In addition, these models rely on their ability to explain how practical parameters affect the average power. Nevertheless, their most significant drawback resides on the fact that they are not extensible to a wide range of parameters [3], [4]. Empirical models are useful at predicting average power on Wimax.

Finally, models that combine stochastic and theoretic methods can be another alternative to calculate the behavior of a radio channel in a fairly accurate way. Their computational cost is lower than in theoretic models whereas they are more flexible than empirical ones. Models such Stanford University Interim (SUI) [5] can be classified into this group. Moreover, SUI models are the choice of Wimax

developers for Fixed Wireless Access (FWA). Due to their great acceptance, for this work SUI models have been chosen as the starting point to foresee the effect of environment on the transceiver.

2. Methodology/ approach

For this research, the SUI model is implemented and tested in Matlab 7.0. An important requirement for assessing technology for Broadband Fixed Wireless Applications is to have an accurate description of the wireless channel. Channel models are heavily dependent upon the radio architecture. According to [5] the wireless channel is characterized by:

- Path loss (including shadowing).
- Multipath delay spread.
- Fading characteristics.
- Doppler spread.
- Co-channel and adjacent channel interference.

The SUI propagation model parameters depend upon terrain, tree density, antenna height and beamwidth, wind speed, and season (time of the year). The three typical terrains are associated with A, B or C letters. For A-type, a hilly topology with a high foliage density is considered, while for C-type terrains a mostly flat environment with low foliage density is considered. Lastly, B-type terrains satisfy a medium foliage density as well as a moderate hilly ground. It is obvious that there are many possible combinations of parameters to obtain such channel descriptions. A set of six typical channels were selected for the three terrain types that are typical of the continental US [5].

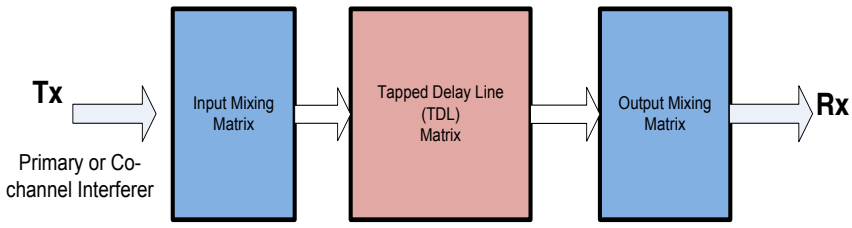

Figure 1: Generic Structure for SUI Model

2.1. SCENARIO FOR MODIFIED SUI CHANNELS

The following parameters to initialize SUI channels:

- Cell size: 7 km.
- BTS antenna height: 30 m.
- Receive antenna height: 6 m.
- BTS antenna beamwidth: 120^{o}
- Receive Antenna beamwidth: directional Antenna $(30)^{o}$
- Vertical Polarization only applied.
- 90% cell coverage with 99.9% reliability at each location covered.

For 30^{o} antenna beamwidth, 2.3 times smaller RMS delay spread is used when compared to an omni-directional antenna RMS delay spread [6]. Consequently, the 2nd tap power is attenuated an additional 6 dB and the 3rd tap power is attenuated an additional 12 dB (effect of antenna pattern, delays remain the same). For the receiver with omni-directional both theoretical and measurement-base propagation models indicate the average received signal power decreases logarithmically with distance, whether outdoor or indoor radio channels are considered.

3. Result and discussion

The IEEE 802.16 channel models [7] for fixed wireless applications are proposed for scenarios where the cell radius is less than 10 km, the directional antennas at the receiver are installed under-the-rooftop/windows or on the rooftop, and the base station (BS) antennas are 15 to 40 m in height. The channel model has 3 paths: the first path is Rician which is a stochastic model for radio propagation anomaly caused by partial cancellation of a radio signal by itself — the signal arrives at the receiver by two different paths (hence exhibiting multipath interference), and at least one of the paths is changing (lengthening or shortening). Rician fading occurs when one of the paths, typically a line of sight signal, is much stronger than the others, in Rician fading, the amplitude gain is characterized by a Rician distribution, while the remaining two are Rayleigh which is the specialized model for stochastic fading when there is no line of sight signal, and is sometimes considered as a special case of the more generalized concept of Rician fading. In Rayleigh fading, the amplitude gain is characterized by a Rayleigh distribution [8].

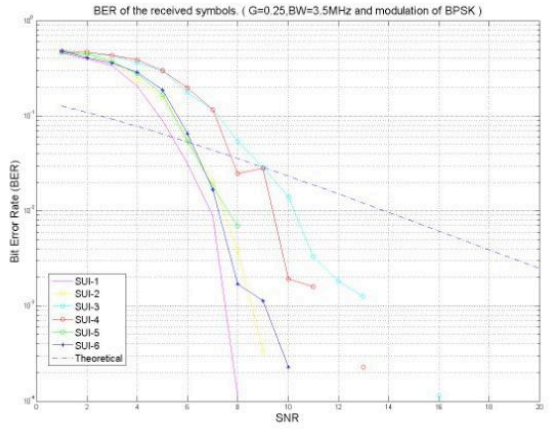

Figure 2. BER of the received symbols for different SUI channels with guard equal to ¼, channel bandwidth is 3.5MHz with BPSK modulation technique

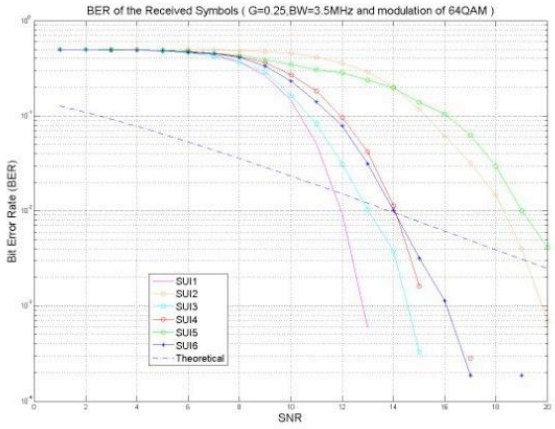

Figure 3. BER of the received symbols for different SUI channels with guard equal to ¼, channel bandwidth is 3.5MHz with 64QAM as a modulation technique

In the simulation model two antennas are used for transmission side and one antenna for reception. The correlation coefficient between the two signals on each path is taken equal to the antenna correlation. We carry out the simulation through different SUI channels (1 to 6). In this section, we have presented various BER vs. SNR plots for all the essential modulation profiles in the IEEE

Wimax-2004 standard with the same ratio of cyclic prefix and equal channel bandwidth. Figures 2 and 3 displays the performance of SUI models under different modulation types, BFSK and 64 QAM respectively.

4. Conclusion

The research study is a comparative study between different SUI channel models. Each one of them is described by appropriate parameters and for specific environment of propagation were implemented using different modulation schemes. Implementation of the channels under BPSK is quite satisfactory, while its need a higher SNR value is required using the 64QAM modulation scheme. The Bit Error Rate (BER) plot obtained in the performance analysis shows that models work well on Signal to Noise Ratio (SNR) less than 20 dB. The performance of the system under BPSK modulation is quite satisfactory as compared to other modulation techniques. The figures were plotted showing the theoretical AWGN channel compared with simulated one under different modulation schemes.

It is clear that the SUI channels in category A and B contain more noise than category C; the figures demonstrate this with a variety of modulation schemes, even with BPSK which is reliable for long distance communication. Category A channel curves also contain more errors than other curves as we can see in figure 3, which is due to its hilly terrain environment with high foliage density.

REFERENCES

[1] IEEE. Standard 802.16-2004. Part16: Air interface for fixed broadband wireless access systems. October 2004.

[2] Andrews, Jeffrey; Ghosh, Arunabha; Muhamed, Rias. “Fundamentals of Wimax”. *Prentice Hall. ISBN:0132225522*. 2007.

[3] Rial, Alvaro Valcarce, et al. "Empirical propagation model for Wimax at 3.5 GHz in an urban environment." *Microwave and optical technology letters*, 2008

[4] Betancur, L., Hincapie, R.C., and Bustamante, R. “Wimax Channel - PHY Model in NS2” *ACM International Conference Proceeding Series,* 2006.

[5] IEEE 802.16.3c00/49r2. “Interim Channel Models for G2 MMDS Fixed Wireless Applications”. *IEEE 802.16 Working Group*, 2000.

[6] IEEE. 802.16e IEEE “Physical and Medium Access Control Layers for Combined Fixed and Mobile Operation in Licensed Bands”, 2005.

[7] V. Erceg et.al, “A model for the multipath delay profile of fixed wireless channels,” IEEE JSAC, vol. 17, no.3, March 1999, pp. 399-410.

[8] Lindsey, W. Error probabilities for Rician fading multichannel reception of binary and N-ary signals, IEEE Transactions on Information Theory, Volume 10, Number 4, October 1964

Facilitating Mobile Communication with Annotated Messages

Ghaidaa Al-Sultany, Sadaqat Jan, Maozhen Li and Hamed Al-raweshidy
Electronic & Computer Engineering
School of Engineering, Brunel University
Uxbridge, UK
{Ghaidaa.Bilal, Sadaqat.Jan, Maozhen.Li, Hamed.Al-Raweshidy}@brunel.ac.uk

Abstract

The widespread usage of the SMS messaging system reflects its importance for the users of mobile phones. However, it is becoming extremely laborious for users to manually write, read and reply to every single SMS message due to an increasingly high volume of SMS messages received. This paper presents SAMS a semi-automated message annotation system, which facilitates mobile communication with annotated messages. Two scenarios are presented showing that SMS messages can be replied to automatically by a software agent on behalf of mobile users. As a result, the workload of users in using SMS messages can be significantly reduced.

Keywords- Mobile computing; message annotation; context aware computing.

1. INTRODUCTION

Since the first commercial use of mobile textual messaging services, it has been embraced and became one of the most popular services in mobile phone networks environment [1][2]. The cost, efficiency and privacy have encouraged text message reciprocation particularly in social communication networks [3]. The number of mobile users using text messaging in the United States from 2003-2010 has increased from about 32 million to 100 million customers and over 48 billion messages are sent monthly [4]. In the UK, the outgoing messages in only one month were more than 6.5 billion [5]. It is shown in [2] that most text messages are concentrated on special occasions and festivities such as New Year, Christmas Eve and Birthdays. During the Chinese New Year in 2007, about 15 billion messages had been exchanged among users [2][6].

It has become a real challenge for mobile phone users to read and reply to all the received messages instantly due to the growing number of these messages. It is stated that the generic greeting messages, for example 'Happy New Year!', are less likely to be responded immediately and the recipients of these messages usually use a predefined template to reply to the messages [2].

This paper proposes a novel approach of developing a Short Text Messaging Service through releasing the overload working that result from responding to the text messages constantly. A Semi-automated Annotated Messaging System (SAMS) framework is proposed and implemented in this paper. The main objective is to redirect the manual messaging service to a Semi-automated Messaging Service by developing a context aware messaging system. This paper mainly concentrates on Annotating Short Text Messages, which is a part of the proposed framework. Two scenarios are tested to evaluate the prototypes working.

2. RELATED WORK

In spite of much research having been focused on adopting metadata and context awareness in wireless networks environment, to our knowledge this research is the first study concentrating on annotating textual messaging and converting the manual service to a semi-automated service. Some previous research works have been summarized about managing metadata with messaging services and using context awareness with semantic based technologies in mobile phone networks environment.

Metadata has been widely used for information retrieval [1][7]. Much research has suggested using metadata with the applications that run on limited resources devices. In [2], Cui searched the awareness of

using text messaging services during special occasions and festivities. It was observed that in spite of there being a massive number of greeting messages sent for a group of users, they were the least likely to get an instant response as numerous users have neither the time nor the patience to interact with such an amount of received messages for different reasons. Therefore, the author mentioned some improvements that would partially solve this issue by offering some navigation support such as adding some metadata about the sender, following them up and unifying the fragment information [2]. Gunner et al in [1] proposed AMMS, which is the Annotated Multimedia Messaging Service. In this research the MMS messages included some spatiotemporal metadata (time of MMS recording, the place where MMS was composed in, and the position to track places) based on the metadata capability of SMIL1 language. The framework Been-There-Done-That has been used to test and implement the AMMS concept. It has two parts, the first to help the users to compose the annotated messages and send them to the server while the other is the local acquisition program. Karypidis et al in [8] presented a method for annotating files automatically with some contextual metadata on portable devices with limited resources. This was managed by combining two system components; the context distribution mechanism that maintains a shared collective contextual awareness and a storage management system to automatically merge the created files with annotations.

Context awareness and semantic based technologies have formed a primary part in designing the ubiquitous pervasive services to improve the mobile phone systems services [9]. A middleware, called AIDAS is presented by Toninelli et al in [10], which adopts context-aware discovery of services based on the mobile users' requirements and preferences. It utilizes some semantic techniques to providing tailored views on services and supports semantic-based adaptation between demanded and existing service facilities. Also, Dietze et al in [11] illustrated an approach depicting learning processes semantically via Situation-driven Learning Processes (SDLP) to link learning contexts and learning resources. The notion of this research depends on two perspectives: that of the user and of the system. The first deals with the learning process as a course of learning objectives while the later perspective concentrates on Semantic Web Services (SWS) technology to describe learning goal resources within a particular learning situation. Contextual Pedestrian Guiding framework is performed by Patkos et al [12] to explore the intelligent pedestrian navigation. The efficient processing and diffusion of context-based knowledge was the aim of the research that was achieved by modeling context using Semantic Web technologies.

The aforementioned works investigated either the possibility of improving new applications working on limited resources devices or adapting metadata annotating to helping file (images or videos) organization and retrieval. This paper has aimed to use both the metadata and context awareness to contribute to developing short Text messaging services.

3. SAMS STRUCTRUAL DESIGN

The key design objective of SAMS architecture is to optimize the conventional text messaging system. Basically, it is composed of two basic parts: the Annotating Layer and the Intelligent Helper Mobile Software Agent (HMSA), as demonstrated in figure 1.

The Annotating layer is the base part of the framework, which is described as a message translator. It plays a vital role in the system's structure (see figure 1 – Annotation part). Mainly, the track of the annotating layer is accomplished by using three procedures: the Convertor, the Annotator and the Parser. The Converter is the core part in the annotating layer. It is in charge of converting the whole outgoing text message into XML format to be ready for sending as an XML document. The Annotator undertakes augmenting text messages with some extra beneficial metadata. The created XML document is based on predefined tags, which include the content of the sending text message and any attached metadata. The main cause behind changing the format of the text messages is increased usability and readability by the intelligent software agent (which will be the second part of SAMS). In addition, the use of the XML format gives text messages the flexibility to be readable on different kind of networks. Last, but not least, the Parser is the last stage in the annotating layer that is responsible on parsing the created XML document to get the involved information of received messages.

The complete performance of the Annotating layer is divided between message sender and message recipient. On the sender end all outgoing messages are annotated automatically, whereas on the receiver end the task will be to extract the whole annotated data of received message using the XML parser.

The helper software agent (HMSA) is the second part of SAMS, whose task is being started after the parsing stage on the receiver side. It deals with the output of annotating XML tags to predict the appropriate answer for the incoming message.

HMSA is running based on two approaches. The first way follows a specific format of the message sent. According to the given format criterias, HMAS will be able to find out the exact reply for the received messages. In this way, the agent does not need to predict or use its ontology tree (As will be demonstrated in the subsequent scenarios). The second way is dealing with non-uniform formatting messages. In this case, context aware ontology will be used to analyze the message context to get the ideal reply for the received message (which will be the next stage of the research).

The initial prototype has been applied based on three main steps. Firstly, setting up the mobile phone network to send and receive the ordinary short text messages. The connection between the nodes depends on standardized communications protocols that allow the interchange of messages between mobile phone devices using wireless messaging APIs. Peer to Peer connection is adopted with the proposed prototype.

Next step is the annotation layer as mentioned above. DTD (Document Type Definition) is approved to define the structure of an XML document to avoid the overhead in sending a message. An XML document will be passed to the kXML Parser to extract the data. The performance of the parser will concentrate on reading the XML document, comparing it with the predefined tags and then to retrieve the metadata and message content. It appeared that kXML is the fully evaluated parser in terms of the parsing time and saving consuming resources. The third step is developing HMSA to predict the suitable reply on behalf of the mobile phone user.

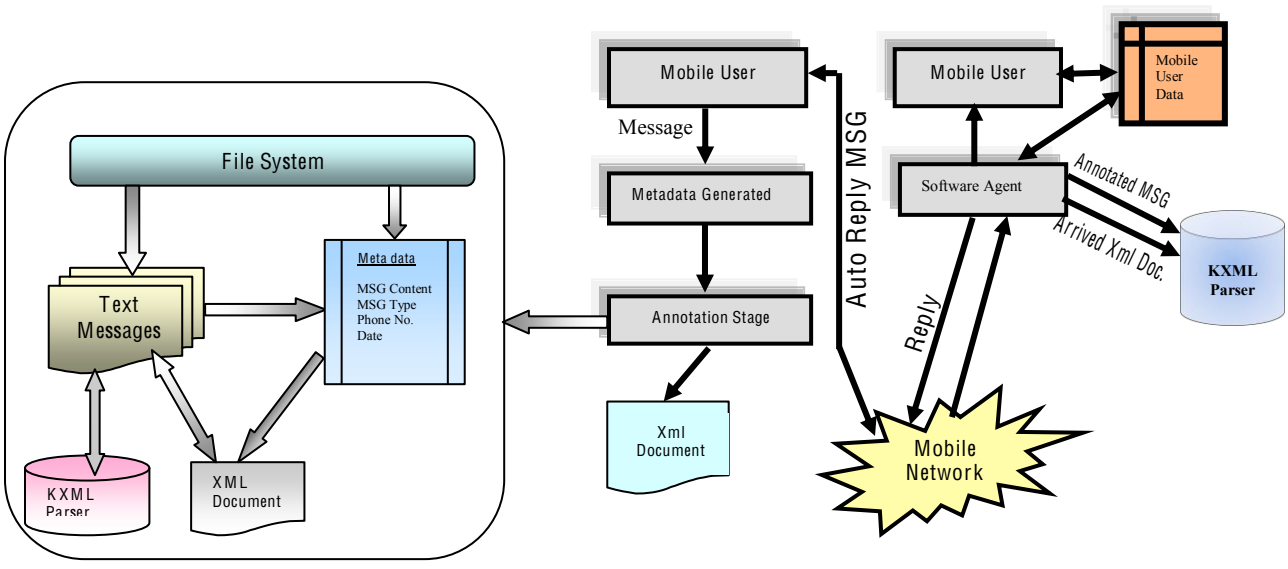

Figure 1. SAMS Architecture

4. CONCLUSION AND FUTURE WORK

This paper described the SAMS framework in evaluating the Textual Messaging Service. It has been proposed to send a XML document instead of ordinary text messages. It is based on two main layers: the Annotation layer to annotate text messages automatically with some information either obtained from the file system of device or added by the messaging writers themselves as predefined tags. The Helper Mobile Software agent, comprising the second main layer, is to redirect text messaging services to semi-

automated services by suggesting different scenarios. MIDlets in J2ME and a kXML parser are implemented in evaluating the application.

Currently, we are in the process of trying some different experimental approaches to adapting semantic based technologies to the framework, such as OWL using context awareness to predict the message content automatically. To summarize, a novel aspect of this study is to move further towards an automated messaging system.

REFERENCES

[1] G. Misund and M. Lindh, "Annotating mobile multimedia messages with spatiotemporal information," Journal of Geographic Information Sciences, vol. 1992, 2005.

[2] Y. Cui, "Messaging Design and Beyond: Learning from a User Study on Holiday Greeting Messages," Analysis, vol. 07, 2007, pp. 11-13.

[3] D. Reid and F. Reid, "Insights into the Social and Psychological Effects of SMS Text Messaging," 2004, pp. 1-11.

[4] P. Moloney, F. Specialist, T.P. October, and C.R. Report, "Text and Multimedia Messaging: Emerging Issues for Congress," 2009.

[5] Digital Britain / the Interim Report, Department for Culture, Media and Sport and Department for Business, Enterprise and Regulatory Reform, 2009.

[6] Xinhua, “Chinese send 15 billion messages during Spring Festival,” 28 /02/2007. Available at: www.chinadaily.com.cn/

[7] W. Does, M. Do, S. Metadata, M. Schemes, E. Sets, C. Metadata, F. Directions, and M. Information, "Understanding Metadata,” 2004.

[8] A. Karypidis and S. Lalis, "Automated context aggregation and file annotation for PAN-based computing," Personal and Ubiquitous Computing, vol. 11, 2007, p. 33–44.

[9] S. Dietze, A. Gugliotta, and J. Domingue, "Bridging the Gap between Mobile Application Contexts and Semantic Web Resources,” 2008.

[10] A. Toninelli, A. Corradi, and R. Montanari, "Semantic-based discovery to support mobile context-aware service access," *Computer Communications*, vol. 31, 2008, pp. 935-949.

[11] S. Dietze, A. Gugliotta, and J. Domingue, "Supporting Interoperability and Context-Awareness in E-Learning through Situation-driven Learning Processes” 2008.

[12] T. Patkos, A. Bikakis, G. Antoniou, M. Papadopouli, and D. Plexousakis, "A Semantics-based Framework for Context-Aware Services: Lessons Learned and Challenges," 2007.

SED Student Research Conference
Brunel University
21 – 23 June 2010

Electron-sample interactions in gamma irradiated glass by CASINO and PENELOPE simulations

Ruzalina Baharin, Peter R. Hobson and David R. Smith
Centre of Sensors & Instrumentation, School of Engineering and Design, Brunel University
Uxbridge, Middlesex, UK
Ruzalina.Baharin@brunel.ac.uk

Keywords: CASINO, PENELOPE, dosimetry

There is much interest in optical response of ionizing irradiated glass particularly for potential dosimeter use. A commercial glass [1] and coloured glass [2] available at market are the glass types that draw the most attention in dosimetry research. In previous work, the glass characteristics and capability of glass as a dosimeter have been investigated. Subsequently, we inquired into the electron interactions and charge-deposition distributions in gamma irradiated glass. In this study, a model of thin silica glass was considered being irradiated with parallel electron beams of 1.17 and 1.33 MeV. Using the CASINO [3] and PENELOPE [4] simulation, among the Monte Carlo technique, the electrons transport profiles in the glass have been obtained.

Introduction

Research on glass as a dosimeter has taken place for many years. It shows promise to the radiation processing industry in terms of dosimetric systems that need low-cost, simple measurement and easy-to-handle equipment [5,6,7]. The most extensive application in industries is for medical products, health care product sterilization, food processing and polymer modifications [8]. Generally, proper dosimetric systems are a prerequisite in order to confirm that the products are treated correctly.

This application has made an increase in the study of the transport of electrons through glass [9]. Recent developments on Monte Carlo simulations investigating the transport of electrons are the CASINO, which is the acronym from 'monte Carlo Simulation of electron trajectory in sOlid' and PENELOPE which is 'PENetration and Energy Loss of Positron and Electrons'. The CASINO program is specially designed for user easy-interpretation of electron trajectory of low-energy beam interaction in bulk or thin film samples. This software also can be used to generate backscattered electrons. On the other hand, PENELOPE allows the simulation of electrons, positrons and photon transportation in any material. The energy ranges between a few hundrend eV and 1 GeV for electrons and positrons. Both programs can be downloaded and are available commercially on the internet.

In this work, these two codes were used to simulate the electron-sample interactions in silica glass. A simple model of thin silica glass exposed to a Co-60 source was used. The model depends on different parameters such as sample thickness, atomic number of sample and electron energy. Observation on the profiles acquired was used to explain the mechanism that occurred in the irradiated sample.

Methodology

The model used in both simulations is of 0.1 cm 0.1 cm of silica (SiO_2) glass, exposed to 1 MeV electrons. The energy of two parallel beam of 1.17 and 1.33 MeV of electrons are considered.

Result and Discussion

Figure 1 shows the energy of transmitted electrons from both simulations. It indicates that the electrons can penetrate to the bottom of silica glass and escape the surface. The energy of transmitted electrons released was in range of 520-620 keV accelerating voltage (from Figure 1 (a)). This indicates that electrons most likely have lost nearly half of their energy when travelling deeper in the silica glass via inelastic scattering. In PENELOPE simulation, the transmitted electron energy is at 600 keV quite similar with result simulated by CASINO.

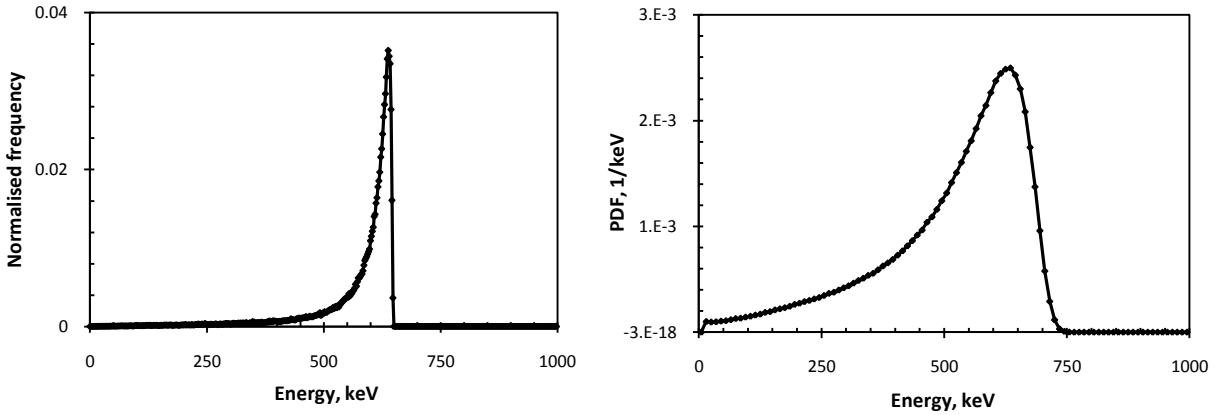

(a) (b)

Figure 1. The transmitted energy of electrons from (a) CASINO and (b) PENELOPE simulations. The model used is 0.1 cm of silica exposed to 1 MeV electrons.

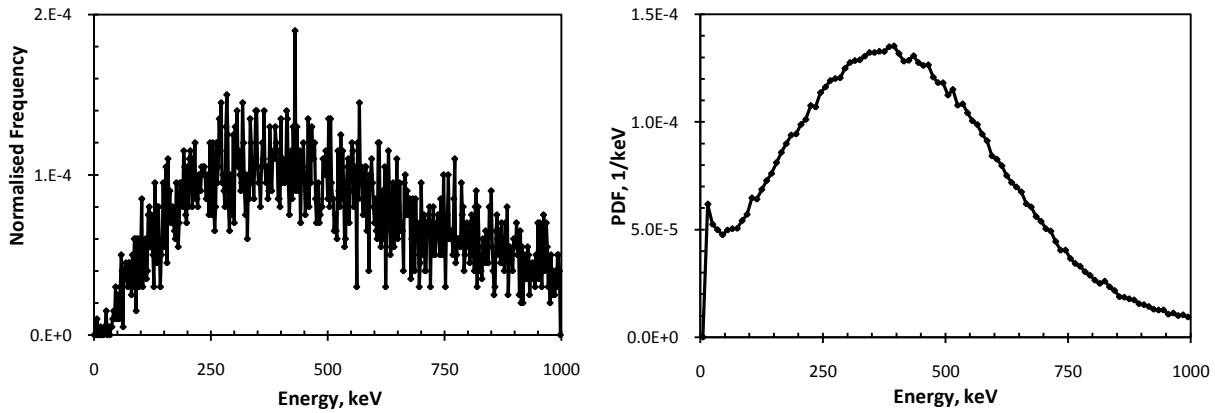

(a) (b)

Figure 2. The energy distribution of backscattered electrons from (a) CASINO and (b) PENELOPE simulations. The model used is 0.1 cm of silica exposed to 1 MeV electrons.

In Figure 2 above, show the distribution energy of backscattered electrons from the sample. These backscattered electrons may have contributed into the final image, but are not discussed in this paper. From CASINO (Figure 2(a)) and PENELOPE (Figure 2(b)) simulations, the optimum energy is at 400-500 keV and may also generate a response in the detector.

The results below are showing the depth-dose distribution of electrons in sample. Figure 3 (a) shows the result from CASINO simulation with the maximum distribution at 0.04-0.05 and uniformly distribute throughout the depth at 0.05-0.06 cm in Figure 3 (b), from PENELOPE simulation.

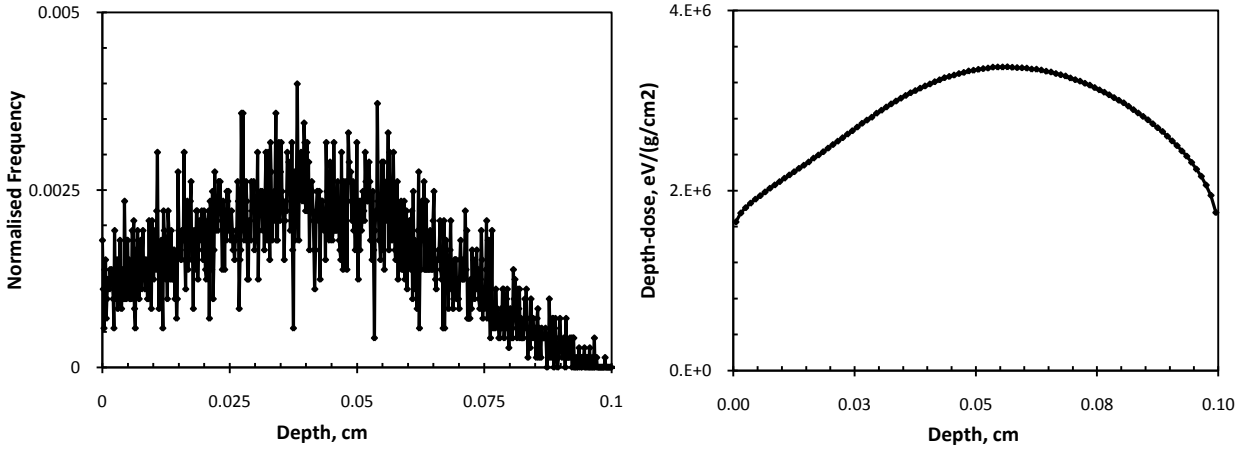

(a) (b)

Figure 3. The depth dose distribution of electrons from (a) CASINO and (b) PENELOPE simulations. The model used is 0.1 cm of silica exposed to 1 MeV electrons.

Comparing these two simulations, PENELOPE has provided more description than CASINO, but CASINO is a more user-friendly program. However, because of the fluctuations in CASINO data, further analysis is required to interpret these data. PENELOPE allows electron, photon and positron transportation; however CASINO only permits trajectory electrons. Both simulations can develop 2D views while PENELOPE has further features for 3D view and distribution.

Conclusion

The results obtained in this work indicate that CASINO and PENELOPE simulations are very useful tools to present the description of different radiation effects on different materials. They are easy to understand and provide detailed validation data to support experimental work. However, a good knowledge in computer programming language is highly recommended.

Future work

For the next study, the simulations will be run on the same model with the addition of silica glass-quantum-dots-doped. Quantum-dots now have received great attention in many fields due to their tunable optical and electronics properties [10]. These advantages drive our motivation to optimize the capability of silica glass as a dosimeter.

References

[1] Khan HM and Ali SW 1995 *Radiation Physics and Chemistry* 46 1203.
[2] Teixeira MI, Ferraz GM and Caldas LVE 2007 *Nuclear Instruments and Methods in Physics Research B* 263 67.
[3] Salvat F and Fernandez-Varea JM 2009 *Metrologia* 46 S112.
[4] Drouin D, Couture AR, Joly D, Tastet X, Aimez V and Gauvin R 2007 *Scanning* 29 92.
[5] Rodriques Jr. AA and Caldas LVE 2002 *Radiation Physics and Chemistry* 63 765.
[6] Teixeira MI, Ferraz GM and Caldas LVE 2005 *Applied Radiation and Isotopes* 62 365.
[7] Farah K, Kovacs A, Mejri A and Ouada HB 2007 *Radiation Physics and Chemistry* 76 1523.
[8] Narayan P, Senwar KR, Vaijapurkar SG, Kumar D and Bhatnagar PK 2008 *Applied Radiaton and Isotopoes* 66 86.
[9] Obata S, Yoshida T, Tanabe T, Allen C, Okada M and Xu Q 2006 *Nuclear Instruments and Methods in Physics B* 250 169.
[10] Nazmitdinov RG 2009 *Physics of Particle and Nuclei* 40 71.

SED Research Student Conference
Brunel University
21-23rd June 2010

A Personal Mobile Grid

Heba Kurdi, Hamed Al-Raweshidy, Maozhen Li
Wireless Networks & Communication Centre (WNCC)
Electronic & Computer Engineering, School of Engineering and Design
Brunel University, Uxbridge, Middlesex, UK
heba.kurdi@brunel.ac.uk

Keywords (3): Grid computing, resource scheduling, Next Generation Grids

Introduction

The overall aim of this project was to introduce Personal Mobile Grids (PM-Grids) as a novel paradigm in grid computing [1] that scales grid infrastructures to mobile devices and extends grid entities to individual personal users. In this project, an architectural design as well as simulation models for PM-Grids were developed and evaluated as a proof of concept.

A PM-Grid is a grid environment which can be owned and utilised by an individual user. It is constructed over her/his devices and might be extended to other devices which s/he trusts. PM-Grids aim to enable the mobility of both, users requesting access to grid resources and resources that are part of a grid. This opens the doors to have the grid processing power in more widespread geographical locations and social settings, such as emergency communications in fire fighting and natural disasters, as well as many of the newly emerged mobile applications in e-learning, e-healthcare, e-wallet and m-gaming among others.

The main motivation of PM-Grids is the need for grid systems which support the vision of Next Generation Grids (NGG) [2] to scale grids to a larger number of entities and smaller devices. The NGG vision has placed scalability, openness to wider user community, pervasiveness and ubiquity, transparency and user-centricity among its top desirable properties. However, neither existing third generation grid technologies nor great extensions to them can satisfy the NGG requirements. Therefore, the way forward is to design an architecture based on the NGG properties and implement it [3].

Hence, the PM-Grid design has not adopted any of the already available grid architectures. Instead, the design is based on Personal Networks (PN) [4] architecture and as a natural extension to them, seeing that these features have been explicitly addressed in their design [5].

Methodology

The work in this project started by surveying the area of grid computing and distributed systems for paradigms relevant to PM-Grids. The survey revealed two main findings. First, there are few research projects which have addressed the mobility issue in grid computing but only at the organisational level. Second, fewer research projects have targeted grid systems at the personal level, but the focus has only been on facilitating file sharing applications. Therefore, an architectural design of PM-Grids was developed to address both personalisation and mobility issues in grid computing.

The most important aspect of realising a grid system is a scheduler that efficiently utilises its resources. However, the extremely dynamic nature, diversity and limited

capabilities of resources, as well as difficulties in predicting the nature and timing of incoming jobs, are all factors that increase the complexity of the scheduling problem in PM-Grids.

Therefore, a survey on resource scheduling frameworks was conducted to address design features required for a resource scheduler that can cope with the extraordinarily difficult scheduling conditions in PM-Grids. The survey revealed that decentralised, cooperative, local, adoptive, non-clairvoyant and self-scheduling schemes are among the top requirements to deal with the complexity of this problem. Consequently, a resource scheduler, HoPe, was proposed and implemented based on these requirements. HoPe was augmented with techniques analogous to those utilised by the honeybee colony, while allocating worker bees to nectar sources under the extraordinarily difficult conditions of weather unpredictability and food variability.

Next, PM-Grid designs and HoPe implementation were evaluated thoroughly through a strictly controlled empirical study considering two main grid design issues:

- Scalability to a larger number of nodes.
- Sustainability under different loads.

The controlled study involved the following steps:

1. Identifying the critical elements inherent in the design of grid systems and deciding on the set to be considered: job interarrival time, number of nodes, job size and processor capacity.
2. Varying the experimental variables, job interarrival time and number of nodes, to simulate a representative sample of grid environments. Values of the number of nodes (workers) were selected in the range of the expected number of devices per cluster available for an individual user or a small business: from 4 to 16 nodes. Values of interarrival time were selected in the range of two extreme cases of the expected usage of PM-Grids: from 4 to 180 sec.
3. Controlling extraneous variables, job size and processor capacity, by randomisation to ensure a representative sample in all experiments. Heterogeneity in processor capacity was modelled assuming three types of machines (P_a, P_b, P_c) with different capacities. Heterogeneity in job size was modelled assuming three types of jobs (J_a, J_b, J_c) with different sizes. During running time, a uniform random number R_{proc} from one to three was generated describing the processor capacity and another random number R_{job} following the same distribution was generated to describe job size heterogeneity. Basically, the processor capacity and job size were generated based on similar lines of research conducted by [7].
4. Identifying a benchmark algorithm. The opportunistic scheduling heuristic (OSH), a well established heuristic in high throughput computing, was selected for this purpose.
5. Identifying suitable performance measures:
    - Stability where the rates of job entering and job leaving the system are equal.
    - Mean turnaround time (TT) which represents the elapsed time from when a client submits a job until the client receives the corresponding results.
    - Net throughput which represents the amount of work completed by the system over a period of time. It is measured as the number of jobs completed from time zero to time t.

- Speedup which refers to how much a parallel system is faster than a corresponding sequential system.

6. Comparing the performance of both HoPe and OSH to optimum values and lower bounds and analysing the main findings.
7. Improving the accuracy of this simulation-base study through:
   - Running ten simulations and accepting the mean outcome.
   - Ignoring simulation results generated in the first 60 seconds.
   - Measuring the uncertainty in data using the standard deviation.
   - Calculating absolute and relative errors to examine the quality of results.

Results and Discussion

Figure 1- Figure 8 show simulation results obtained after running each experiment for five hours. Jobs were generated using four clients with a Poisson process and exponential interarrival times with means in the range from 4 to 180 sec. Computational jobs were implemented as divisible load cryptography applications to factor large integers (up to 4,293,001,441). Each job was contained in one packet and produced one output file. For simplicity, the communication cost was not considered at this stage. It was assumed that one machine can process only one operation at a given moment (resource constraints) and once task started, operation runs to completion (no pre-emption condition).

Experimental results indicate the dominance of HoPe performance and demonstrate the ability of HoPe to considerably reduce the effect of variations in grid scale and job interarrival times, illustrating better scalability and sustainability, when compared to the OSH. HoPe has successfully maintained optimum stability and throughput in more than 95% of the experiments, with HoPe achieving three times better than the OSH under extremely heavy loads. Regarding the turnaround time, HoPe has effectively achieved less than 50% of the value incurred by the OSH while doubling its speedup in more than 60% of the experiments.

Conclusion

In this project, PM-Grids were introduced as grid environments owned and utilised by individual personal users. An architectural design of PM-Grids based on PNs architectures was proposed. A lightweight, self-managed and adaptive scheduler was implemented and evaluated as the core component of a middleware system for PM-Grids. The results indicate the potential of PM-Grids in realising futuristic grid visions to scale the grid entities to larger number of entities and smaller devices and to widen the grid application areas to span more geographical and social settings than ever before. Therefore considering the deployment of PM-Grids in real life scenarios and the utilisation of HoPe in other parallel processing and high throughput computing systems are recommended.

References

[1] I. Foster and C. Kesselman, Eds., *The Grid2: Blueprint for a Future Computing Infrastructure*. San Francisco: Morgan Kaufmann, 2003.

[2] Expert Group, "Future for European grids: Grids and service oriented knowledge utility," Expert Group Final Rep., Jan. 2006.

[3] K.G. Jeffery, "Next generation grids for environmental science," *Environmental Modelling & Softw.,* vol. 22, no. 3, pp. 281–287, 2007.A.

[4] IST.MAGNET Beyond (IST-FP6-IP-027369) [online]. Available: http://www.magnet.aau.dk.

[5] B. Jiang, V. Kaldanis and A. Markopoulos "User requirements & demand for services and applications in PNs," presented at IST mobile & wireless communication summit, Lyon, France, 2004.
[6] K. Li, "An average-case analysis of online non-clairvoyant scheduling of independent parallel tasks," *J. Parallel Distrib. Comput.,* vol. 66, no. 5, pp. 617-625, 2006.
[7] CoreGRID, "Comparative evaluation of the robustness of DAG scheduling heuristics," FP6-004265, Tech. Rep. TR-0120, Dec. 5, 2007.

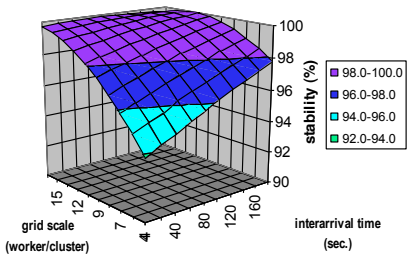

Figure 1: HoPe stability

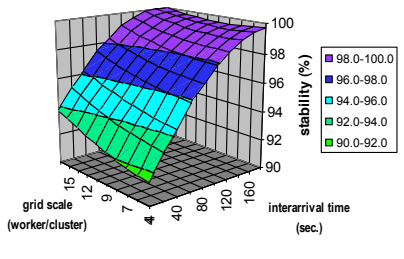

Figure 2: OSH stability

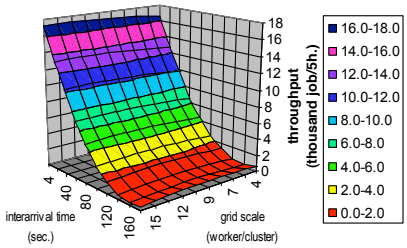

Figure 3: HoPe net throughput

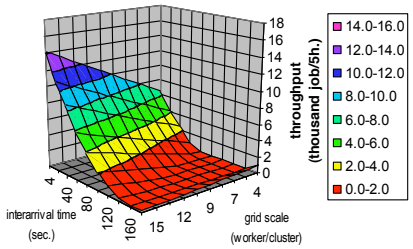

Figure 4: OSH net throughput

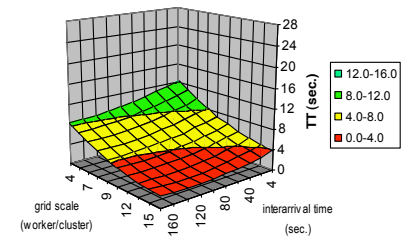

Figure 5: HoPe TT

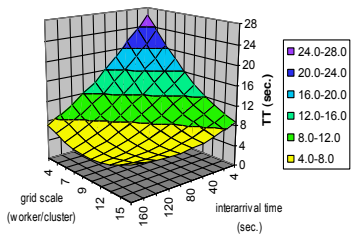

Figure 6: OSH TT

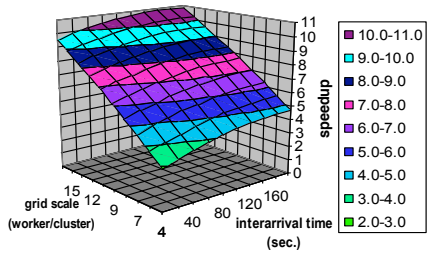

Figure 7: HoPe speedup

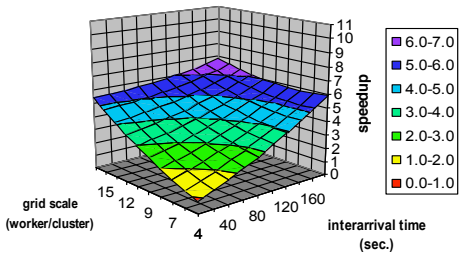

Figure 8: OSH speedup

Digital Radio over Fibre for Wireless Access Network Application

Seyed Reza Abdollahi, IEEE Student Member

E-mail: Seyedreza.abdollahi@brunel.ac.uk

Abstract

Digital signal processing has revolutionized modern communication systems by offering unprecedented performance and adaptivity. Since digital systems are flexible and more conveniently interface with other systems, and are more reliable and robust against additive noises of devices and channel and achieve better dynamic range than analogue systems. Analogue to digital and digital to analogue converters (ADC and DAC, respectively) are the link between the analogue world and the digital world of signal processing and data handling. In an Analogue system, bandwidth is limited by device, element performance and parasitic introduced. Thermal noise generated in active and passive components limits the dynamic range of an analogue system. The ratio between the maximum allowable analogue signal and the noise determines the dynamic range of the system.

Radio over fibre technology is currently receiving large attention due to its ability to provide simple antenna front ends, increased capacity and wireless access coverage. In this paper, we present the simulation and performance investigation of the proposed digital radio over fibre link for wireless standard signal transportation. In this research work, we have used the photonic analogue to digital conversion (PADC) technique to digitize the analogue radio frequency (RF) signal. Wideband analogue to digital conversion is a critical problem encountered in broadband communication and radar systems. The recent electronic analogue to digital conversion systems suffer the following problems: jitter in sampling clock, settling time of the sample and hold circuit, speed of comparator, mismatches in the transistor thresholds and passive component values, these limitations imposed by all these factors become more severe at higher frequencies. Photonic ADCs by using the Mode-locked laser and Mach Zehener Modulator (MZM) which are able to scale the timing jitter of the laser sources to the sub-femtosecond level resolution by many orders of magnitude beyond what electronic sampling systems can achieve currently [1]. Figure 1, shows a generic analogue radio over fibre link that includes an optical source, modulator, optical amplifier & filters, optical channel and photodiode as a receiver and electrical domain amplifiers and filters. In some cases the optical source is directly modulated by the RF signal, but as the laser is usually a significant source of noise and distortion in a radio over fibre link, and laser diode normally exhibits nonlinear behaviour. When it is driven well above its threshold current, its input/output relationship can be modelled by Volterra series of order 3, [2]. So, in the recent radio over fibre systems, semiconductor laser is used for the optical source and the external modulator, usually a Mach Zehnder interferometer fabricated from LiNbO3, impress the RF signal on the optical intensity. A wide range of other modulator can be used as reviewed in [3][4].

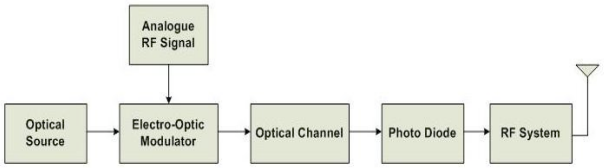

Figure 1: A generic Analogue Radio over Fibre Link.

Analogue optical link suffer from nonlinearity of both microwave and optical components that make up the optical link. The digital radio over fibre link can maintain the dynamic range more independent of the optical fibre link distance and can employ the present infrastructure for transporting the digitized radio traffic.

Figure 2 shows the proposed digital radio over fibre system. In this system, first we have digitized the analogue RF signal by using the PADC techniques and with regenerating the digital data and multiplexing of them together we modulated the digital data over optical carrier by external modulators. In this design, we can transport both the baseband data traffic and digitized RF signal over core and metro networks by using wavelength division multiplexing technique. At the receiver side or base stations, we can demutiplex and regenerate the original transmitted data.

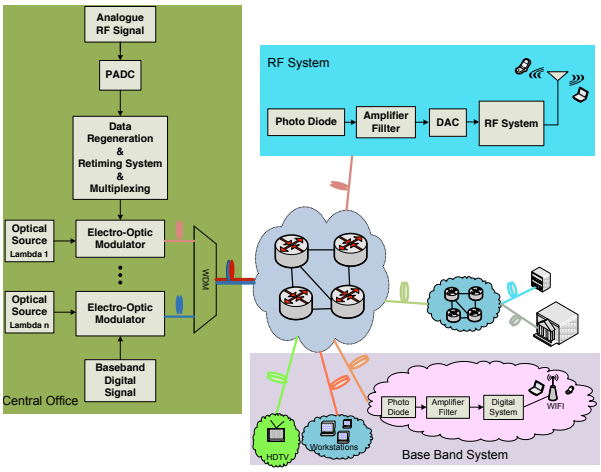

Figure 2: Proposed Digital Radio over Fibre Network Implementation.

With employing this technique, we could be able to use the core and metro networks infrastructure free capacity to transport the traffic of broadband wireless and wireline users, and centralise the signal processing, system management and monitoring. Therefore, Wireless networks could easily be integrated with existing and future broadband optical and high-speed networks that reduce the system implementation overhead and service cost for each bit per second to end-users.

Conclusion:

In this paper, we present the simulation and performance investigation of the proposed digital radio over fibre link for wireless, mobile and fixed users standard signal transportation that used the PADC to digitize the analogue radio frequency (RF) signal. We have digitized the RF carrier modulated signal and then transporting the resulting digital baseband signal optically over the fibre. In the digital radio over fibre, the dynamic range is independent of the fibre distance up until the distance that passed the receiver error free signal detection level.

References:

[1] P. A. Gamage, A. Nirmalathas, C. Lim, D. Novak and R. Waterhouse, " Design and analysis of digitized RF-Over-Fiber Links," J. of Lightwave Technology, Vol. 27, No. 12,pp. 2052-2061, 2009.

[2] H. Al-Raweshidy and S. Komaki, Radio over Fiber Technology for Mobile Communication Networks, Artech House, 685 Canton Street, MA 02062, 2002. Pp 136-138.

[3] C. H. Cox, III, Analog Optical Links, Cambridge University Press, Cambridge UK, 2004.

[4] G. L. Li. and P. K. L. Yu, "Optical intensity modulators for digital and analog applications," J. of Light wave Technology. Vol. 21, PP. 2010-2030, 2003.

[5] S. Yang, Z. Shi, H. Chi, X. Zhang, S. Zheng, X. Jin and Jiang Yao, " Photonic analog-to-digital conversion using multiple comparators and Mach-Zehnder modulators with identical half-wave voltages," Elsevier B. V., Optic Communications, Vol. 282, pp. 504-507, 2009.

SED Research Student Conference
Brunel University
21st – 23rd June 2010

Rapid Prototyping of Finite Radon Transform (FRAT) for Medical Imaging Applications

Afandi Ahmad, Abbes Amira
Electronic and Computer Engineering, School of Engineering and Design,
Brunel University, Uxbridge, Middlesex, UK
afandi.ahmad@brunel.ac.uk

Keywords: Finite Radon transform (FRAT), field programmable gate array (FPGA), medical imaging

Introduction

Digital image and signal processing is one of the fastest growing areas of the electronic industry. Recently, the technological advances have had a particular strong impact, especially in the field of medical applications and this has provided an impetus to the development in medical image processing applications such as compression, segmentation, registration, denoising and quantification.

The finite Radon transform (FRAT) was first introduced in [1] and the algorithm is inherently serial, iterative and has large latency. To overcome this limitation, hardware implementation with parallelism capabilities appears as a good solution. Field programmable gate arrays (FPGAs) with massive parallelism options, multimillion gate counts and special low power packages makes FPGAs an attractive platform for FRAT hardware implementation.

A thorough survey of literature [2–6] indicates that the research is still in its infancy as demonstrated by the limited contributions for the FRAT and their FPGA implementations. The aim of this paper is to investigate the exploitation of Xilinx AccelDSP for rapid prototyping of FRAT used in medical imaging applications. Two architectures have been proposed with direct implementation of pseudo-code (sequential and pipelined descriptions), and an area-efficient version. Analysis for both software simulation as well as the hardware implementation with different medical image modalities has been carried out and discussed.

Methodology

Two architectures of direct implementation of pseudo-code and an area-efficient version have been studied. For direct implementation of pseudo-code, architectures exploration with loops rolled and unrolled has been examined for two types of descriptions: sequential and pipelined as shown in Figs. 1(a) and (b), while the area-efficient model implementation is shown in Fig. 1(c). In both architectures, pseudo-code has been written in MATLAB and the Xilinx AccelDSP has been used for architecture and synthesis exploration.

Results and analysis

Three medical images have been used for software simulation and hardware implementation: medical resonance imaging (MRI) scan of human brain (940×940), real chest body computerised tomography (CT) (512×512), and real positron emission tomography (PET) scan of normal human brain (109×109).

For the software simulation, the PSNR values of the reconstructed medical images with various block sizes is depicted in Fig. 2. Results obtained have shown that the PSNR of the reconstructed image drops by 6.58, 7.20 and 12.10 dB for MRI, CT and PET, respectively when the block size increases from $p = 5$ to $p = 17$. This is because as p increases, the rounding error becomes more significant. Using a divider with greater precision can reduce the rounding error.

For the case of block sizes $p = 17$, the FRAT domain visualisation for MRI and PET test images is shown in Figs. 3(a)-(f). It can be observed that the averaging effect of the FRAT and the blockiness of the image in the transform domain become clearly visible as p increases. It is worth mentioning that the filtered back projection (FBP) is a mathematically perfect inversion for the FRAT and peak signal to noise ratio (PSNR) depends only on the accuracy required. In order to illustrate the effect of bit-width limitations on PSNR, reconstruction has been carried out on standard images in the FRAT domain.

On the other hand, results obtained for the hardware implementation demonstrate various tradeoffs with sequential and pipelined descriptions yielding better achievement for maximum frequency and throughput, respectively. Moreover, an area-efficient implementation version also exhibit less area occupied and better maximum frequency. Comparison of performance metrics for the proposed FRAT architectures with existing work is presented in Table 1.

Conclusion

Two architectures of FRAT which are obtained from the direct implementation of algorithm and an area-efficient version have been proposed. Analysis and performance evaluation with various medical imaging modalities have been conducted. Evaluation of the implementation results indicate promising tradeoffs achievement in terms of maximum frequency, throughput and area.

References

[1] E. D. Bolker. The finite Radon transform. In S. Helgason, R. L. Bryant, V. Guillemin, and R. O. Wells, Jr, editors, Integral Geometry (*Contemporary Mathematics*), volume 63, pages 27 – 50. 1987.

[2] J. Wisinger and R. Mahapatra. FPGA based image processing with the curvelet transform. *Tech Report TR-CS-2003-01-0*, Texas A & M University, TX, 2003.

[3] C. A. Rahman and W. Badawy. Architectures the finite Radon transform. *IEE Electronic Letters*, 40(15):931–932, July 2004.

[4] I. S. Uzun and A. Amira. Design and FPGA implementation of finite ridgelet transform. In *Proceedings of the IEEE International Symposium on Circuits and Systems*, volume 6, pages 5826 – 5829, May 2005.

[5] S. Chandrasekaran and A. Amira. High speed/low power architectures for the finite Radon transform. In *Proceedings of the International Conference on Field Programmable Logic and Applications,* pages 450 – 455, August 2005.

[6] S. Chandrasekaran, A. Amira, S. Minghua and A. Bermak. An efficient VLSI architecture and FPGA implementation of the finite ridgelet transform, *J. Real-Time Image Process.*, pages. 183 – 193, 2008.

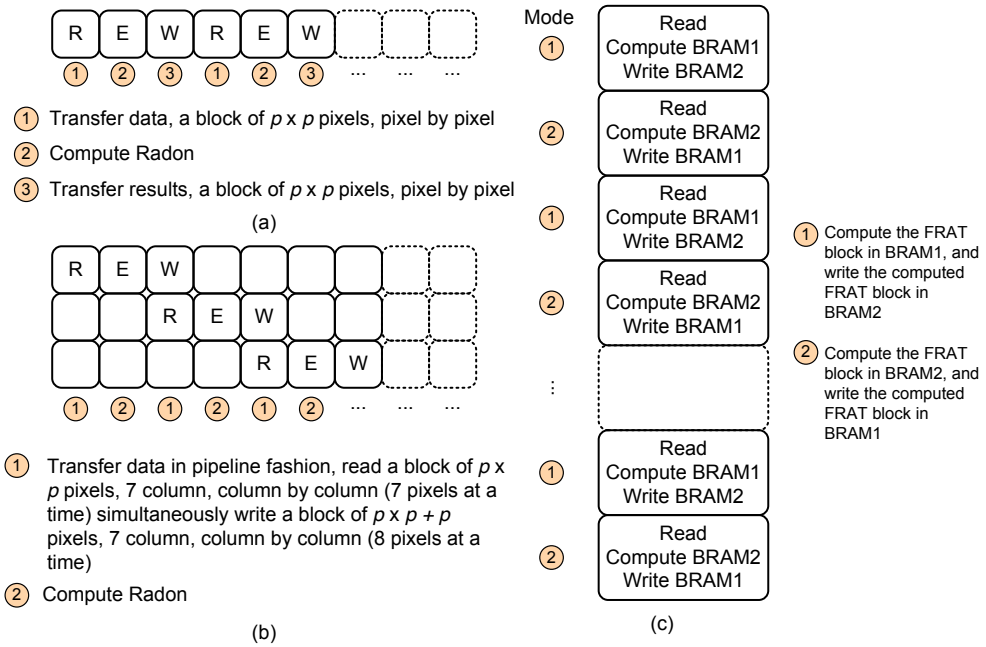

Fig. 1: Implementation descriptions. (a) Sequential (b) Pipelined (c) Area-efficient.

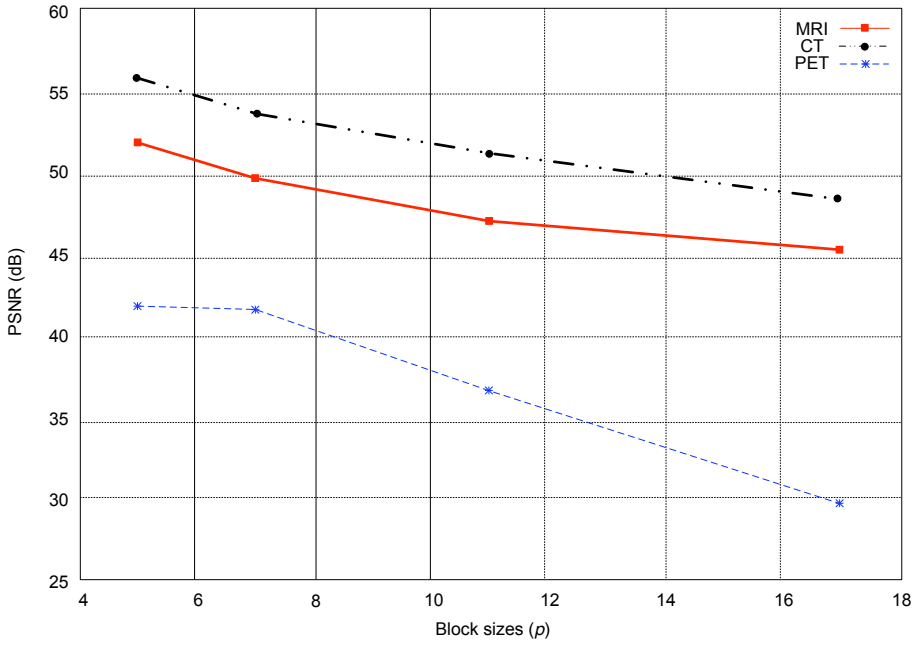

Fig. 2: Analysis of PSNR and different block sizes.

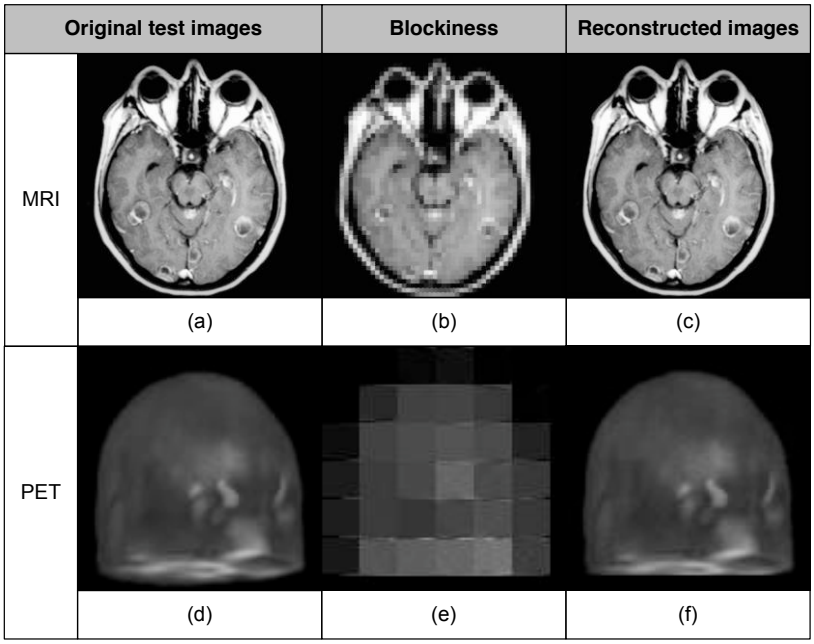

Fig. 3: Original and reconstructed images.

Table 1: Comparison of proposed architectures performance with existing architectures for the case of $p = 7$.

Type	Platform	References	Maximum frequency (MHz)	Throughput (MSPS)	Area (Slices)
Sequential	Virtex-II	[3]	100.13	9.87	159
		[4] – Arch. 1	112.87	11.13	198
		[4] – Arch. 2	67.30	6.64	131
		[6]	79.97	37.32	215
	Virtex-E	[5]	69.00	6.90	345
		[6]	94.46	45.01	245
	Virtex-5	Proposed - LR	174.30	0.12	669
		Proposed - LU	127.80	8.52	2,704
Pipelined	Virtex-5	Proposed - LR	161.40	13.31	2,044
		Proposed - LU	103.50	48.30	5,286
Area-efficient	Virtex-5	Proposed	188.90	6.30	637

Note: LR: Loops rolled, LU: Loops unrolled

SED Research Student Conference
Brunel University
21-23rd June 2010

Risk Analysis in Supplier Selection and Behaviour Model of supplier in supply chain linked to SCOR Model

Harris Makatsoris 1, Bilal Akbar Chuddher 2
1. Mechanical Engineering, School of Engineering and Design, Brunel University, Uxbridge, Middlesex, UK
2. Advanced Manufacturing and Enterprise Engineering (AMEE), Brunel University, Uxbridge, Middlesex, UK
Bilal.chuddher@brunell.ac.uk

Keywords (3): SCOR Model, supply chain, credit and behaviour modelling

Introduction:

The concept of supply chain management was introduced in 1960s; however it has been discussed in literature in 1970s and 80s due to Toyota's production approach. Now it is a very hot topic in research and literature. The supply chain literature/research can be divided into three groups: design of system, operations of supply chain and strategic planning for the entire process. Pittiglio Rabin Todd (PRTM) & McGrath and Advanced Manufacturing (AMR) have introduced a process reference model for supply chain management, which later was improved and called supply chain operational reference (SCOR) model by Supply Chain Council with involvement of more than 65 companies. SCOR is designed to integrate business re-engineering, benchmarking and process measurement into a cross functional framework to enable companies to examine, communicate, measure and compare supply chain practices to improve their supply chain process internally and externally[1], [2]. SCOR Model consists of five basic processes, which covers all aspects of supply chain from manufacturing to end-user of product: Plan, Source, Make, Deliver and Return. Planning process involves the execution and communication of plan for entire supply chain including business practices, logistics, demand and supply, resources assessment, production including entire supply chain to deliver the best performance. In sourcing phase scheduling, identification of resources and sources, inventory, capital assets, risk in supply etc are being taken in account [3, 4]. The literature shows that so much work has been done previously in planning phase of supply chain management, which includes location decision to operate, optimize effectively entire supply chain to gain the competitive advantages [6], [7]. Operational research area of supply chain management focuses on issues relating to daily operation like scheduling, production, and inventory etc [8], [9], [10]. However due to changed nature of manufacturing outsourcing has become very crucial for last decade as agile and customise manufacturing. There is a high need of more effective supplier selection and risk measuring tool intergraded with SCOR Model to make supply chain more sustainable and agile through SCOR model philosophy.

The following research paper will discuss the potential parameters for the supplier selection in supply chain from literature review and SCOR model (level2 which describe supplier selection) and needed risk analysis methodology can be implemented. In stage two a mathematical approach will be used to develop a model which predicts the risk associated with new supplier in partnership and behaviour modelling of supplier already in business partnership.

Methodology/Approach:

The paper content will be investigated through a literature review and a mathematical approach will be deployed for model development. The methodology adopted for this research paper will be aimed to develop a concept for risk prediction related to supplier and behaviour modelling of supplier in supply chain through a mathematical model. In stage one important parameters of supplier selection will be discussed from literature review. In stage two a mathematical methodology will be explained and possibly can be implemented to develop a model to predict risk and behaviour modelling of suppliers in market.

Conclusion:

The paper is aimed to introduce the concept of risk analysis and behaviour modelling of suppliers and possible mathematical tool which can be integrated with SCOR Model, possible outcomes can be summarized as:

- The concept will be a new idea of supplier scoring and behaviour modelling, which can be useful in assessing the risk involved with new supplier and old supplier already in partnership.
- This will also provide a concept to improve SCOR Model for agile and customise supply management chain.

References:

1. Huan, S.H., Sheoran, S.K.,Wang, G., 2004. A review and analysis of supply chain operations reference (SCOR) model. Supply Chain Management 9 (1), pp. 23–29.
2. Harelstad, C., Swartwood, D., Malin, J., 2004. The value of combining best practices. ASQ Six Sigma Forum Magazine August, 19–24.
3. Supply-Chain Council (SCC), 2006. Supply-chain operations reference model version 9.0 overview, /http://supply-chain.org.
4. Stephens, S., 2001. Supply chain operations reference model version 5.0: A new tool to improve supply chain efficiency and achieve best practice. Information Systems Frontiers 3 (4), 471–476.
5. Lockamy, A. McCormack, V. (2004); “Linking SCOR planning practices to supply chain performance An exploratory study” International Journal of Operations & Production Management Vol. 24 No. 12, 2004 pp. 1192-1218.
6. Cohen,M.A. and Lee, H.L. (1989), “ Resource Deployment Analysis of Global Manufacturing and Distribution Network”, journal of manufacturing and operation management, Vol.2, pp.81-104.
7. Towill, D.R.(1991), “Supply Chain Dynamic”, international journal of computer integrated manufacturing, Vol.4, issue 4, pp.197-208.
8. Lambert, D.M. and Cooper, M.C. (2000), “Issue in Supply Chain Management”, industrial marketing management, Vol29, pp65-83.

9. Li,L. and Lederer, P.J.(1997) “Pricing, Production, Scheduling and Delivery-Time Competition”, operation research, Vol.45, No.3, pp.407-420.
10. Zipkin, P.H. and Cachon, G.P. (1997), “Competitive and Cooperative Inventory Policies in a Two-Stage Supply Chain” Management Science, Vol.45, No. 7, PP. 936-953.

The Strategic Role of Human Resources Management: A Case of Health Care Management in Saudi Arabia

Faisal Basahl * , Susan Grant
Engineering Management, School of Engineering and Design
Brunel University, Uxbridge, UK

*Faisal.basahl@brunel.ac.uk

Introduction

Human Resources Management (HRM) is a department in any organisation that functions with the basic aim of enhancing the productivity of employees while helping individual employees achieve their career goals. According to Kabene (2006), HRM deals with people. From simply being involved in hiring and firing of employees to being a strategic partner in the organisation, HRM has undergone tremendous changes over the years, passing through many phases. It is in this respect that HRM plays an important role in the health care industry of Saudi Arabia, which has been undergoing a change in terms of planning and priorities in health care, with the private sector also playing an increasingly pivotal role. In such a scenario human resources are assets that an organisation can strategically use to gain competitive advantage over its competitors. This paper examines the significance of HRM in health care and the ways in which it can critically influence the effectiveness of health care systems. The study also investigates the ways in which most challenges faced by health care systems are HRM related.

Literature Review

Khatri, Wells, McKune, and Brewer (2006) point out the importance of the human factor in health care even though health care organisations have yet to manage it effectively. According to Khatri et al.(2006), healthcare organisations use only up to about 70% of

their human resource capacity. Health care is one of the services where practitioners have intimate contact with customers' lives and where customers react to such services in a special way (Hogan, Moxham, & Dwyer, 2007). In such cases human resources become a fundamental element of the service strategy, but existing literature does not focus on HRM-specific issues in strategic HRM, hindering the effective management of human resources.

Methodology

This research is primarily a qualitative explanatory study with the aim of providing in-depth analysis of the significance of HRM as a strategic partner in health care organisations. The research question will be addressed by questionnaires and observations of managers of health care service providers performing well, rather than by collecting only numerical data. At least two health care institutions in Saudi Arabia will be targeted for the study; one from the private sector and one a government agency. The two institutions will be chosen by purposive sampling, and organisations from both sectors will be chosen to avoid biasing of the findings towards either sector. Data collection methods will be questionnaires and semi-structured interviews of employees and human resource managers of the two health care organisations. The analytical tools will be a Likert 5-point scale of agreement and disagreement with statements, and a thematic analysis will also be done. SPSS (Statistical Package for the Social Sciences) will be used to analyse the results from the responses collected.

Results

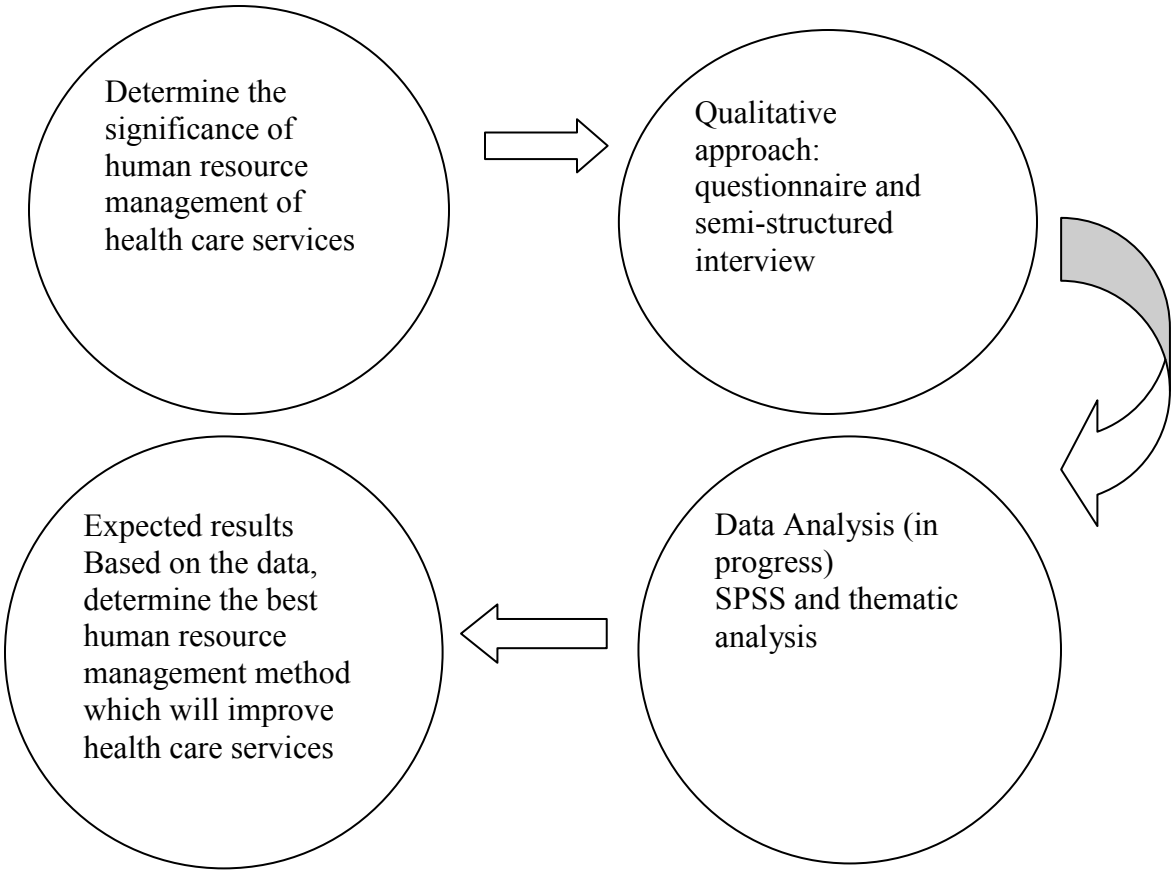

Conclusion

The findings will be discussed in relation to the research question, and recommendations will be made for the areas of HRM where required. It is anticipated that the findings of the study will influence the techniques used in strategic human resource management in the domain of health care management in Saudi Arabia.

References

Hogan, P., Moxham, L., & Dwyer, T. (2007). Human resource management strategies for the retention of nurses in acute care settings in hospitals in Australia. *Contemporary Nurse: A Journal for the Australian Nursing Profession, 24*(2), 189-199.

Kabene, S. M. (2006). Importance of human resources management in health care: A global context. *Human Resources for Health, 4*(20), 114-125.

Khatri, N., Wells, McKune, J., & Brewer, J. (2006). Strategic human resource management issues in hospitals: A study of a university and a community hospital. *Hospital Topics, 84*(4), 9-20.

Day Two
Proceedings

SED Research Student Conference
Brunel University
21-23rd June 2010

Analysis of Fluid-Structure Interaction (FSI) by Numerical Simulation for a cylinder-A literature review

Hossein Madani, Prof. Hamid Bahai, Dr. Jan Wissink
Mechanical Engineering, School of Engineering and Design, Brunel University,
Uxbridge, Middlesex, UK
Hossein.madani@Brunel.ac.uk

Keywords: Fluid-Structure interaction (FSI), Cylinder, Vortex-Induced vibration (VIV)

Introduction

In the past decades, significant effort [1,2,3] has been developed to improve understanding of the complicated Fluid–Structure Interaction (FSI) problem of Vortex-Induced Vibration (VIV) of long flexible cylindrical structures (e.g., risers, mooring lines, tendons, conductors). However, major challenges persist with regard to riser VIV modelling and response prediction [4].

In the presence of even moderate currents, risers can undergo significant VIV. In ultra-deepwater, the suspended lengths of these risers can be in excess of 5,000 meter [5], which constitutes challenges in both physical testing and also computer simulations for the sake of improving their design. Without an accurate method of measuring the forces exerted on them, risers have to be designed and built to very high margins of safety, which increases their cost and creates practical limitations on the depths at which they can be used.

The response of cylinders subjected to cross flow has been a major subject of research in fluid-structure interaction. Each time the cylinder sheds a vortex, a force is generated in both the in-flow and cross-flow direction. Vortex shedding causes an oscillatory multimode vibration of risers, which in turn, can cause fatigue or even collisions with other risers. Riser designs can be tested practically but scaling effects can limit the accuracy of the results. Down scaled models are typically limited to Reynolds numbers and short spans. What makes vortex induced vibration so challenging to predict in the case of risers is their very large length/diameter ratio, complex fluid-structure interaction with multiple vibrational modes, and, typically, the wide range of different cross currents along their spans [5].
In simulating riser VIV, it is necessary to model not only the fluid flow around the riser but also the motion of the riser in response to the flow. Fluid structure interaction (FSI) problems require the concurrent application of techniques from two separate fields: Computational Fluid Dynamics (CFD), and Computational Structural Dynamics (CSD). As the shape of the fluid domain changes during the calculation due to riser motion, solving the fluid flow in the deformed configuration requires the movement and recalculation of the computational mesh, or the CMD (Computational Mesh Dynamics) solution. The fluid flow solution provides the hydrodynamical loads to be used as boundary conditions for the CSD solver. Once a CFD calculation has been performed, at each time step, the computed velocities, pressures and temperatures are passed to the structural mechanics solver, where the deflection in the structure and the resulting stress are computed independently. The results from the CSD calculation are then fed back to the CMD to rebuild the mesh and then the CFD solver where the flow field is recalculated. This is the so-called two-way coupling approach which is needed when the computation of the flow field in the deformed domain is crucial (when the structural displacements are of the same order of magnitude as the smallest scale of interest in the fluid flow model). Many techniques can be used for this purpose as will be discussed in this paper.

Approach

The Fluid-Structure interaction for a cylinder has been studied extensively through experiment for a long time. Vast majority of research efforts in the past were focused on the study of flexibly mounted rigid bodies, with one degree of freedom (transverse motion) [1,2,3]. Recently, important differences in the dynamic response of flexible bodies arise due to the intrinsic nature of body, its capacity to vibrate at high mode numbers, the complex added mass and hydrodynamic damping distributions while in motion and in-line and transverse to the flow responses, added extra complexity to study FSI of a long flexible cylinder [6, 7, 8]. On the other hand, over the past decade work has been undertaken using a computational approach as well [10, 11, 12]. However, this technique does have limitations in that, it is difficult and so time consuming to simulate three dimensional flow with moving mesh and turbulence. This has not been popular so far, because of the complexity of the coupling with structural analysis and the large computational demands. In spite of these challenges, the great potential for improved design and better physical understanding means that research work in this field is attracting increased attention.

One approach is to cast both the fluid and structure solution frameworks monolithically using a finite element or finite volume formulation, Thereby solving the coupled problems directly. This approach requires purpose-designed software and the large nonlinear system demands higher computational resources both in terms of memory and processor speed. To overcome this difficulty, loose sequential coupling methods were proposed and widely adopted [13]. These normally use separate solvers for the fluid, the structure and the mesh. By maintaining the modularity of individual fields, this technique allows the use of existing software. However, loose sequential approaches sometimes suffer an asynchronization problem, which may cause numerical instability and give erroneous results. A third approach, block-iterative coupling, which still falls into the classification of sequential coupling but uses subiteration to synchronise the two fields, attempts to combine the benefits of the above two methods. It has been successfully applied to the coupling of simple fluid and solid mechanics solvers [14, 15]. Also the block iterative Gauss–Seidel method has been extended to study FSI with turbulence modelling, boundary layer treatments, and other features (field coupling and the field non-linearity)[16]. In addition to the question of coupling the fluid and the structural analyses, mesh movement is an important issue in FSI studies.

Moving mesh problems in computational fluid dynamics (CFD) have become of great interest due to their wide area of applications. Blood flow through the arteries of the human heart, aircraft wing flutter, free surface flows, parachute inflation, airbag explosion and several other kinds of flow–structure interaction problems can be classified in this category. In order to simulate the fluid dynamical problem with moving mesh and boundaries, several approaches have been proposed, such as the Arbitrary Lagrangian–Eulerian (ALE) scheme [17], the space–time approach [18,19], and the immersed boundary method [20-21].

The space–time approach is based on a finite-element formulation of the governing equations which is written over a sequence of space–time slabs. In this formulation, the finite-element interpolation polynomials are functions of both space and time.

In the immersed boundary method, a body in the flow field is considered as a kind of momentum forcing term in the Navier–Stokes equations rather than a real body. In this method, the choice of accurate interpolation schemes satisfying the no-slip condition on the immersed body is crucial because the mesh does not generally follow the immersed body boundary [22].

The ALE formulation is based on the description of the flow field on a moving frame of reference which is typically attached to the moving surface(s). In the ALE finite-volume method, the mesh follows the motion of the interface between the fluid and solid boundary. Hence, the mesh velocity appears in the convective flux term of the formulation. For the

stable and accurate simulation on moving meshes, the time integration scheme should be developed such that it preserves its stability and accuracy of its fixed mesh counterpart. Furthermore, the motion of the mesh should not deteriorate the stability, accuracy, and the preservation of uniform flow. Ahn and Kallinderis for the validity of the ALE formulation with moving mesh source term, drove the moving mesh source term from the original conservation laws, and address its significance in moving mesh simulations [22].
Also, for the coupling of the flow and structural solvers, two different strategies can be employed, namely strong and weak coupling, the strong coupling is based on the predictor–corrector method [22].
In addition, to calculate the FSI responses of slender models, the elastic analysis of the structure needs to be included. In structural engineering, modal analysis is the most popular approach for vibration studies. The modal approach has been carried over to investigate FSI problems when coupling the structural analysis with the Navier–Stokes solver. To do this, however, poses another difficulty for the mesh algorithm, due to the discrepancy in the degrees of freedom for the structure and the fluid. The structural response must be faithfully transformed into the motions of boundary conditions to satisfy the kinematic relation at the fluid–structure interface. One way is to use the features of elastic line-like elements to devise a mesh algorithm for a three-dimensional FSI study that links the structural motion to the mesh movement of the fluid domain [16].
Furthermore, the turbulence of the flow is critical in both experimental and numerical studies of vortex induced vibrations of oil risers. For that reason the selection of a CFD turbulence model plays a critical role in the simulation of riser VIV. The three most commonly used models are the Reynolds-Averaged Navier-Stokes (RANS), Large Eddy Simulation (LES), and Detached Eddy Simulation (DES) models. However there are some simulations without modelling turbulence in literature (DNS method) such as the work has been done by Dong and Karniadakis at Re=10000 for the flow past a stationary and oscillating cylinder [23].
Most conventional simulations are carried out with traditional RANS methods, which perform a time-average on the flow variables and extract the contribution that results from turbulence. The turbulence effects are then captured using techniques that employ one, two, or several additional equations. Two of the most popular RANS turbulence models are the k-epsilon and Reynolds stress models. Problems arise with RANS When the turbulent contribution is large and has the same order as the mean. Examples are unsteady flow in general, wake flows, or flows with large separated regions. For these types of flows, it is more appropriate to use LES, in which averaging is applied to only the smallest turbulent eddies, those that are smaller than a typical cell size. Larger eddies are computed directly (resolved) in this time-dependent model. In order to extend LES to high Reynolds number flows, new methods have recently been developed. The DES model uses LES in the core turbulent region and RANS in the wall-dominated region [5].

Results and discussion

There are numerous related parameters in the fluid-structure interaction subject which critically affect the behaviour of the flexible oil riser in deep water in the oceans. On the other hand, there are complicated theories and methods to simulate these parameters and physical phenomena. Also some disagreements persist in VIV problems. For example, controversy regarding added mass [2]. Further ideas have been developed, which the use of an effective elasticity concept will reduce the number of parameters to define in VIV. We may expect new more fundamental contributions to emerge, and further universal or generic characteristics to be discovered which carry across from one VIV system to another, specially for higher Reynolds numbers [2].

Conclusion

Although in the past decades excellent work has been done in cross flow around a long flexible cylinder both experimentally and numerically, there is still inadequate full-scale data for FSI to verify all conditions of interest. For instance, study of the VIV behaviour (for high length/diameter cylinder) at large Re with different turbulent modelling and different FSI modelling. Interestingly, the most important limitation for this subject will be the computational power.

References

1. C.H.K. Williamson, R. Govardhan, Vortex-Induced Vibrations, Annu. Rev. Fluid Mech. 2004. 36:413-55.
2. C.H.K. Williamson, R. Govardhan, A brief review of recent results in vortex- induced vibrations, Journal of wind engineering and industrial aerodynamics 96 (2008) 713-735.
3. T. Sarpkaya, A critical review of the intrinsic nature of vortex-induced vibrations, journal of fluids and structures 19 (2004) 389-447.
4. H. Mukundan, F. Chasparis, F.S. Hover, M.S. Triantafllou, Optimal lift force coefficient databases from riser experiments, journal of fluids and structures 26 (2010) 160-175.
5. D. Scnowalter, R. Menon, D. Allen, Computer simulation shows potential challenge of modelling Deepwater risers. Article for *Hart's E&P*, April 2007.
6. M. Brankovic, P.W. Bearman, Measurments of transverse forces on circular cylinders undergoing vortex-induced vibration, journal of fluids and structurs 22 (2006) 829-836.
7. G.R. Franzini, A.L.C. Fujarra, J.R. Meneghini, I. Korkischko, R. Franciss, Experimental investigation of vortex-induced vibration on rigid, smooth and inclined cylinders, journal of fluids and structures 25 (2009) 742-750.
8. F.J. Huera-Huarte, P.W. Bearman, Wake structure and Vortex-Induced vibrations of long flexible cylinder-part1:Daynamic response, Journal of fluids and structures 25 (2009) 969-990.
9. F.J. Huera-Huarte, P.W. Bearman, Wake structure and Vortex-Induced vibrations of long flexible cylinder-part1:Drag coefficients and vortex modes, Journal of fluids and structures 25 (2009) 991-1006.
10. Z.Y. Pan, W.C. Cui, Q.M. Miao, Numerical simulation of vortex-induced vibration of a circular cylinder at low mass-damping using RANS code, Journal of fluid and structures 23 (2007) 23-37.
11. M.R.H. Nobari, H. Naderan, A numerical study of flow past a cylinder with cross flow and inline oscillation. Journal of computers and fluids 35 (2006) 394-415.
12. R.H.J. Willden, J.M.R. Graham, Numerical prediction of VIV on long flexible circular cylinders, Journal of fluids and structures (2001) 15 659-669.
13. Farhat, C., Lesoinne, M., Maman, N., 1995. Mixed explicit/implicit time integration of coupled aeroelastic problems: three-field formulation, geometric conservation and distributed solution. Int.J.Numer.Meth.Fluids 21, 807–835.
14. Matthies, H.G., 2002. Partitioned but strongly coupled iteration schemes for non-linear fluid–structure interaction. Comput.Struct. 80, 1991–1999.
15. Codina, R., Cervera, M., 1996. Block-iterative Algorithms for Nonlinear Coupled Problems. CIMNE, Barcelona.
16. D. Sun, J.S. Owen, N.G. Wright, K.F. Liaw, Fluid–structure interaction of prismatic line-like structures, using LES and block-iterative coupling, Journal of Wind Engineering and Industrial Aerodynamics 96 (2008) 840–858.
17. C. Hirt, A. Amsden, J.L. Cook, An arbitrary Lagrangian–Eulerian computing method for all flow speeds, Journal of Computational Physics 14 (1974) 227–253.
18. T. Tezduyar, M. Behr, J. Liou, A new strategy for finite element computations involving moving boundaries and interfaces – The deforming-spatial-domain/space–time procedure: I. The concept and the preliminary numerical tests, Computer Methods in Applied Mechanics and Engineering 94 (1992) 339–351.
19. T. Tezduyar, M. Behr, S. Mittal, J. Liou, A new strategy for finite element computations involving moving boundaries and interfaces –The deforming-spatial-domain/space–time procedure: II. Computation of free-surface flows, two-liquid flows, and flows with drifting cylinders, Computer Methods in Applied Mechanics and Engineering 94 (1992) 353–371.
20. C. Peskin, Numerical analysis of blood flow in the heart, Journal of Computational Physics 25 (1977) 220–252.
21. L.T. Zhang, A. Gerstenberger, X. Wang, W.K. Liu, Immersed finite element method, Computer Methods in Applied Mechanics and Engineering 193 (2004) 2051–2067.
22. H.T. Ahn, Y. Kallinderis, Strongly coupled flow/structure interactions with a geometrically conservative ALE scheme on general hybrid meshes, Journal of Computational Physics 219 (2006) 671–696.
23. S.Dong, G.E. Karniadakis, DNS of flow past a stationary and oscillating cylinder at Re=10000, Journal of fluids and structures 20 (2005) 519-531.

SED Research Student Conference
Brunel University
21-23rd June 2010

Investigation of the dislocation of hemp fibres by FTIR

Dasong Dai and Mizi Fan
Civil Engineering Department, School of Engineering and Design, Brunel University, Kingston Lane, Uxbridge, Middlesex, UB8 3PH, UK
Corresponding author: e-mail address: mizi.fan@brunel.ac.uk

Keywords: Hemp fibre; FTIR spectra; Hydrogen bonds

Introduction

Fourier transform infrared spectroscopy (FTIR) has been considered one of the best tools to study the change of native cellulose super molecular structure [1]. This paper employs this technology (FTIR) to study the dislocations in hemp fibres aiming at a better understanding of the fracture behavior, structure and bonding systems within dislocation regions of the hemp fibres.

Methodology/Approach

Test procedures are outlined in Figure 1 and the details of main tests are given as follows:
A. Optical microscopy examination (OM)
B. FE-SEM characterization
C. Tensile test
D. FTIR analysis
E. XRD analysis

Results and discussion

1 Morphologies of dislocation

The results from FE-SEM shows that overall the surface of dislocations of hemp fibres looks more amorphous than that of hemp fibres without dislocations. This may be due to the loss of hemicelluloses or lignin. It is also evident that the fibrils distort in the dislocation regions, which could affect the stiffness and stress of fibres with the stiffness and stress decreasing with the increase of dislocation angle.

2 Crystallinity index of dislocation

In this study, the ratios of absorption band A_{1423}/A_{896} and A_{1368}/A_{662} are 55.76% and 49.30% respectively. The value calculated by using Segal empirical method is 56.03%, indicating that the ratio of absorption band A_{1423}/A_{896} is more suitable for CI evaluation. The CI (IR) in dislocation regions is only 45.25%, which is lower than that of normal region of hemp fibres. This means that there exists a higher content of crystalline regions in the hemp without dislocation than in dislocation regions. According to two-phase model theory [2].

3 Hydrogen bonds of cellulose in dislocations

The deconvoluted four bands of the OH stretching region gave rise to a clear indication of changes in the valence vibration of Hydrogen bonded OH groups. The weaker inter- and intra-molecular hydrogen bonding in the dislocations could be the main cause that induced the decrease of tensile strength in the hemp fibres, especially the intramolecular hydrogen bond of O(3)H---O(5).

4 Hemicelluloses and lignin in dislocations

The disappearance of bands of 1368 cm^{-1} and 1362 cm^{-1} may be due probably to the removal of the hemicelluloses in dislocation regions. The deconvoluted FTIR spectra from 1330 cm^{-1} to 1220 cm^{-1} showed the S ring stretching, CH2 rocking at C6 in cellulose, G ring stretching and COH bending at C6 in cellulose, indicating a significant reduction of lignin content in the dislocation regions. The ratio of G (Guaiacyl, 1261 cm^{-1})/S (syringyl, 1323cm^{-1}) was 0.61 for the hemp without dislocations comparing to 1.15 for the dislocation regions, indicating higher cellulose content in the dislocation regions.

Conclusion

1) The developed morphologies of the dislocations showed that the surface of hemp fibres within the dislocation regions were more amorphous than those without dislocations. The fibrils within the dislocations regions were distorted.

2) Both XRD and FTIR were able to examine the crystallinity index of the dislocations. The CI examined by FTIR was 55.79% for the hemp without dislocations and 45.25% for those within dislocation regions, showing a significant reduction in the crystallinity due to the dislocations. The CI produced by XRD was 56.03%.

3) The deconvoluted four bands of the OH stretching region gave rise to a clear indication of changes in the valence vibration of Hydrogen bonded OH groups. The weaker inter- and intra-molecular hydrogen bonding in the dislocations could be the main cause that induced the decrease of tensile strength in the hemp fibres, especially the intramolecular hydrogen bond of O(3)H---O(5).

4) The FTIR spectra from 1370 cm^{-1} to 1330 cm^{-1} illustrated that the band at 1368 cm^{-1} and 1362 cm^{-1} disappeared in dislocation regions, indicating the removal of the hemicelluloses in dislocations and hence possible loss of lignin. The deconvoluted FTIR spectra from 1330 cm^{-1} to 1220 cm^{-1} showed a significant reduction of lignin content in the dislocation regions..

References

[1] http://en.wikipedia.org/wiki/Fourier_transform_spectroscopy

[2] Hearle, JWS. A fringed fibril theory of structure in crystalline polymers. J. Polym.Sci.1958; 28(117):432-435.

SED Research Student Conference
Brunel University
21-23rd June 2010

How Users Differ in Using Instruction Manuals?

Abdusselam Selami Cifter[1], Hua Dong[2]
1. HCDI, School of Engineering and Design, Brunel University, Uxbridge, Middlesex, UK
2. HCDI, School of Engineering and Design, Brunel University, Uxbridge, Middlesex, UK
a.cifter@brunel.ac.uk

Keywords: Instruction Manuals, Users, User Characteristics

Introduction

When we are faced with new products there are two main information sources to understand the usage; the first one is the product itself and the second one is instruction manuals. Design of the instruction manual and design of the product itself are equally important; both of them can prevent the user from making mistakes or can lead them to misuse. However it is not always possible to predict all the usage problems through the design process, due to the complexity of user characteristics. According to Smith [1], "too often, consumers act in a way that is inconsistent with what the manufacturer intended." For example some people may not prefer to use instruction manuals and might try to understand the usage through their own understanding [1].

According to Horen et al [2][3], many people end up with complaining about the manuals when they first time try to use an electronics device. They also argue that instruction manuals are inaccessible and difficult to use for many user groups particularly for older people due to their impaired capabilities [2][3]. Knowing the people who are likely to use the instruction manual is crucial to produce them easy to understand and usable. Therefore designers should be aware of the diversity of the users [4]. This paper investigates the differences between three user groups (i.e. younger people, older people and people with cognitive disabilities) regarding their approach to understanding of instruction manuals.

Methodology/Approach

The study involved three groups of people:

- 10 able-bodied young people (Aged between 18-64)
- 10 healthy older people (65+)
- 10 people with cognitive disabilities (Aged between 18-64)

The study was conducted as product interaction trials which involved the completion of given tasks by the volunteer participants through interacting with two selected digital devices and their instruction manuals. The products used in the user observation study are a digital camera (Sony DSC-S730) and a digital automatic blood pressure monitor (Omron R7). Observation was used as a primary method for capturing user data [5].

The study involves three parts. In the first part the participants were invited to fill in a general questionnaire before they started the trial. This questionnaire asked about their age range, gender, education level and contact details. In the second part a task list was given to them and they were asked to complete the tasks by using the devices provided along with their instruction manuals. There were seven tasks in total (refer to Table 1); the first three related to the Blood Pressure Monitor (BPM); and the rest related to the digital camera. The session was video recorded to capture the participants' behaviour and emotional reactions during the tasks.

Table 1: The task list

Blood Pressure Monitor (BPM)	
Task 1:	**Prepare the device to be used.**
Task 2:	**Measure your blood pressure and write down the score.**
Task 3:	**Switch off the device as if it will not be used for a long time.**
Digital Camera	
Task 4:	**Prepare the device to be used.**
Hidden Task:	*This task was designed only for younger participants. The memory stick used for the study was left full hence the participants were expected to create space in the memory stick by erasing the pictures or formatting the card to be able to continue the following tasks. The purpose of this task was to enable the observation of the response of the participants when they encounter an unexpected situation.*
Task 5:	**Take your own picture reflected in the mirror provided. Please try to take at least one good picture.**
Task 6:	**Take a picture of the toy car. Please try to take at least one good picture.**
Task 7:	**Erase the unwanted pictures and switch off the device.**

As a last part another questionnaire was given to them to capture the thoughts of their experience during the study. The participants were also encouraged to give any verbal feedback about their experience.

Results and Discussion

Figure 1 shows the number of participants who used the instruction manuals for each task and from each of the user groups.

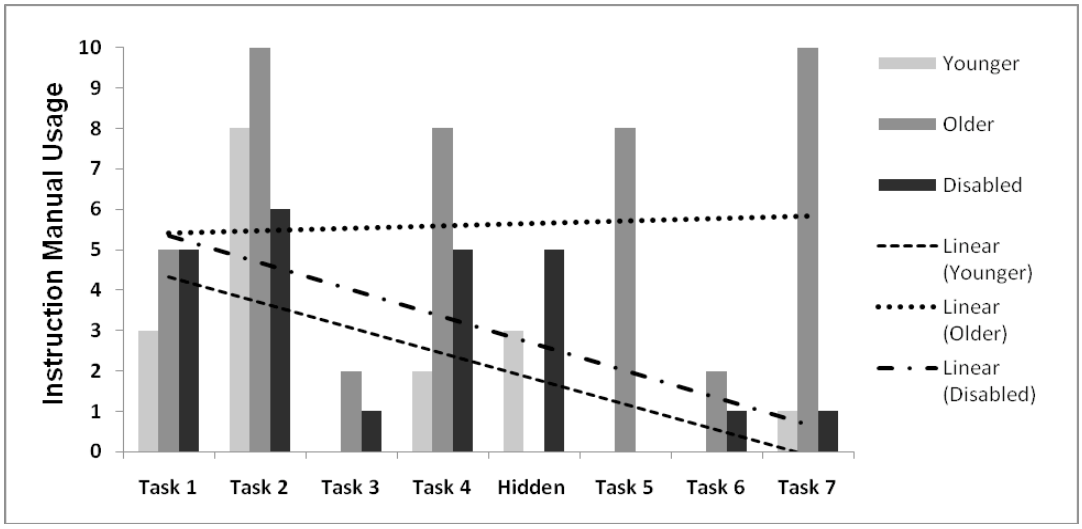

Figure 1: Number of people referred to the instruction manuals during the tasks

The younger participants performed better than the other user groups. The majority of the younger participants used their previous experience as their primary information source, and they referred to the instruction manuals when it was deemed necessary to do so. As a result they were more successful and confident in using the digital camera when compared with the BPM.

As suggested by the literature, older people encountered more problems in using the instructions due to their impaired capabilities [2] [3]. As can be seen from Figure 1, older participants used the instruction manuals more than all the other user groups. Particularly during Task 2 and Task 7, all of the older participants preferred to use the instructions. However due to their lack of motivation, they had a tendency to give up and as a result blame themselves on failing to complete the tasks. They experienced difficulty in reading the instruction manuals due to the small font size and frequently complained about it.

Regarding the disabled participants, their reading skills, comprehension, impatience and attention issues did prove to hinder them in their understanding of what was described within the manuals, which, in turn unmotivated them to use the instruction manuals. As a result half of the disabled participants did not use the instruction manuals for most of the tasks although they could not complete them. Most of the disabled participants who used instruction manuals experienced reading difficulties, and reading comprehension deficiency was prominent, this was consistent with the research done by Gardill and Jitendra [6].

Some of the explanations caused confusion for all user groups. Even though they read the explanations several times, some of the users from all user groups could not manage certain actions explained within the manuals. This was more prevalent with the older participants. Wording was another problem, sometimes participants experienced difficulty in understanding the explanations due to the terminology used.

Conclusion

Instruction manuals are critical for the product usage. Preparing good instruction manuals is important, since poorly designed ones can mislead the users. In addition it is up to users to

decide whether or not to use the instruction manuals, hence the design of the instruction manual should be appealing to the users.

All the different user groups presented different characteristics regarding their approach to using instruction manuals. Younger participants were found to be the most successful user group in using the instruction manuals. Therefore it is critical to understand the diversity of the users before preparing an instruction manual.

The effects of the prior experience were generally positive for all of the users, however during the BPM tasks some of the younger participants misused the device because they did not refer to the instructions due to their prior experience with similar products.

The design of the instruction manuals for the two products was found to be more appropriate for the younger user group. Some of the older participants and disabled participants experienced various difficulties regarding their understanding of the visual and text based explanations which resulted in their failure. Some of the older users were excluded by the design of the instruction manuals due to the small font size.

References

[1] Smith T. P.: Manufacturer's Guide to Developing Consumer Product Instructions. US Consumer Product Safety Commission (2003).

[2] Horen F. M., Jansen C., Meas A., Noordman L.G. M.: Manuals for the Elderly: Which Information Cannot Be Missed. Journal of Technical Writing and Communication, Vol. 31, pp 415—431 (2001)

[3] Horen F., Jansen C., Noordman L., Maes A.: Manuals for the Elderly: Text Characteristics That Help or Hinder Older Users. In: 2005 IEEE International Professional Communication Conference Proceedings, International, pp. 334—342, 10-13 July (2005)

[4] The Department of Trade and Industry: Instructions for Consumer Products: Guidelines for Better Instructions and Safety Information for Consumer Products. Her Majesty's Stationery Office, London (1989)

[5] Robson C.: Real World Research: A Resource for Social Scientists and Practitioner-Researchers. Blackwell Publishing (2002)

[6] Gardill M. C., Jitendra A. K.: Advanced Story Map Instruction: Effects on the Reading Comprehension of Students with Learning Disabilities. The Journal of Special Education, Vol. 33, pp. 2—17 (1999)

SED Research Student Conference
Brunel University
21-23rd June 2010

On Demand Electrochemical Production of Hydrogen for Mobile Applications

S. K. Raza, J. Silver, P. Kathirgamanathan, R. Withnal
Wolfson Centre for Material Processing, Brunel University, Uxbridge, Middlesex, UK
SyedKhurram.Raza@brunel.ac.uk

Keywords (3): Hydrogen generation, Electrolysis, electrolyser

Introduction

Global warming and the energy crisis are two of the greatest challenges that face mankind. This has forced governments and other organisations to think how to protect the environment and how to reduce fuel costs. A variety of new and exciting technologies are being investigated to address the problem.

Solar powered devices, although they solve the problem of carbon emissions, are not suitable in every environment and unable to fulfil the whole of the energy requirement; the same is true of wind and tidal power. Attractive and promising solutions include hybrid systems, for example liquefied petroleum gas cars, and electric vehicles based on fuel cells.

Current research is moving towards the hydrogen economy and hydrogen based energy systems. Hydrogen can be produced in many ways, most commonly by steam reforming of hydrocarbons (70% to 85% thermal efficiency based on the high heating value but the downside is that it releases carbon dioxide (CO_2)) [1], compared with commercial PEM electrolysers where performance has been reported to be 56 -73%[1] at normal temperature pressure with zero carbon emissions. Electrochemical production of hydrogen has several advantages:

- It produces pure hydrogen.
- Allows portability for example solar energy can be used to power the electrochemical cell.
- Hydrogen can be produced on demand.

Electrolysis of $1m^3$ of water can be the source of 108.7 kg of hydrogen which is equivalent of to 422 litre of gasoline [2]. This work will explain the approach towards electrochemical hydrogen generation by electrolysis.

Methodology/Approach

Electrochemical production of hydrogen is usually performed in alkaline conditions (33% potassium hydroxide (KOH) or sodium hydroxide[1]) by using either solid electrodes (efficiency 50% – 60%[1]) or porous electrodes (efficiency 55% – 70% [1]) where expensive proton exchange membranes are employed.

The aim of the hydrogen generation project is fourfold:

1. To improve the efficiency of production of hydrogen by enhanced hydrodynamics and novel cell design.
2. To identify low cost membranes for the separation of H_2 and O_2.
3. To improve the efficiency of the electrochemical production of hydrogen by means of nanostructured electrodes.
4. To understand the mechanism of catalytic activity of nanostructured electrode.

Results and Discussion

In this study, an electrochemical cell for hydrogen generation was designed (Figure1). The design is based on careful consideration of hydrodynamics (using continuous flow cell), bubble discharge and low cost system design. Cell performance was tested at different current densities using different low cost microporous membranes (8 in all) in 30% KOH.

An efficiency of up to 94% has been observed for total (mixed) gas generation. As opposed to an efficiency of 88% which was achieved when the membrane was employed.

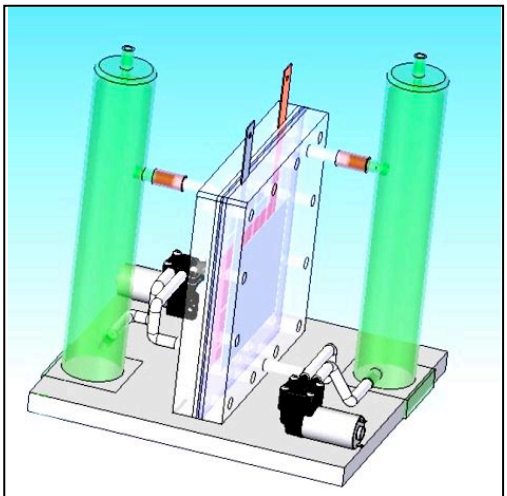

Figure 1: Electrochemical Hydrogen Generator design

Table 1: Micro porous membrane

Membrane	Thickness (um)	Ion Exchange Capacity (mmol/g)	Porous	Strength	Residue	Description
1001	180	0.5	Fully Blocked	Fragile	Yes	Not suitable
1007	171	0.68	Porous	Strong	less	Gas mixing on high pressure
1008	140	0.5	Fibber structure	strong	no	Gas mixing on high pressure
1009	125	0.69	Woven Fibber	strong	no	Gas mixing on high pressure
1010	32.51	1.11	very	very strong	no	suitable for high pressure and chemical

Membrane 1001 was found not suitable for the purpose. From the images shown in figure 2, it is clear that there are few problems. The general problem is one of fragility, the second, as observed in figure 2A and B is that residue is clearly presented in B. Thirdly expansion of the membrane is evident comparison of studies (C) and (D), before and after KOH processing respectively.

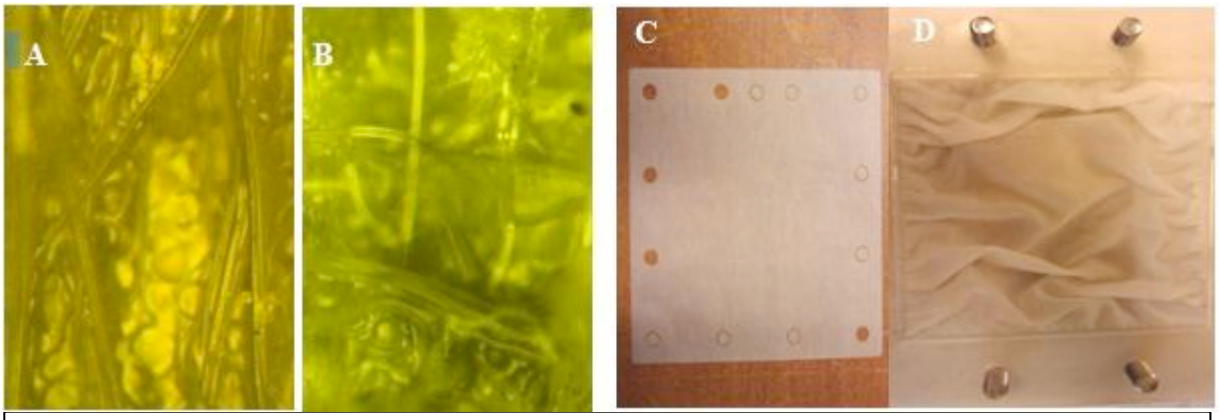

Figure 2: Optical microscope images of membrane 1001, (A) before process and (B) after processed in 30% KOH. (C) and (D) are digital camera images before and after KOH process respectively.

The physical structure of membranes 1007 to 1010 (Table 1) has good strength properties; overall the best result was achieved with membrane 1010, that has a high degree of strength capability for ion exchange, suitable reliability, it does not appear to contaminate the electrolyte by releasing residue and most importantly provides pure hydrogen. Therefore 1010 is the membrane of choice for the next phases of our program.

From the consideration of the results in figure 3 when the pump is on the hydrogen yield is significantly better. This shows that the increases in fluid pressure/flow is probably adding evolution and enhancing the efficiency of the cell. The increase in hydrogen production was potentially noticeable for membrane 1010 and increases of over 6% were verified.

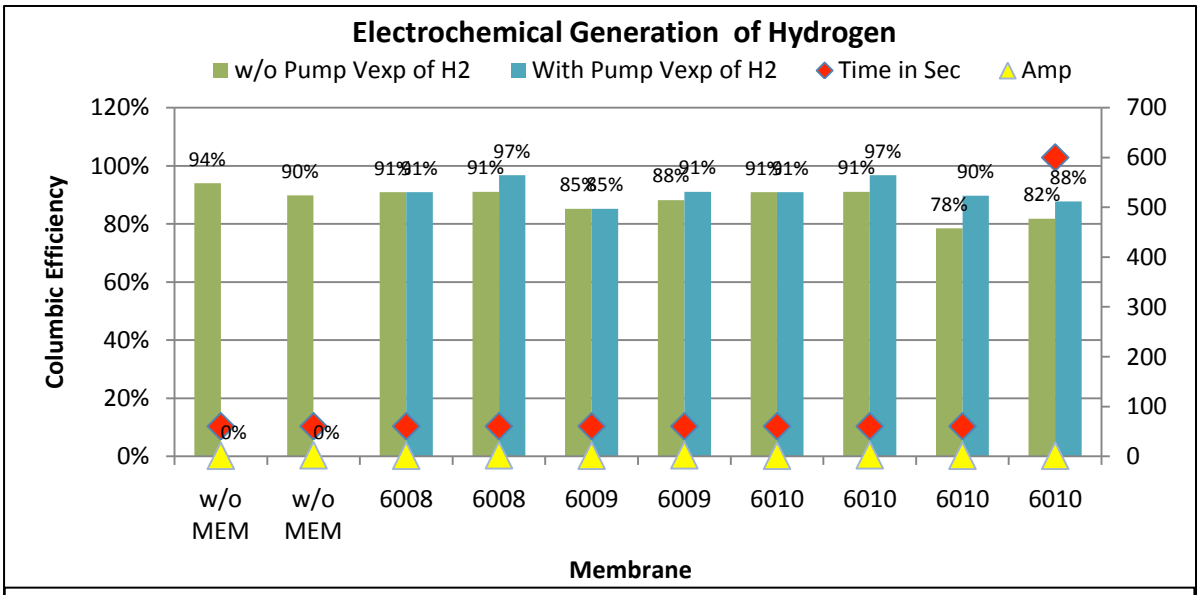

Figure 3: Graph of columbic efficiency compression on with and without membrane, with and without continues turbulence.

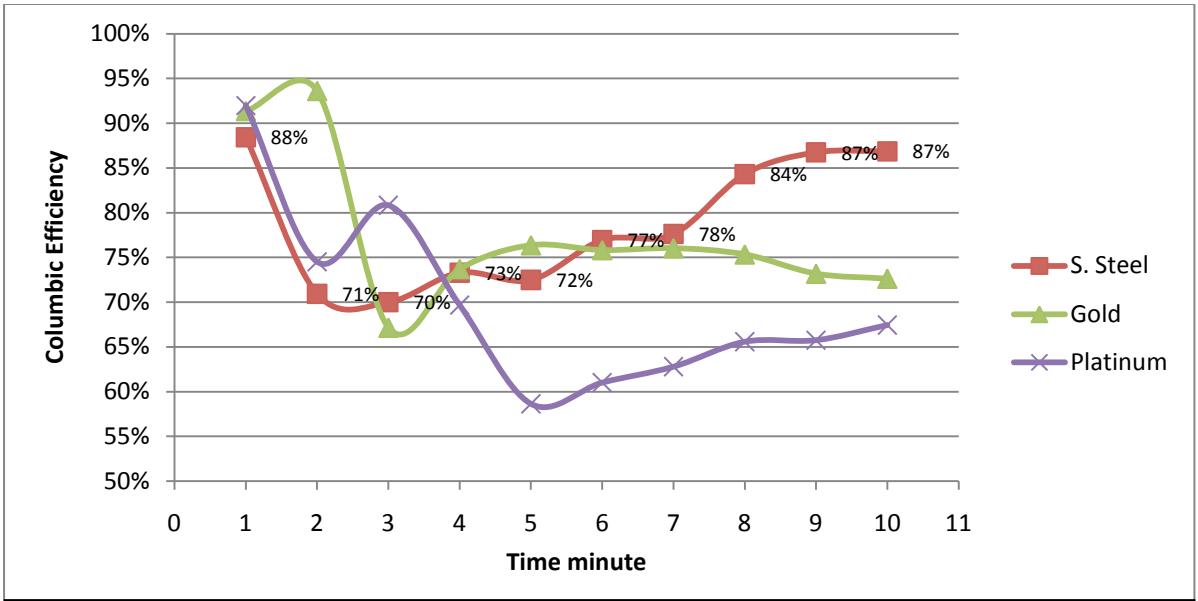

Figure 4: 70nm Sputter coated electrode Columbic efficiency compression.

To establish the optimum electrode structure, the different cathodes were tested. The first was stainless steel, the second was stainless steel sputter coated with 70nm of gold. The third was stainless steel sputter coated with 70nm of platinum. Each electrode was monitored for 10 minutes under identical conditions. The first four minutes of each run can be ignored as in this time ionic diffusion layers are forming near the electrode surface. The succeeding minutes shows that these layers then perform with time as seen in figure 4. From the results presented in figure 4 it appears that there is no noticeable advantage in using the sputter coated samples, as plain stainless steel gains the best result.

Future work will be aimed at optimising the electrode materials and electrode structure on the micrometre and nanometre scale.

Conclusion

There are many ways to produce hydrogen, but water electrolysis is one of the best methods to produce hydrogen without carbon emission. Some breakthrough results were obtained using low cost membranes. This work suggests that there is a great potential for future research in multi stack hydrogen production cell for the production of clean hydrogen for on demand application.

References

[1] J.D. Holladay, J. Hu, D.L. King, Y. Wang. An overview of hydrogen production technologies. Catalysis today 139 244-260 (2009).
[2] Umar K. Mirza et al. A vision for Hydrogen economy in Pakistan. Renewable and Sustainable Energy Reviews 13 1111-1115 (2009),.
[3] Shepard, Jr et al. Electrolytic hydrogen storage and generation. U.S. Patent no .4,737,249, 12 April 1996.
[4] Klein. Electrolytic hydrogen storage and generation. U.S. Patent no.5,540,831, 30 July 1996.

SED Research Student Conference
Brunel University
21-23rd June 2010

SchoolAir: Air Quality in Primary Schools and Children's Health
(a pilot study)

Yulia Anopa[1,2], Anna Koulkova[1,2,3], Benjamin J. Jones[2], Ariana Zeka[1].
1. Institute for the Environment, Brunel University, Uxbridge, UB8 3PH, UK
2. Experimental Techniques Centre, Brunel University, Uxbridge, UB8 3PH, UK
3. Institutet för miljömedicin (IMM), Karolinska Institutet, Stockholm, Sweden
yulia.anopa@brunel.ac.uk

Keywords: air quality, children's health, exposure measurements

Introduction

Burden of evidence suggests that indoor air quality is a major contributing factor to observed increases in respiratory symptoms among young children. Particulate matter (PM) [1,3], nitrogen dioxide (NO_2) [1,2,3,4,5,6], sulphur dioxide (SO_2) [1,6], carbon dioxide (CO_2) [2,4], ozone (O_3) [4,6], total volatile organic compounds (TVOCs) [2] and formaldehyde [4,6] have all been identified as having the potential to affect health.

The SchoolAir study is aiming to assess the hypothesis that poor indoor and outdoor air quality in schools is associated with increased prevalence of asthma, respiratory and allergic symptoms among primary school children, and assess the feasibility of a bigger full-scale research project in the future. The study is unique in the way that it is looking simultaneously at many air components and parameters (5 gaseous components: CO, CO_2, NO_2, TVOC and formaldehyde; particles, temperature, and humidity), as well as assessing personal exposure and respiratory health effects in children.

Methodology

Study design: Four primary schools were selected for the pilot study conducted within the academic year 2009-2010. The four schools are of diverse size and socioeconomic backgrounds: two suburban (referred to as S1 and S2), one urban (referred to as U) from North–West of Greater London; and one rural school from South–East England (referred to as R). All children of school Year 3 (ages 7 to 8) where offered participation in the study in urban and suburban schools, whereas participation was offered to all pupils in the rural school (ages 5 to 11), due to its small size. The study has been ethically approved by Brunel University.

Air quality monitoring: The first round of measurements in schools took place in September-November 2009. All in all four rounds of exposure measurements were planned to be carried out throughout 2009-2010 school year in order to capture seasonal variability of indoor and outdoor levels of air pollutants in these schools. Each round involves a five day school week's monitoring in four arbitrary chosen representative locations: three indoors and one outdoor.

Particulate matter concentration levels are measured with particle counters (Aerocet 531; Met One Instruments, Inc., USA) for the length of a school day (7-8 hours). The counters are used for two particle size ranges: particles with aerodynamic diameter of more than 0.5μm and more than 5.0μm. We calculated the difference for PM >0.5μm and PM >5.0μm to estimate particle count for PM size range 0.5–5.0μm and used this in the analyses.

Continuous measurements of the following gaseous pollutants: carbon dioxide (CO_2), nitrogen dioxide (NO_2), carbon monoxide (CO), formaldehyde and total volatile organic compounds (TVOCs), as well as temperature and relative humidity of the air are monitored

with wireless automatic concentration monitor (PPMonitor Wireless unit; PPM Technology, UK).
In addition, monitoring and recording children's activity during the day is performed to see how occupancy of a particular room affects measured parameters such as concentration of PM and various gases and also to create a representative exposure pattern for each child according to time spent in different environments.

Health and background questionnaire survey: The questionnaire used for the pilot study was based on the questionnaire designed by the International Study of Asthma and Allergies in Childhood (ISAAC) [7,8,9], that was slightly modified to this study needs. The questionnaire included questions on child's name, gender and ethnicity, questions on respiratory symptoms, such as wheezing, cough and asthma (ever and in the last 12 months), questions on rhinitis and irritation (ever and in the last 12 months), and finally there was a general questionnaire part, with questions on other illnesses of a child and medication taken, on asthma and allergies in the immediate family, on home area, on cooking and heating sources at home, and on socio-economic status of the family.

Preliminary results and discussion

In this abstract we will represent the results of the first round of the study (conducted in September-November, 2009). Whereas exposure monitoring was conducted in four primary schools, in one of them (S2) the respiratory health questionnaire response rate was not high enough to include that school into health outcomes. Response rates in the remaining three schools (S1, U and R) were between 50 and 60%.

Question	School		
	S1	U	R
Wheezing or whistling in the chest ever	26.4%	18.2%	15.5%
Wheezing or whistling in the chest in the last 12 months	9.3%	6.8%	10.3%
Asthma ever	18.5%	14.0%	10.3%
Medication for wheezing or asthma used in the last 12 months	17.0%	7.1%	6.9%
Wheeze in the chest during or after exercise in the last 12 months	9.4%	4.8%	1.8%
Dry cough at night in the last 12 months (apart from a cough associated with a cold or chest infection)	24.5%	9.8%	10.3%
Sneezing, or a runny, or a blocked nose ever (not associated with cold or flu)	33.3%	27.9%	19.0%
Sneezing, or a runny, or a blocked nose in the last 12 months (not associated with cold or flu)	31.5%	25.6%	19.0%
Itchy, watery eyes in the last 12 months	20.4%	20.9%	14.0%
Hayfever ever	26.9%	31.7%	22.8%

Table 1. Prevalence of selected allergic and respiratory symptoms by school (S1 = suburban; R = rural; U = urban school)

Prevalence of respiratory symptoms varied between the schools (Table 1) and was overall higher in school S1 compared with the two other schools. One explanation of the observed higher prevalence may be report bias. However, schools S1 and R have similar parental socioeconomic background, including educational background, hence expected to respond similarly. Other explanations are the contribution of other factors to this difference, including environmental. The analysis of performed measurements shows that there is variability in air quality both during the day and during the week. Furthermore, a significant variation between schools has also been observed (Table 2). For example the levels of CO_2 were significantly higher in S3 compared to other schools, which could be a sign of insufficient ventilation. Table 2 shows weekly means of different pollutant concentrations by location within each school. Overall, pollutant levels indoors and outdoors were generally higher in schools S1 and S2.
There is contribution of outdoor levels of pollutants to indoor concentrations, and this contribution is larger for the schools with greater ventilation rate (data not shown).

Figure 1. Concentrations of particles of aerodynamic diameter 0.5µm–5.0µm coincident with Year 3 child location over a period of one school day.

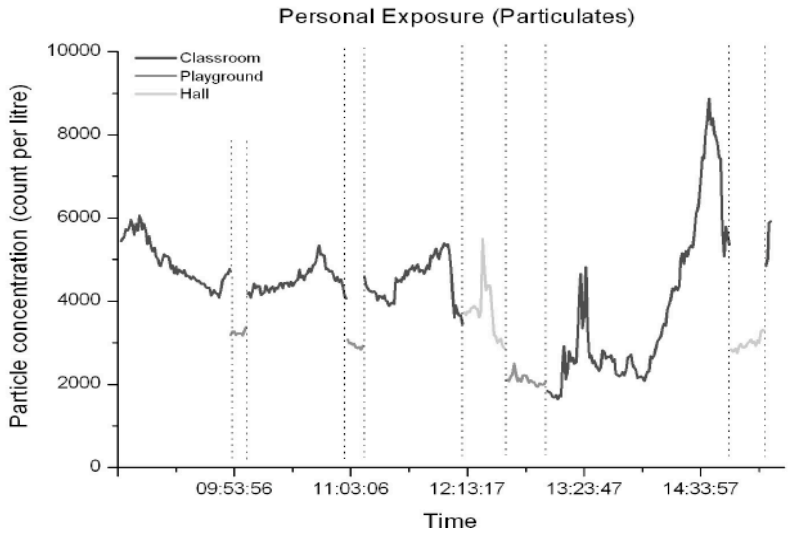

	School			
Exposure	S1	U	R	S2
	PM(0.5-5.0); particles / L			
Classroom 1	6372 (2298)	5264 (2221)	5556 (2594)	6717 (2408)
Classroom 2	-	5182 (1830)	-	8373 (3226)
Hall	6070.14 (2600.04)	5763.36 (2345.2)	-	10207 (5899)
Corridor	-	-	4797 (2134)	-
Outdoors	15098 (16319) †	6969 (6467)	4386 (2575)	12368 (13796) ¤
	CO2; ppm			
Classroom 1	1824 (846)	993 (262)	1450 (694)	3416 (941)
Classroom 2	2085 (960)	869 (249)	-	3089 (1118)
Hall	-	725 (186)	918 (313)	955 (381)
Corridor	1397 (566) ¤	-	775 (217)	-
Outdoors	442 (162)	407 (22)	395 (23)	450 (42)
	CO; ppm			
Classroom 1	0.9 (0.55)	0.46 (0.09)	1.03 (1.1)	0.74 (0.25)
Classroom 2	0.99 (0.57)	0.29 (0.15)	-	0.65 (0.21)
Hall	-	0.38 (0.075)	0.43 (0.19)	0.55 (0.23)
Corridor	0.53 (0,16) ¤	-	0.58 (0.61)	-
Outdoors	0.4 (0.1)	0.43 (0.062)	0.39 (0.05)	0.47 (0.28)
	NO2; ppm			
Classroom 1	0.051 (0.007)	0.056 (0.005)	0.05 (0.006)	0.048 (0.005)
Classroom 2	0.043 (0.005)	0.051 (0.006)	-	0.043 (0.005)
Hall	-	0.052 (0.006)	0.046 (0.004)	0.049 (0.007)
Corridor	0.049 (0.006) ¤	-	0.044 (0.005)	-
Outdoors	0.067 (0.006)	0.067 (0.007)	0.057 (0.005)	0.071 (0.008)
	TVOC; ppm			
Classroom 1	0.11 (0.11)	0.0044 (0.007)	0.11 (0.14)	0.23 (0.1)
Classroom 2	0.058 (0.03)	0.011 (0.01)	-	0.26 (0.1)
Hall	-	0.006 (0.02)	0.087 (0.02)	0.034 (0.04)
Corridor	0.4 (0.55) ¤	-	0.035 (0.03)	-
	Formaldehyde; ppm			
Classroom 1	0.0012 (0.0005)	0.0011 (0.0003)	0.0012 (0.0005)	0.0013 (0.0007)
Classroom 2	0.0021 (0.0031)	0.0019 (0.003)	-	0.0019 (0.002)
Hall	-	0.0015 (0.00084)	0.0011 (0.0007)	0.0023 (0.001)
Corridor	0.002 (0.002) ¤	-	0.0016 (0.002)	-
Outdoors	0.0014 (0.001)	0.0018 (0.001)	0.0015 (0.001)	0.0016 (0.001)

Table 2. Numbers in cells are 5-day means (standard deviation) for occupied part of the day (8:45 to 15:30);S1, S2 = suburban schools; R = rural school; U = urban school;† Data for day 2 are missing; ¤ Readings for days 2-5 only (data for day 1 are missing); - No measurements

The measured variability in pollutant concentrations by location (classroom, hall, outdoor) supports the proposed method of this study of using several point locations for exposure measurements (indoors and outdoors) to represent personal exposure of children during the course of a school day.

Figure 1 shows the daily pattern of exposure of a Year 3 child (in school R) based on the daily activity of the class in school by location. Particle concentrations in this example vary by time of the day and the length of time a child spends in each location.

Conclusion

The results from the first round of measurements suggest that there is significant air quality variability between locations in each school and between different schools. This demonstrates the need to develop an assessment of an individual's personal exposure to air quality in the immediate environment. Moreover, results show that outdoor levels of pollutants contribute to indoor pollutant concentrations.

Health survey results showed that respiratory symptoms occurrence was higher in one of the schools where the levels of pollutants were overall higher (in different locations indoors and

outdoors of school environments). Thus these findings may suggest that there is a relationship between air quality in schools and pupils respiratory health.

The SchoolAir study demonstrated that important variability of indoor air pollution occurs in school environments. This study is an improvement over existing methodologies in indoor air pollution studies and air pollution personal exposure assessment. However, only four locations measured are not fully representative of each child's exposure pattern during a school day. Also, such confounding factors as residential exposure (home- and area-based) are not controlled for in the preliminary analysis. Further work is yet to be done.
The success of this pilot study will provide useful methodology and evidence for future studies as well as create the foundation for a large scale study intended by the same investigators.

References

[1] Liu, L., R. Poon, L. Chen, A. M. Frescura, P. Montuschi, *et al.* (2009). "Acute effects of air pollution on pulmonary function, airway inflammation, and oxidative stress in asthmatic children." Environ Health Perspect 117(4): 668-74.

[2] Khalequzzaman, M., M. Kamijima, K. Sakai, N. A. Chowdhury, N. Hamajima, *et al.* (2007). "Indoor air pollution and its impact on children under five years old in Bangladesh." Indoor Air 17(4): 297-304.

[3] Belanger, K., J. F. Gent, E. W. Triche, M. B. Bracken and B. P. Leaderer (2006). "Association of indoor nitrogen dioxide exposure with respiratory symptoms in children with asthma." Am J Respir Crit Care Med 173(3): 297-303

[4] Mi, Y. H., D. Norback, J. Tao, Y. L. Mi and M. Ferm (2006). "Current asthma and respiratory symptoms among pupils in Shanghai, China: influence of building ventilation, nitrogen dioxide, ozone, and formaldehyde in classrooms." Indoor Air 16(6): 454-64.

[5] Pilotto, L. S., M. Nitschke, B. J. Smith, D. Pisaniello, R. E. Ruffin, *et al.* (2004). "Randomized controlled trial of unflued gas heater replacement on respiratory health of asthmatic schoolchildren." Int J Epidemiol 33(1): 208-14.

[6] Zhao, Z., Z. Zhang, Z. Wang, M. Ferm, Y. Liang, *et al.* (2008). "Asthmatic symptoms among pupils in relation to winter indoor and outdoor air pollution in schools in Taiyuan, China." Environ Health Perspect 116(1): 90-7. 1.

[7] "Worldwide variation in prevalence of symptoms of asthma, allergic rhinoconjunctivitis, and atopic eczema: ISAAC." The International Study of Asthma and Allergies in Childhood (ISAAC) Steering Committee. Lancet, 1998. 351(9111): p. 1225-32.

[8] Austin, J.B., et al., "Hay fever, eczema, and wheeze: a nationwide UK study (ISAAC, international study of asthma and allergies in childhood)". Arch Dis Child, 1999. 81(3): p. 225-30.

[9] Pearce, N., et al., "Worldwide trends in the prevalence of asthma symptoms: phase III of the International Study of Asthma and Allergies in Childhood (ISAAC)". Thorax, 2007. 62(9): p. 758-66.

SED Research Student Conference
Brunel University
21-23rd June 2010

Design and Implementation of Roof-top Wind Turbine Monitoring System

Sivanantharasa Panchadcharam, Gareth A. Taylor and Qiang Ni
School of Engineering and Design, Brunel University, Uxbridge, UB8 3PH, UK
s.panchadcharam@brunel.ac.uk

Key words: Renewable Energy Sources, Wind Turbine, Monitoring and Control

Introduction

Integrating renewable energy sources (RES) is now a research topic of national and global interest. Low carbon emission projects are encouraged and funded by governments worldwide and the European Union (EU) supports a large number of renewable energy-related research projects. Both environmental and cost implications have to be communicated to the public to effectively support and encourage them in utilizing small scale embedded generation (SSEG) units such as Wind Turbines (WTs). In the future scalable data analysis and communication systems will play a vital role and smart metering deployment in UK will be essential to such systems in the near future [3]. In recent years the Low Carbon Buildings Programme (LCBP) by Energy Saving Trust has provided grants for the installation of micro-generation technologies [4]. The Brunel University roof-top WT installation investigates the potential benefits of deployment of WTs around UK and cost effective monitoring of these WT data using the novel ICT solutions. Brunel Institute of Power System (BIPS) is already using a data monitoring and control system for a photovoltaic installation in Brunel University and similar technology will be investigated for the WT installation with some changes to the devices being used.

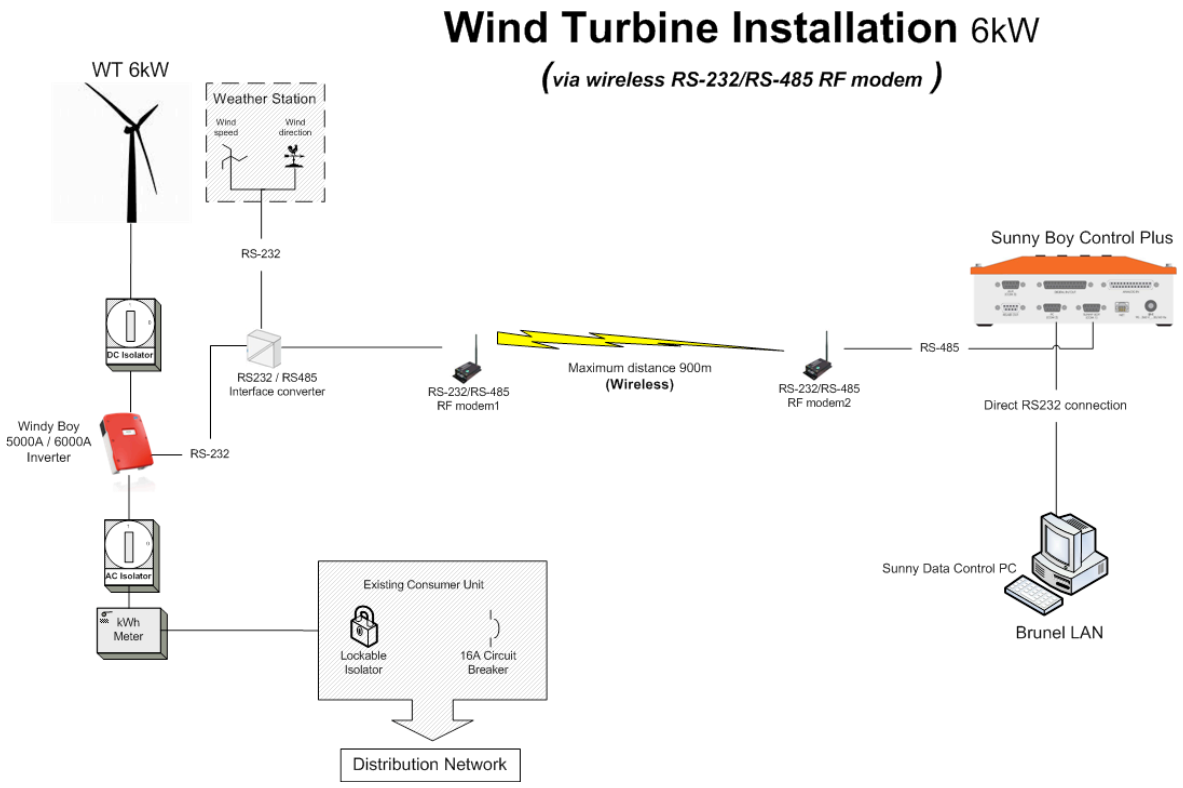

Figure 1: Schematic for WT Installation in Brunel University

Methodology

Figure 1 shows the schematic diagram for the WT installation which will take place in spring 2010. The SMA data logger and the wireless RF modem technology will be used to monitor and control the WT data including wind direction and speed measures from the weather station. The daily report generated by this monitoring tool will be used to evaluate the daily and monthly statistical energy production and carbon reduction information by the WT. These statistical data will be displayed in real time so that performance of the WT is readily available for monitoring.

Discussion

The existing Sunny Boy Control Plus (SBC+) data logger will be replaced by the Sunny WebBox which will monitor the WT and PV installations at the same time along with the two weather stations. As the UK government is interested in providing funds for WT installation for home-owners, there is a potentially high demand in the market and the environmental benefit attracts many people. Figure 2 & Figure 3 show the comparison of payback and avoided cost when the WT 6kW is considered as a case study [2].

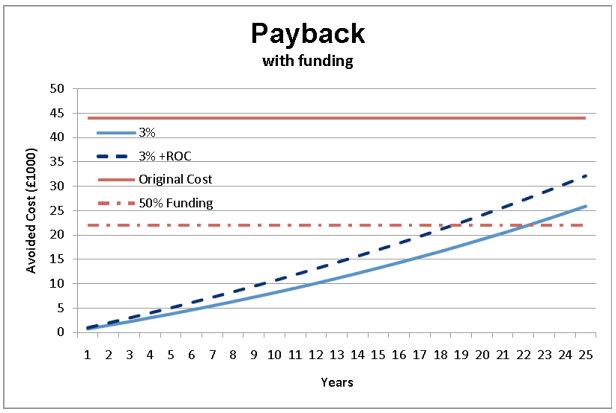

Figure 3: Revised Payback comparison [2]

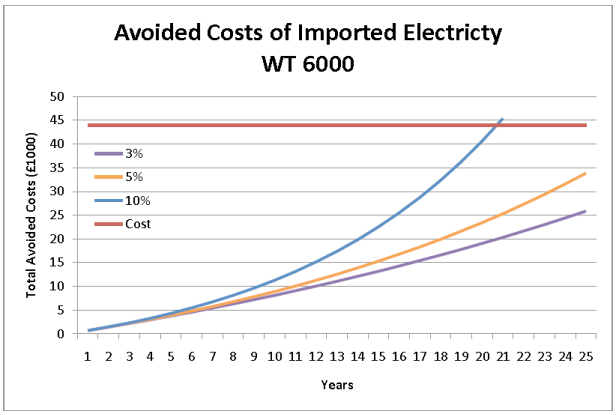

Figure 2: WT 6kW Avoided Cost Comparison [2]

Conclusion

The above case study proves that the expected payback can be achieved within the life time of the plant and could also achieve some savings. In order to achieve these results effectively, monitoring of the WT will play a crucial part. Wireless technology for transferring the WT data to the monitoring location has been considered, as shown in Figure 1, which provides enhanced flexibility in deciding the location of the monitoring equipments. Setting up a dedicated laboratory facility for the PV and WT installations will add value to the existing ICT in monitoring and control of the SSEG units.

References:

[1] S.Chowdhury, P.Day and G.A Taylor, "Supervisory Data Acquisition and Performance Analysis of a PV Array Installation with Data Logger", IEEE PES General Meeting, Pittsburgh, USA, August 2007

[2] P. Day, "Wide-Area monitoring of small-scale embedded generation", Final Year Project, Electronic & Electrical Engineering, Brunel University, Mar. 2009

[3] Fotis Konstantinos Paterakis, "Monitoring and Control of Small-scale Embedded Generation", MSc Thesis, Sustainable Electrical Power, Brunel University, Sep. 2008

[4] LCBP: http://www.lowcarbonbuildings.org.uk/ (Last accessed: March 2010).

SED Research Student Conference
Brunel University
21-23rd June 2010

Economic Benefits of Sustainable Design Standards in Industry

Alexander V. C. Plant, David J. Harrison, Brian J. Griffiths and Busayawan Lam
School of Engineering and Design, Brunel University, Uxbridge, Middlesex, UK
Alexander.Plant@brunel.ac.uk

Keywords: Sustainable, Profit, Production

Introduction

Conventional industry is reliant on the linier processes of extraction, production, consumption and disposal. These deplete natural resources, use energy and cause pollution. The aim of this study is to evaluate the business implications of applying sustainable design strategies. By designing for disassembly, product service life can be extended through repair and maintenance. This design approach also facilitates efficient remanufacture, refurbishment, and recycling. These retain embodied value and energy within post consumer products. Disassembly prior to recycling can permit some materials to be processed with negligible degradation. Such material may be suitable for use in exacting applications and reduce the demand for virgin material. Design requirements for products as part of a closed loop manufacturing system were formalised by British Standards Institution (BSI) in BS 8887-1 (2006), entitled 'Design for Manufacture, Assembly, Disassembly and End-of-Life Processes' [1].

For the purposes of this conference paper, the scope has been limited to establishing the business case for sustainable design whilst at the same time understanding the practical challenges faced by responsible manufacturers. This is the first time that opinions and case studies relating to the standard have been gathered from industry.

Method

The research approach was qualitative using methods from the social sciences. After receiving clearance from the school's Ethics Committee, companies that had purchased BS 8887-1 were contacted and interviews arranged. The necessary details were acquired through collaboration with BSI. Recordings of meetings or notes were transcribed. Documentation was forwarded to participants, mainly Design, Production and Quality Engineers, for editing and approval. Transcripts and notes were processed with NVivo qualitative data analysis software. By coding the text at nodes within the software, related data was clustered such that it was possible to view everything that had been said about any given topic by all participants [2]. The quotations within this work are taken from the interviews.

Results and discussion

The design for manufacture approach to reducing production costs and improving quality is well established but has been updated within BS 8887-1. "Design should aim to minimise material usage as this is good for the environment, and if less material is used there is less cost in the product... A design saving of 2% in the use of material in a component will give a bigger impact than the manufacturer can by reviewing their processes... The design has an impact." Minimising the component count, standardising colours and types of material and increasing commonality between products, further reduced costs. "We have to do it; it is part of being successful. If we didn't, we would produce more waste and increase costs... The

automotive industry is good at reducing costs throughout the supply chain. The environmental gains are a by-product." Often requirements of the standard were confirmed as existing procedure and best practice especially with regard to the design process, documentation, manufacture and assembly.

Design for assembly is usually a benefit in disassembly and maintenance. "To take something apart, it's got to be easy to put together. So, the easier it is to put a product together, the quicker it can be manufactured, which means more profit for us... Our machines are more industrial, so they are designed for maintenance and built to be overhauled, serviced and repaired. At end of life they should be easy to take to bits." This type of design was helpful for another company in efficiently fulfilling service contracts.

One manufacturer went as far as planning for user maintenance, thus avoiding warranty callouts for minor work, this was especially important when selling internationally. "There are competitive advantages to making things more sustainable!" Product maintainability and serviceability were also instrumental in winning business. "The availability of spares that can be replaced and the cost of those parts have an influence on the decision." Disassembly of returned end-of-life product also reduced the cost of Waste Electrical Electronic Equipment, by leaving only a small amount. It was therefore not necessary to pay for the disposal of complete units. Aluminium and stainless steel were then sold.

In addition to the traditional considerations of material properties and cost, recyclability is increasingly a selection criterion. "All the materials we use could be recycled but only in terms of re-use within the engineering system." In other instances performance requirements took priority, as with certain prestige cars featuring exotic composites and bonded assemblies of multiple materials. "This makes crash repair for these vehicles difficult and expensive... end-of-life processing is very difficult... They have been designed with performance in mind and not end-of-life." Tradeoffs were also made for electrical equipment where ingress protection necessitated the use of potting compound or over-moulding.

A commercial kitchen equipment manufacturer used ease of disassembly, recyclability and residual value as a selling point, and to motivate customers to take responsibility at end-of-life. Electrical panels were removable rather than integrated, leaving only high value stainless steel. "The standard talks about the principles that are insisted upon by customers. The customers want things designed such that they can be serviced and will have a residual value." For an industrial refrigeration company, large customers were able to negotiate the price of the product they were buying with regard to end-of-life cost. "The customer will calculate the cost of disposal at the end-of-life and they are passing that back." BS 8887-1 and lifecycle planning supported the manufacturer in these negotiations.

Conclusion

The applications of the principles within BS 8887-1 have significant financial and environmental advantages. "One of our drivers isn't so much the environmental side, although that's a great benefit, what we believe is that there is a great, great cost benefit for being environmentally friendly."

References

[1] BS 8887-1:2006, Design for Manufacture, Assembly, Disassembly and End-of-Life Processing (MADE) - Part 1: General Concepts, Process and Requirements.
[2] Bazeley, P. 2007, "Qualitative Data Analysis with NVivo", SAGE Publications Ltd, London.

SED Research Student Conference
Brunel University
21-23rd June 2010

Product Design for Low Carbon Refurbishments

Mark Dowson[1], Prof. David Harrison[1], Dr. Salmaan Craig[2]
1. School of Engineering and Design, Brunel University, Uxbridge, Middlesex, UK
2. Buro Happold Ltd, 17 Newman Street, London, W1T 1PD, UK
mark.dowson@burohappold.com

Keywords: Aerogel, Insulation, Refurbishments

Introduction

The aim of this research is to develop a new cost effective retrofit product to reduce the environmental impact of buildings. The product must provide a measurable benefit across its entire lifecycle. Key objectives are a proof of concept prototype with a streamlined lifecycle assessment (LCA) by the midway viva, and a fully functional prototype with a detailed LCA by the final viva. It is anticipated that contributions will arise from the design development, in-situ testing and theoretical analysis of each prototype. A further contribution is anticipated to arise from the LCA comparing the energy used to manufacture the prototypes against its operational savings.

Methodology / Approach

A review of conventional retrofit measures has identified scope to improve the thermal efficiency of homes with single glazing and solid walls. In 2006, over 7 million homes in the UK had solid walls and 8.1 million homes still had single glazed windows [1]. New double glazing is not cost effective, with estimated payback lasting up to 98 years. Solid wall insulation is disruptive, limited by spatial requirements and has paybacks lasting up to 22 years [2].

There is scope to develop new retrofit solutions using translucent insulation materials. These materials perform a similar function to opaque insulation, yet they have the ability to transmit useful solar energy. Currently, there are few examples of translucent insulation in use due to a lack of design guidance and the perception that capital costs will be too high. Countering this, recent research has calculated that paybacks for these materials could be as low as 3-4 years [3].

An experiment was conducted to measure the thermal and optical performance of a single glazed window retrofitted with a 10mm polycarbonate panel filled with granules of high performance ‘aerogel’ insulation. Aerogel is an emerging translucent insulation material with a nanoporous silica structure containing 95% air. The high porosity of aerogel means it retains up to 4 times as much heat as conventional insulation, whilst being transparent to solar radiation [4].

Results and Discussion

In-situ testing revealed the prototype reduced 80% of heat loss through single glazing without detrimental reductions in light transmission. This performance is comparable to high performance double glazing and even some triple glazing units. Based on the one-off cost of the prototype, the theoretical payback could be as low as 3.6 years.

Two concepts arising from this study are translucent aerogel 'shutters' and an aerogel 'trombe wall'. Shutters could insulate windows on cold days without blocking out useful natural light. A trombe wall is a type of solar-heated wall consisting of a cavity between a concrete wall and a south facing translucent element, heated up by incoming solar radiation. This generates free heat that can be vented into the building, or left to permeate and warm up the internal wall. A fully functional variation of the aerogel trombe wall will be built and monitored for the second phase of research.

From a range of translucent insulation, aerogel is the best performing, yet the extent of its environmental impact is unclear. To date, there have been no peer-reviewed LCA of aerogel. A literature review found that some methods to produce the material consume a lot of energy, CO_2 and solvents, which may be harmful to the environment [5]. As a result, arrangements have been made to produce samples of aerogel and log the inputs and outputs to each process. This will enable an LCA to be compiled and assessed.

Conclusion

This research forms part of a systematic approach to improving UK homes, while considering the impacts of manufacture vs. operational savings - a balance that is typically ignored. Aerogel is a unique material, with potential for many fascinating applications in new insulation products. Innovative materials such as this should not be overlooked in the effort to improve the UK's vast stock of hard to treat homes.

References

[1] CLG, 2006. Summary Statistics - Insulation and Homes, Communities and Local Government, Accessed [15/04/2010], Available online at: www.communities.gov.uk/documents/housing/xls/summarystats2006.xls

[2] Shorrock L, Henderson J and Utley J, 2005. Reducing Carbon Emissions from the UK Housing stock, Watford, Watford, BRE Press

[3] Wong L, Eames P and Perera R, 2007. A Review of Transparent Insulation Systems and the Evaluation of Payback Period for Building Applications, Journal of Solar Energy, Volume 81, pp. 1058-1071

[4] Yokogawa h, 2005. Handbook of Sol-Gel Science & Technology, Volume 2, Chapter 13 Thermal Conductivity of Silica Aerogels, Sumio Sakka (editor), Kluwer Academic Publishers, New York, USA

[5] Soleimani-Dorcheh A and Abbasi MH, 2008. Silica Aerogel - Synthesis, Properties and Characterization, Journal of Materials Processing Technology, Volume 199, pp 10-26

SED Research Student Conference
Brunel University
21-23rd June 2010

DIBR Algorithm for 3D Video Services

Abubakar Umar[1], Abdul Sadka[2]

Electronic & Computer Engineering, Brunel University, Uxbridge, Middlesex, UK

Abubakar. Sadiq.Umar@brunel.ac.uk

Keywords (3): Depth Image Based Rendering (DIBR), Video-plus-depth format, mobile UMTS

Introduction

With recent advances in the multimedia processing fields, 3-dimentional TV (3DTV) is expected to become one of the most dominant markets in the next generation broadcasting system [1][2]. The basic concept of 3D video is to provide user with interactivity, 3D depth perception and immersion. User interactivity means that when users are able to move and perform interaction in 3D space. Some researchers reconstruct a complete 3D from 2D images and render them from the desired viewpoint. This consists of estimating the 3D depth information and integrating this depth information to generate a complete 3D of a given scene. The difficulties of generating complete 3D of a scene have caused these approaches to be used in limited applications.

Recently, the European Information Society Technologies (IST) project "Advanced Three-Dimensional Television System Technologies (ATTEST 3DTV)"[3] has proposed depth-image based rendering (DIBR) technique, in which one or more 'virtual' views of a real-world scene can be generated rapidly at the receiver. DIBR is expected to be the most efficient way to solve the above problems of the end-to-end stereoscopic chain as described in details in [4][5]. Based on this direction of 3DTV service developments, we propose the DIBR technique for the evaluation of 3D video services over 3G (UMTS) networks. We intend to solve some problems of DIBR, such as depth pre-processing and transmission of 3D video services using DIBR over error –prone UMTS networks [5].

Methodology/Approach

MPEG-C Part 3 [6] defines a video plus depth representation of the stereo video content. Depth is generated at the sender side for instance by estimation from an original left and right views. One view is transmitted simultaneously with the depth signal. At the receiver the other view is synthesized by depth image based rendering (DIBR) algorithm. Compared to video, a depth signal can in most cases be coded at a fraction of the bitrates at sufficient quality for view synthesis. Nonetheless errors in depth estimation and problems with disocclusions introduce artefacts in the rendered view.

In Centre for Media Communication Research (CMCR), we used two cameras simultaneously with adjustable but known geometry, for the calculation of distance between the two cameras and the distance between the cameras and the object. After capturing, the

two tapes are digitised and converted to the right format (AVI) using the MediaCorder Codec, and video frames from both cameras are compared and the offset between the frames after digitisation/conversion can be used to capture depth for both close and distant objects, hence 3D video based on 2d-video-plus depth is realised.

Figure 1 shows the block diagram of the proposed scalable Multiple Description Coding for stereoscopic 3D video employing DIBR algorithm. The depth data, which will be combined with the texture data using a depth image base rendering technique to produce left and right views, is placed in enhancement layer. This type of stereoscopic video coding configuration has better coding efficiency compared to left and right coding and interlaced coding. H.264/SVC in both encoder A and B produces scalable layers that can be exploited for MDC. The odds and even frames are separated before the encoding process starts for both texture and depth. The even frames for the texture are coded in the base layer (Layer 0) while the odd frames for the texture are coded in the enhancement layer (Layer 1). The even frames for the depth are coded in the enhancement layer (Layer 2) and the odd frames for the depth are coded in the enhancement layer (Layer 3). With the interlayer prediction switched off, it can be assumed that layer 1 is also the base layer for the scalable MDC.

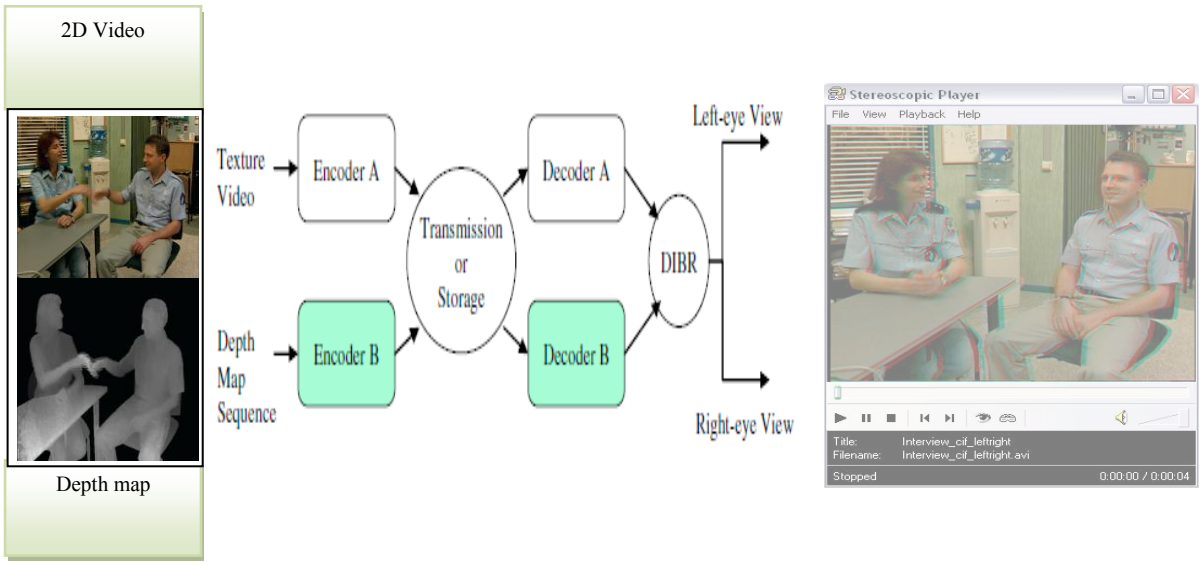

Figure 1: Block diagram of the proposed 3D video coding architecture (Source [9])

Results and discussion

Two sequences were selected for the simulations. The video frames with frame numbers 3 for Interview and Orbi each consisting of the reference sequence and the corresponding depth map are used for our test. 'Interview' and 'Orbi' sequences were acquired from Heinrich-Hertz- Institute (HHI) [7]. The two frames are each 300 frames long and captured at 30fps. The frame size for both videos is 176x144 pixels, which is also known as Quarter Common Intermediate Format (QCIF). The QCIF format is used because it is a typical format for streaming video over mobile networks [8][9][10].

Figure 2: two test sequences and their depth maps (Source [1] and [2])

In the simulation the loss of one packet is assumed to mean the loss of one video frame. The results are presented on the R-D curves where the resulting Bit Rate (Kbps) was plotted against PSNR.

The main achievement in this work is the performance evaluation with depth pre-processing and without depth pre-processing for both video sequences as in figure 3 and 4 under error free condition. In the future, the UMTS simulator which has four packet loss error patterns, namely 3%, 5% 10% and 20% will be use to simulate the loss pattern in high error conditions.

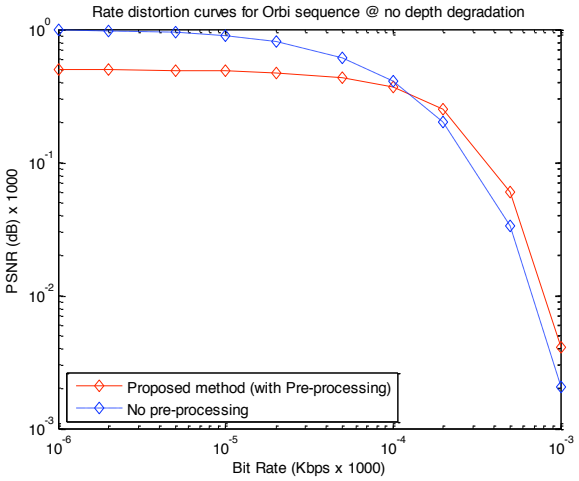

Figure 3: R-D curves for orbi sequence under error-free channel condition

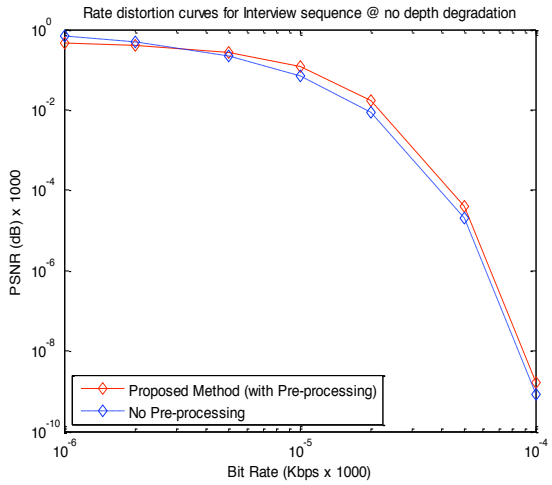

Figure 4: R-D curves for interview sequence under error-free channel condition

Conclusion

This paper presented a method of 2D video-plus-depth transmission by means of DIBR techniques. The main advantage of the proposed method (with depth pre-processing) compared to no depth pre-processing is that it provides high quality 3D video with smaller bandwidth requirement for transmission.

In the future work, we aim at developing a new model for the R-D performances based on subjective quality assessment metrics to evaluate user experiences and perception in 3D video.

References

[1] H. Karim, a. Sali, S. Worrall, A. Sadka, and a. Kondoz, "Multiple description video coding for stereoscopic 3D," *IEEE Transactions on Consumer Electronics*, vol. 55, 2009, pp. 2048-2056.

[2] P. Kauff and O.Schreer, "An immersive 3D video conferencing system using shared virtual team user environments ", *Proceedings of the 4th international conference on Collaborative virtual environments – VCE '02*, 2002, pp. 105-112.

[3] A. Redert, M. de Beeck, C. Fehn, W. Ijsselsteijn, M. Pollefeys, L. Van Gool, E. Ofek, I. Sexton, and P. Surman, "Advanced three-dimensional television system technologies," *Proceedings. First International Symposium on 3D Data Processing Visualization and Transmission*, 2002, pp. 313-319.

[4] P. Kauff, N. Atzpadin, C. Fehn, M. Muller, O. Schreer, a. Smolic, and R. Tanger, "Depth map creation and image-based rendering for advanced 3DTV services providing interoperability and scalability," *Signal Processing: Image Communication*, vol. 22, 2007, pp. 217-234.

[5] W. Chen, Y. Chang, S. Lin, L. Ding, and L. Chen, "Efficient depth image based rendering with edge dependent depth filter and," *interpolation, in: Proceedings of International Conference on Multimedia and Expo*, 2005, pp. 1314-1317.

[6] P.K. C, Fehn, K. Schuur, I. Feldmann, "International Organisation for standardisation, coding of moving picture," *Methods*, 2002, pp. 1-3.

[7] International Organisation for Standardisation, ISO/IEC, "Coding of moving pictures and associated audio information", December 2002, Awaji Island.

[8] Abdul. H. Sadka "Compressed Video Communications" *John Wiley & Sons Ltd, 2002*.

[9] H. Karim, C. Hewage, A. Yu, S. Worrall, S. Dogan, and A. Kondoz, "Scalable multiple description 3D video coding based on even and odd frame," *PCS-2007, Lisbon, Portugal*, 2007, pp. 10-13.streaming system," *Proceedings of SPIE*, 2008, pp. 680310-680310-8.

[10] O. Schreer, P. Kauff, and T. Sikora, *3D video communication*, West Sussex, John Wiley & Son Ltd., pp. 29-37, 2005.

SED Research Student Conference
Brunel University
21-23rd June 2010

3D MULTIRESOLUTION ANALYSIS FOR SEGMENTING REDUCED FEATURE MEDICAL VOLUMES USING PCA

Shadi AL-Zu'bi and Maysam Abbod
Electronic and Computer Engineering, School of Engineering and Design,
Brunel University - Uxbridge, Middlesex, UK
shadi.alzubi@brunel.ac.uk

Keywords: Segmentation, Multiresolution analysis, Feature reduction.

3D volume segmentation aims at partitioning the voxels into 3D objects (sub-volumes) which represent meaningful physical entities. This paper focuses on the implementation of a medical volume segmentation technique using 3D Discrete Wavelet Transform (3D-DWT). Principle Component Analysis (PCA) has been presented to reduce the dimensionality of the volume as a pre-processing step of 3D-DWT to accelerate the segmentation process.

Introduction

Volume segmentation allocates the voxels in 3D images into partitions or 3D regions that represent meaningful physical entities. The goal is to distinguish between different regions in the 3D volume and cover the extracted contours from the entire volume. Voxels' classification into regions is performed according to which certain region are the voxels belong, and some shared, predefined properties. Those voxels comprise an isolated or segmented Object Of Interest (OOI) from the input volume.

Segmentation can be manually performed by a human expert who simply examines an image, determines borders between regions, and classifies each region. There are many other existing techniques used for medical image segmentation, including Multiresolution Analysis (MRA), statistical methods, thresholding techniques and clustering based techniques [1,2].

PCA is the most conventionally used technique for dimensionality reduction in image processing. It is widely used in face recognition for its ability to reduce the dimensionality of a data set while retaining as much characteristic features as possible. In PCA, while discarding a large number of minor components, a small number of principal components are retained on a linear and low dimensional subspace.

The aim of this paper is to accurately detect the Region Of Interest (ROI) in medical volumes using 3D Discrete Wavelet Transform (3D-DWT) and exploring a Feature Reduction (FR) techniques such as Principal Components Analysis (PCA) to speed up the segmentation process.

PROPOSED SEGMENTATION SYSTEM

The most common way for generating 3D data set in medical applications is from tomographic devices such as Computed Tomography (CT) scanners. Such devices are capable of slicing an object in a physical sectioning. 3D data of those devices can be presented as parallel slices stacked to form a 3D volume. Each of these slices is a 2D medical image which represents a specific section from the human body. All slices are stacked using an algorithm explained in [3] to form a 3D matrix which evaluates the 3D medical volume.

3D-DWT is used for medical image feature extraction. Segmentation techniques such as thresholding have been used to detect the ROI. The problem with 3D-DWT is the computation time which depends on the dimensionality of the image. As illustrated in Fig. 1, PCA can be applied to reduce the number of slices in medical volumes to reduce the computation time.

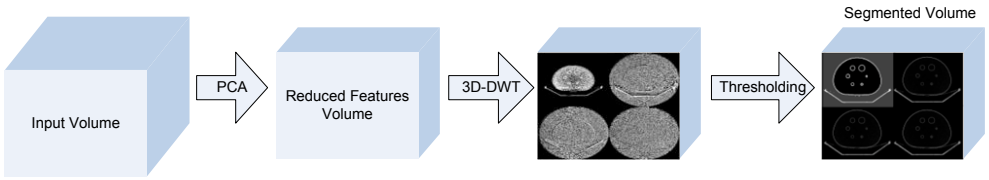

Fig. 1: Proposed segmentation system.

MATHEMATICAL BACKGROUND

The mathematical backgrounds of the developed medical volume segmentation techniques are performed in this section.

Wavelet Transform

DWT operates by convolving the target function with wavelet kernels to obtain wavelet coefficients representing the contributions of wavelets in the function at different scales and orientations. DWT can be implemented as a set of high-pass and low-pass filter banks. In standard wavelet decomposition, the output from the low-pass filter can then be decomposed further, with the process continuing recursively, DWT can be mathematically expressed by equations (1) and (2) [4]:

$$a^j(n) = \sum_{i=0}^{L-1} l(i).\ a^{j-1}(2n - i)\,, \quad 0 \le n < N_j$$

$$d^j(n) = \sum_{i=0}^{L-1} h(i).\ d^{j-1}(2n - i)\,, \quad 0 \le n < N_j$$

The coefficients $a^j(n)$ and $d^j(n)$ refer to approximation and detailed components in the signal at decomposition level j respectively. The $l(i)$ and $h(i)$ represent the coefficients of low-pass and high-pass filters respectively. Mathematically, 3D-DWT is the process of applying 1D-DWT on each vector in Z-axis that share X-axis and Y-axis coordinates after applying 2D-DWT for all comprising frames, where each frame pixels have the same Z-axis values. Algorithm 1 describes the pseudo code for applying 3D-DWT on 3D data set and the filter architecture of 3D-DWT using Haar filter is illustrated in Fig. 2.

Algorithm 1: Pseudo code for 3D-DWT

```
1 :  Load 3D data set into V
2 :  [x y z]=size(V)
3 :  for k = 1 to z do
4 :       apply 2D-DWT for each plane in Z-axis
5 :  end for
6 :  for i = 1 to x do
7 :       for j = 1 to y do
8 :            apply 1D-DWT for each vector in XY plane
9 :       end for
10:  end for
```

Principal Components Analysis

PCA can be used with 3D volumes to compress a group of slices into one slice that includes most of the input features resulting to reduce the volume dimensions. Five DICOM slices (9-13) of real human chest images [5] have been used for the experiments. Each image is converted into a column vector (X) by concatenating successive rows transposed. According to the algorithm in [6], each of the image vectors is stacked into a training matrix X. Where X = x1, x2, ... , x5. PCA is applied to the data X which returns principal components based on the eigenvectors corresponding to the highest eigenvalues. Fig. 3 illustrates the input slices and the reduced features slices using PCA.

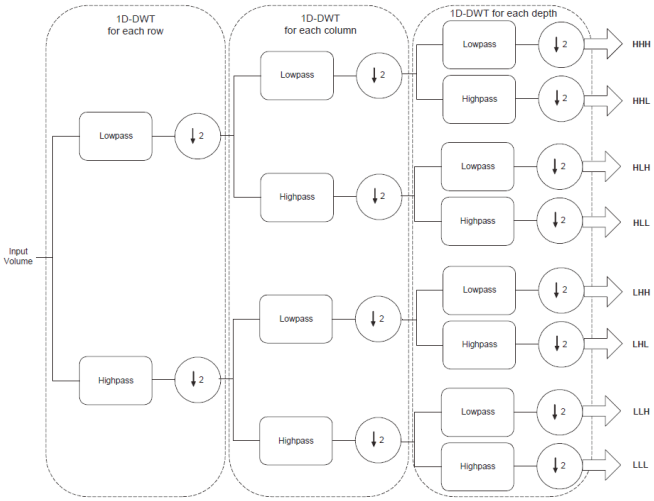

Fig. 2: 3D Haar filter architecture.

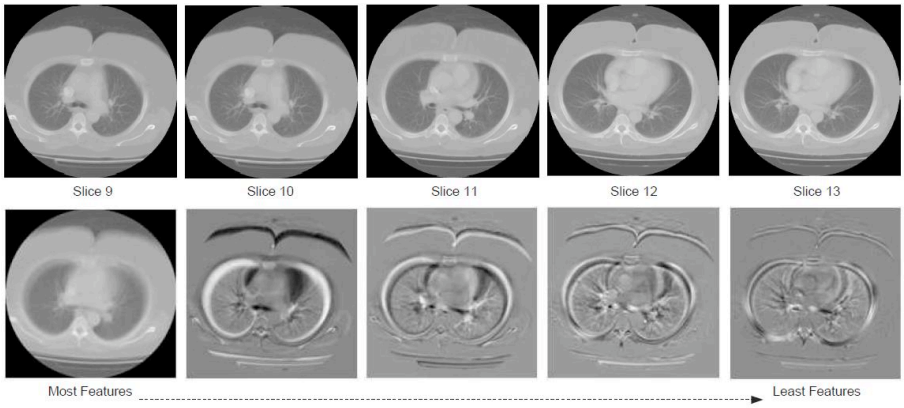

Fig. 3: PCA for 3D volume feature reduction

It can be seen from the output slices in Fig. 4 that the first principal eigenslice has significant portion of contrast/feature details and it decreases rapidly from the second principal eigenslice. This is due to the eigenvalues of this data, as the first image in Fig. 4 has a very large eigenvalue and it decreases significantly. Looking at the perspective of dimensionality reduction of such large data it can be used as a 3D FR technique to reduce the number of tested slices. However segmentation algorithms can be applied on a reduced slices volume rather than the whole volume.

RESULTS AND ANALYSIS

The proposed approach has been tested using NEMA IEC body phantom and real CT chest data. NEMA phantom consists of an elliptical water filled cavity with six spherical inserts suspended by plastic rods of inner diameters: 10, 13, 17, 22, 28 and 37 mm [7]. 3D-wavelet technique is applied on the same phantom data and the included spheres are detected as illustrated in Fig. 4(a).

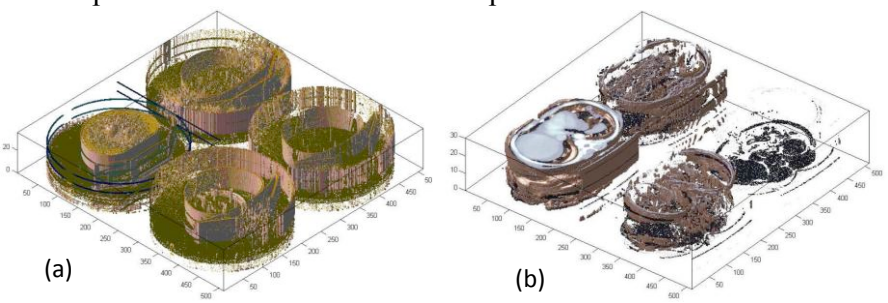

Fig. 4: Wavelet Transform for: (a) NEMA IEC body phantom. (b) Real CT volume for the chest.

Table I compares the errors in spheres diameters using 3DDWT with existing measurements using 2D techniques for slice number 19. Another example of applying 3D-DWT on real CT images for the human chest [5] is illustrated in Fig. 4(b) where the edges are detected and the comprising obstacles can be seen from different angles.

Table 1: The error percentage of spheres measurement using different segmentation techniques

Spheres (mm)	10	13	17	22	28	37
K-means [2]	13.6	11.5	5.77	5.51	5.1	5.01
MRFM [2]	7.41	8.69	4.28	4.06	3.9	3.89
2D Thresholding	-4.8	-8.15	0.06	-0.36	1.07	1.14
2D wavelet+ Thr	-2.9	-2.46	1.35	0.82	0.29	0.05
3D Thresholding	0.59	0.77	0.17	1.11	2.20	6.08
3D wavelet+ Thr	-2.67	-1.93	-0.74	4.75	3.37	0.77

PCA has been used to reduce the third dimension or the number of experimented slices. It compresses a group of slices into one slice which includes most of the features from the input slices. 3D-DWT and thresholding technique can be applied to segment the reduced features volume in less computation time.

Fig. 5 illustrates real chest volume in wavelet domain with reduced features using PCA. The original dimensions for the real chest volume can be reduced using PCA from 512*512*62 to 512*512*9, where PCA compresses each 7 slices together to produce one slice which includes most of the features. The required computation time to apply 3DDWT on the reduced features volume using PCA is 168.38 seconds while PCA spends 13.87 seconds to reduce the dimensions. The overall time is 182.25 seconds which is less than the required time for segmenting the full features volume (280.26 seconds).

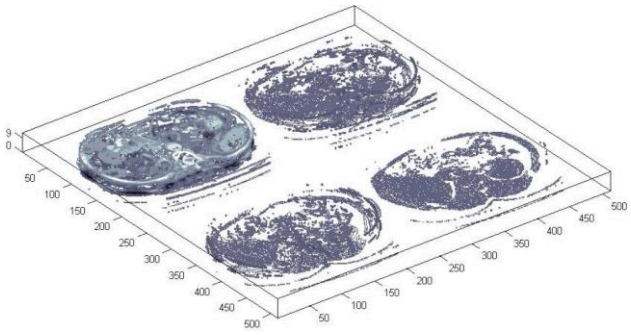

Fig. 5: 3D-DWT for real CT images after FR using PCA.

CONCLUSIONS AND FUTURE WORKS

A novel segmentation system has been developed specifically for 3D data segmentation. This system was tested on phantom data obtained from PIN laboratory. The system is used to quantify tumours within the data of known volume, and these results were compared with those obtained from 2D approaches. This system commonly reduces the percentage error achieved using the traditional 2D segmentation techniques by several percents. In order to speed up computation, PCA was used to reduce the dimensionality of the proposed volumes which is based on reducing the features in a set of slices and include most of those features in one slice. A Graphical Processing Unit (GPU) which is based on parallel processing will be used in the future work with focusing on the implementation of other 3D novel image segmentation techniques based on ridgelet and curvelet transforms for better real time segmentation accuracy.

REFERENCES

[1] P. Schelkens, A. Munteanu, J. Barbarien, M. Galca, X. Giro-Nieto, and J. Cornelis, “Wavelet Coding of Volumetric Medical Data sets,” IEEE Transactions on Medical Imaging, 22(3), pp. 441–458, March 2003.

[2] D. Montgomery, ”Multiscale Compression and Segmentation of Volumetric Oncological PET Imagery,” Ph. D. thesis, Queens University - Belfast, 2006.

[3] Balter, ”Dicom to 3 dimentional”, Copyright (c) Pacific Northwest National Laboratory, 2009.

[4] Uzun and A. Amira, ”Design and FPGA Implementation of Finite Ridgelet Transform,” International symposium on circuits and systems, 5826-5829, vol. 6, 2005.

[5] Computed Tomography scanner, King Abdullah university hospital, Ramtha, Jordan, 2009.

[6] R. Gonzalez, R. Woods, S. Eddins, Digital image processing using matlab, second edition, Lavoisier, JAN 2009.

[7] International Electrotechnical Commission (IEC), 61675-1, Geneva, Switzerland, 1998. And National Electrical Manufacturers Association (NEMA), Standards Publication No. NU2, Washington, D.C., 2001.

SED Research Student Conference
Brunel University
21-23rd June 2010

Medical Volume Analysis using Artificial Neural Network

Mhd Saeed Sharif, Abbes Amira, and Maysam Abbod
Electronic and Computer Engineering
School of Engineering and Design
Brunel University, Uxbridge, Middlesex, UK
mhd.sharif@brunel.ac.uk

Keywords: Artificial Neural Network, Medical Image Analysis, Positron Emission Tomography.

Introduction

Tumour classification and quantification in Positron Emission Tomography (PET) imaging at an early stage of illness are important for radiotherapy planning, tumor diagnosis, and fast recovery. Medical images can be acquired using different medical modalities such as Positron Emission Tomography (PET), Computed Tomography (CT), Magnetic Resonance Imaging (MRI), and Ultrasound (US). PET is a tomography technique which is used to measure physiology and function rather than anatomy by imaging elements such as carbon, oxygen and nitrogen which have a high abundance within the human body. PET plays a central role in the management of tumour beside the other main components such as diagnosis, staging, treatment, prognosis, and follow-up. Due to its high sensitivity and ability to model function, it is effective in targeting specific functional or metabolic signatures that may be associated with various types of diseases [1], [2], [3], [4].

There are many techniques for segmenting medical volumes, in which some of the approaches have poor accuracy and require a lot of time for analyzing large medical volumes. Artificial Intelligence (AI) technologies can provide better accuracy and save a decent amount of time. Artificial Neural Network (ANN), as one of the best AI technologies, has the capability to classify, measure the region of interest precisely, and model the clinical evaluation. ANN is a mathematical model which emulates the activity of biological neural networks in the human brain. It consists of two or several layers each one has many interconnected group of neurons. The main aim of this research is to evaluate the capability of ANN to detect and classify the region of interest (ROI), tumour, in PET volumes. Thresholding, clustering and Multiresolution Analysis (MRA) approaches have been used also to segment the ROI, and they are used as true ground to compare the outputs of the artificial neural network. Promising results have been achieved utilizing phantom and clinical PET volumes.

Methodology

The 3D PET volume acquired from the scanner goes through the preprocessing block. At this stage histogram equalization and median filter are utilized to enhance the quality of

image features and remove most of the noise associated with the image. The enhanced image can be processed using two types of approaches; the first processing block includes a thresholding technique which removes the background and unnecessary information, and a clustering approach which classifies each slice into a certain number of clusters. The second block is the MRA, where the slice is transformed into the wavelet domain using Haar Wavelet Transform (HWT) at different levels of decomposition. This transform decomposes the image and produces the approximation, horizontal, vertical, and diagonal features. The approximation features are fed to the ANN for classifying and quantifying the tumour. The outputs of both blocks are compared in the next step and the best outputs are selected. The generated outputs are finally mapped and displayed.

Results and discussion

The results have shown that HWT method has generated better results in comparison with thresholding, and clustering methods; however in both cases the ROI has been clearly detected using ANN. Fig. 1 illustrates one segmented clinical PET slice.

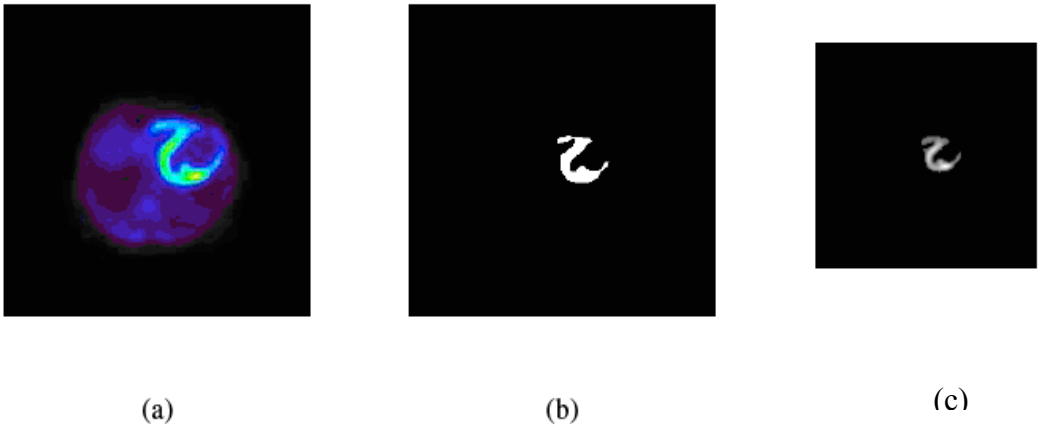

Fig 1: Clinical PET: (a) Original PET image (256x256) [5], (b) Reconstructed image from ANN and thresholding (256x256), (C) Reconstructed image from ANN and HWT (128x128).

Conclusion

Subjective evaluation for the proposed system outputs has been presented in this paper. It is worth mentioning that objective evaluation using phantom images containing a simulated tumor was also carried out. The experimental results have shown good performance for the ANN in detecting and segmenting the tumor in both phantom and clinical PET volumes.

References

[1] D. A. Mankoff, M. Muzi, and H. Zaidi, ”Quantitative analysis in nuclear oncologic imaging”, in Quantitative Analysis of Nuclear Medicine Images. edited by H. Zaidi, Springer, New York, pp. 494-536, 2006.
[2] D. Montgomery, A. Amira and H. Zaidi, ”Oncological PET Volume Segmentation Using a Combined Multiscale and Statistical Model”, Medical Physics (The American Association), 34 (2), February 2007.
[3] P. Dendy, B. Heaton, ”Physics for Diagnostic Radiology” , Institute of Physics, 2002.

[4] A. Webb,"Introduction to Biomedical Imaging", IEEE Press Series in Biomedical Engineering, 2003.
[5] PET Instrumentation and Neuroimaging Lab, Geneva University Hospital, 2010.

SED Research Student Conference
Brunel University
21-23rd June 2010

Discrete Time Simulation of Electrical Power Network with Intermittent Generation

Saharuddin Othman[1], Malcolm Irving[2]
1- Professional Development Unit, UniKL BMI, 53100 Gombak, Selangor, Malaysia
2- Institute of Power Systems, School of Engineering and Design, Brunel University, Uxbridge, Middlesex, UK
shahruddin@bmi.unikl.edu.my

Keywords : Wind power simulation; Power Flow; Intermittent generation

Introduction

Malaysia is moving towards increasing the use of its own natural resources for its energy generation. Islands in Malaysia can gain from wind turbine installations especially when they are jointly equipped with solar panels, since the country is very rich in terms of solar energy. These turbines may not be connected to the main grid because the fluctuating and unpredictable output of a wind turbine can cause the grid some problems. In the daytime, when there is less wind, the solar panels will cover the extra load. At night, the wind turbines will be generating more power. If the solar panels and wind turbines do not create enough power, the diesel generator will automatically run to compensate for the deficiency. Since the back-up generators are fuelled by diesel and turn on only when needed, this can save a lot on fuel cost. Such a situation can be modelled and simulated using a Stepwise Power Flow method created in the MatPower package and executed with MATLAB.

Methodology/Approach

Regular Power flow calculations assume balance between scheduled generation and actual load, but this is formally correct only one or a few times during the hour in a real power system, where the load is always changing, as discussed by Bakken *et al.*[2] A basic Stepwise Power Flow method is demonstrated by using a 6-bus system (Ward-Hale model) as the sample system, the loads are change 30% linearly through the hour, while schedule generation is changed only at the change of hour. The loads on a power system consist of a variety of electrical devices. Some of them are purely resistive; some are motor loads with variable power-frequency characteristics, and others exhibit quite different features. Since motor loads are a dominant part of the electrical load, there is a need to model the effect of a change in frequency on the net load drawn by the system. The main idea is to use a sequence of stationary power flow analyses to capture slow system dynamics in the minutes range. For each time step, loads are updated and generation is distributed among all units according to the schedule.

Results and discussion

The maximum frequency allowed is 52.5 Hz and minimum frequency is 47.5 Hz. Each prime mover's governor (control system) will respond to a change of frequency as a function of the amount of droop that the control system is programmed to have. A 1% change in frequency on a machine with 5% droop will result a 20% change in load, nominally, supposing the machine was running at 80% of load or less to begin with. A unit with 4% droop will respond with a 25% change in load, nominally, again presuming the machine was running at 75% or less than rated load to begin with. When there is no

wind at step 5 the frequency is 45.1Hz and the generator will be forced to shut down. If suddenly the wind turbine generation fails due to lack of wind the frequency will fall below the minimum setting frequency and the diesel generation is forced to shut down.

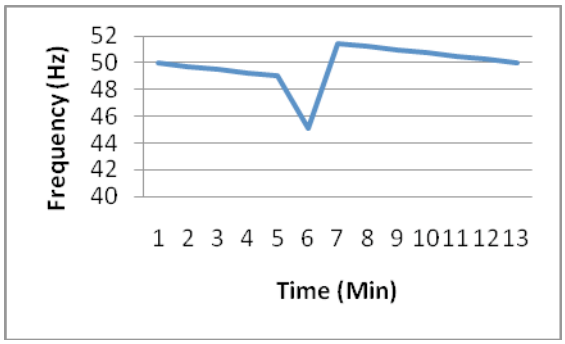

Figure 1: Frequency deviation after the wind generation fails.

Conclusion

In this paper, a method for simulating the integration of wind power in the power system generation is introduced and demonstrated on the Ward Hale system test case. The method is an AC power flow algorithm modified to run typically in 5 minute time steps. This discrete time steady state approach assumes that the operator would have been able to predict that the regulating power was needed. The operator would allocate regulating power if the frequency were to drop below 49.9 Hz provided that no regulating power was already allocated. The simulation shows that wind power development will have an influence on the expected rate-of-change of frequency in the system due to a given load increase, but the frequency control is stable in the selected simulation case. This is mainly because there is less frequency bias in the system if wind power replaces frequency controlled generation.

References

[1] R.D. Zimmermann, C. E. Murillo-Sanchez: "MATPOWER: A MATLAB Power System Simulation Package, Version 3.2",PSERC, December 1997-2007.

[2] B. H. Bakken, A. Petterteig, E. Haugan, B. Walther: "Stepwise Power Flow-a new tool to analyse capacity shortage and reserve requirement", 15th Power Systems Computational Conference, Liege, Belgium, August 2005.

[3] I. Norheim, D. Pudjianto:"Method for Assessing Impact of Large-scale Wind Power Integration on Reseves" Wind Energy Research Article Wiley Interscience, John Wiley & Sons, Ltd, October 2007.

[4] Bakken, B.H, Petterteig, A: "Alternatives to reduce reserve requirements and reserve costs in the Nordel system", SINTEF TR A6034, February 2005.

[5] P. Sorensen, I. Norheim, P. Meibom, K. Uhlen."Simulations of wind power integration with complementary power system planning tools". Elsevier, August 2007.

[6] Wood A. J. Wollenberg B. F. "Power generation, operational and control" 2nd ed. Wiley-Interscience Publication 1996.

[7] J. D. Glover, M. S. Sarma, and T. J. Overbye, Power System Analysis and Design, 4th ed. London: Thompson Learning, 2008.

[8] E.F. Fuchs & M.A.S. Masoum, Power quality in power systems and electrical machines (USA: Academic Press, 2008).

[9] Gilat A."Matlab An Introduction with application" 2nd ed. John Wiley and Sons, Inc. 2005

SED Research Student Conference
Brunel University
21-23rd June 2010

A critical review of the experimental, analytical and simulation techniques for the measurement of heat generation and temperature distribution in the cutting process

Saiful Bin-Che-Ghani, Kai Cheng, Richard Bateman
Advanced Manufacturing and Enterprise Engineering, Brunel University, Uxbridge, Middlesex, UK
mepgsab@brunel.ac.uk

Keywords: heat generation, cutting temperature, metal cutting

In metal cutting a large amount of the external energy supplied to the cutting system is converted into heat [1]. The knowledge of the amount of heat generated is necessary to predict tool life and surface finish, to determine optimum cutting conditions, and is useful in the advancement of tool and machining technology. Therefore, the generated heat has been one of the first and foremost topics investigated in machining [2, 3]. This paper will review works that have been undertaken by using various experimental and computational simulation techniques to measure the generated heat and the distribution of temperatures in the cutting process. In the conclusion, the most promising techniques will be summarised.

1. Introduction

In many manufacturing processes, it is often times vital to have knowledge on the amount of heat generated and corresponding temperature rise as well as its distribution in the conduction media. The temperature rises to critical levels up to 1000 °C in the cutting zone affecting the material behaviour and mechanics of chip formation [1]. The maximum temperature occurs at the tool– chip interface. The tool–wear and fracture considerably increase at higher temperatures. The development of new tool materials as well as the advancement of machining technology will depend to a large extent on the knowledge and limitations of the cutting temperatures on the tool material, as the temperatures influence the life and performance of the tool.

This paper will critically review the experimental and computational approaches that have been carried out to measure temperature quantitatively in material removal machining. However, the analytical approach won't be analysed in details in this paper because of the complex approximations and computational procedures.

This review is important to determine that the most appropriate measurement technique for a given thermal problem depends on the situation under consideration, such as the ease of accessibility of the sensor to the subject location, situation dynamics, spot size, accuracy needed, cost of instrumentation, advancements in sensor technology, and data collection & analysis.

2. Measurement of heat generation

One of the earliest measurements of the mechanical equivalent of heat (J) was done by Benjamin Thomson (Count Rumford) [2] in 1798 by using the Calorimetric method. These experiments not only provided a good correlation to the mechanical equivalent of heat but also provided a new insight into the nature of thermal energy at a time when most people believed the heat was a special form of fluid [3]. The Calorimetric method was later used by Schmidt and Roubik [3] in 1949 to investigate the distribution of the heat generated in drilling. The investigation yielded for the first time that the amount of heat generated in cutting processes was carried out by chips (70-80%), with ca. 10% transferring into the workpiece and the remainder flowing into the cutting tool. It is reported other investigations using Calorimetric technique had also been conducted by Taylor and Quinney in 1934 and 1937, Bever, Marshall, and Thitchener in 1953 and Bever, Holt and Thitchener in 1974. All of the results of

these experiments suggest it is convincing to assume that all of the energy associated with chip formation is converted to thermal energy [1].

On the other hand, for the past fifty years many analytical and computational modelling techniques have been developed including analytical simplified model, slip line solutions, empirical approaches, and finite element analysis techniques. However, in recent years, finite element models have been widely used for simulating metal cutting processes [4, 5, 6], with which temperatures in the tool, chip and workpiece, as well as cutting forces, plastic deformation (shear angles and chip thickness), chip formation and possibility of breaking can be determined faster than using costly and time consuming experiments [6, 7].

3. Temperature measurement techniques

Much effort has been made to measure the temperature at the tool-chip interface zone and the temperatures of the chip, tool and the workpiece, as well as, obtaining the temperature distributions in the cutting tool. In general, the techniques used include (i) embedded thermocouples, (ii) dynamic thermocouples, (iii) radiation pyrometers, (iv) metallographic techniques and (v) a method of using powders of constant melting point [3].

Finite element simulations have been remarkably successful in modelling orthogonal cutting processes. The applications have significantly reduced the simplifying assumptions of analytical models [1, 3, 6]. However, a large number of input parameters, which need to be determined through extensive experimental work and mechanical property tests, are required to perform this FEM simulation in metal cutting studies [3, 4, 6]. These include material models for large deformation, high strain rate, temperature effects, tool-chip contact and friction models, and the separation criterion. Among the commercial codes used to simulate the processes are DEFORM 2D-3D [3, 6], MSC.Marc[5, 6], and Thirdwave AdvantEdge [6].

4. Conclusion

Predictions of heat generation and cutting temperatures are major challenges in metal cutting. This is due to numerous practical difficulties involved in the process. However, for temperature measurement of the cutting process (especially with high speed) the most promising methods at the moment are the fibre-optic pyrometers and infrared thermography techniques due to non-contact measurement, the capability of measuring in transient periods, ease of cooling, accuracy and fast response times. Nevertheless the capabilities of the methods to work at micro-scales and with different emissivity materials are still arguable.

While FEM has been successfully applied for two dimensional analysis of the machining process with reasonable accuracy, the transition to three-dimensional analysis is still problematic. The method is still unable to consistently validate existing conventional machining simulation models accurately.

5. References

[1] M. C. Shaw, *Metal Cutting Principles.* , vol. 3, Oxford: Clarendon, 1984,

[2] B. C. Rumford, "An Inquiry concerning the Source of the Heat Which is Excited by Friction." *Phi,l Trans. of the Roy. Soc. of Lon.,* vol. 88, pp. 80-102, 1798.

[3] R. Komanduri and Z. B. Hou, "A review of the experimental techniques for the measurement of heat and temperatures generated in some manufacturing processes and tribology," *Tribol. Int.,* vol. 34, pp. 653-682, 10. 2001.

[4] E. Ceretti, P. Fallböhmer, W. T. Wu and T. Altan, "Application of 2D FEM to chip formation in orthogonal cutting," *J. Mater. Process. Technol.,* vol. 59, pp. 169-180, 5/15. 1996.

[5] F. Klocke, T. Beck, S. Hoppe, T. Krieg, N. Müller, T. Nöthe, H. Raedt and K. Sweeney, "Examples of FEM application in manufacturing technology," *J. Mater. Process. Technol.,* vol. 120, pp. 450-457, 1/15. 2002.

[6] H. Bil, S. E. Kılıç and A. E. Tekkaya, "A comparison of orthogonal cutting data from experiments with three different FE models," *Int. J. Mach. Tools Manuf.,* vol. 44, pp. 933-944, 7. 2004.

SED Research Student Conference
Brunel University
21-23rd June 2010

Novel State Estimation for Distribution Systems

Nazia Nusrat[1], Gareth A. Taylor[2] and Malcolm Irving[3]

1. Research Assistant, Brunel Institute of Power System, School of Engineering and Design, Brunel University, e-mail: Nazia.Nusrat@brunel.ac.uk
2. Senior Lecturer, School of Engineering and Design, Brunel University, e-mail: Gareth.Taylor@brunel.ac.uk
3. Professor, School of Engineering and Design, Brunel University, e-mail: Malcolm.Irving@brunel.ac.uk

Key words: State Estimation, Distribution System State Estimation, Weighted Least Squares, Weighted Error Modulus.

Introduction: In an electrical power system, the state estimator takes into account all the available measurements and estimates the most accurate value of the different states (voltage, current, power) of a node. The transmitted measurement data may contain noise or wrong information. A good estimator can overcome the effect of these erroneous measurements and determines the actual state of the system. The application of the state estimation techniques to maintain desirable voltage, power flow control and the security of the system is widely used at transmission level. However, the state estimation at a distribution network level has not been common due to lack of measurement data and an accurate measurement model. In addition, distribution networks consist of hundreds of thousands of nodes and dealing with such high volumes of data is extremely challenging. Currently distribution networks are usually passive with very limited communication support and intelligent automation. Hence, the development of a Distribution System State Estimation (DSSE) tool is essential to transform the distribution system to a 'smart grid'. The traditional estimation techniques that have been used at transmission level cannot be utilized effectively at distribution level. Therefore, it is necessary to develop a novel method that will be able to handle the integration of distributed generators as well as data from smart meters in future scenarios.

Overview of DSSE: The measurement model of a DSSE tool consists of voltage angle and magnitude measurements, real and reactive power injection measurements, power and current flow measurements. Each measurement is evaluated by a weighting factor depending upon the accuracy and reliability of measurement from the instrument. The measurements at distribution level are classified as real time, pseudo and virtual measurements. The pseudo-measurement is normally the load data obtained from historical characteristics at a node. The virtual measurement is the zero injection bus, zero flow line (breaker) etc. The weighting factor for a virtual measurement is assumed very high and that of pseudo measurement is taken as low [1].

Development of Novel DSSE: Weighted Error Modulus (WEM): The most commonly used state estimator is the Weighted Least Squares (WLS) method that provides an optimal solution with known measurement variance and normally distributed measurement error [2]. Assuming the

measurement error is e, the measurement vector as z and the measurement equation as $h(x)$, we can obtain:

$$z = h(x) + e \quad \text{..... (1)}$$

Here, x represents the state vector. For an optimum condition, the aim is to achieve the best estimation that contains the least error. The objective function $J(x)$ is such that

$$\text{Min } J(x) = [z - h(x)]^T W [z - h(x)] \quad \text{.....(2)}$$

Here $[z - h(x)]$ is the residual vector of the measurement errors. W is the weighting factor determined from the accuracy of the associated measurement. The estimated result is obtained through an iteration procedure. The equation that fulfills the optimum condition is:

$$H^T W H \Delta x = H^T W [z - h(x)] \quad \text{.....(5)}$$

Here H is the Jacobian matrix of measurement equations and Δx is the mismatch vector. For k^{th} iteration, $\Delta x^k = x^{k+1} - x^k$ [3].

Although the WLS method gives a very good estimation, it is not efficient in detecting and overcoming the effect of gross measurement errors or bad data. To eliminate gross errors, another technique called the Weighted Least Absolute Value (WLAV) method is more effective. The WLAV optimizes the absolute value of the residual vector instead of the quadratic value as in WLS method. In this research, a novel estimator, Weighted Error Modulus (WEM) method is proposed. The advantage of the WEM method is that it extracts the benefits from both WLS and WLAV methods. In this approach, the weighting value is modified iteratively within the WLS method. Equation (2) of WLS can be expressed as

$$\text{Min } \sum_{i=1}^{m} w_i | r_i |^2 \quad \text{..... (6)}$$

Where w_i = diagonal element of 'modified' weighing matrix

$r_i = z_i - h_i(x)$ = residual of the measurement error

m = number of the measurements

If w_i is modified iteratively such that

$$w_i^{k+1} = u_i / |r_i|^k \quad \text{..... (7)}$$

The equation (6) becomes

$$\text{Min } \sum_{i=1}^{m} u_i | r_i | \quad \text{.....(8)}$$

When $| r_i |^k = | r_i |^{k+1}$. Here u_i is the measurement weighting matrix. Equation (8) represents the objective function of the WLAV method [3]. Thus WEM combines both the WLS and the WLAV approach. The flowchart of the proposed method is presented in Figure 1 as follows:

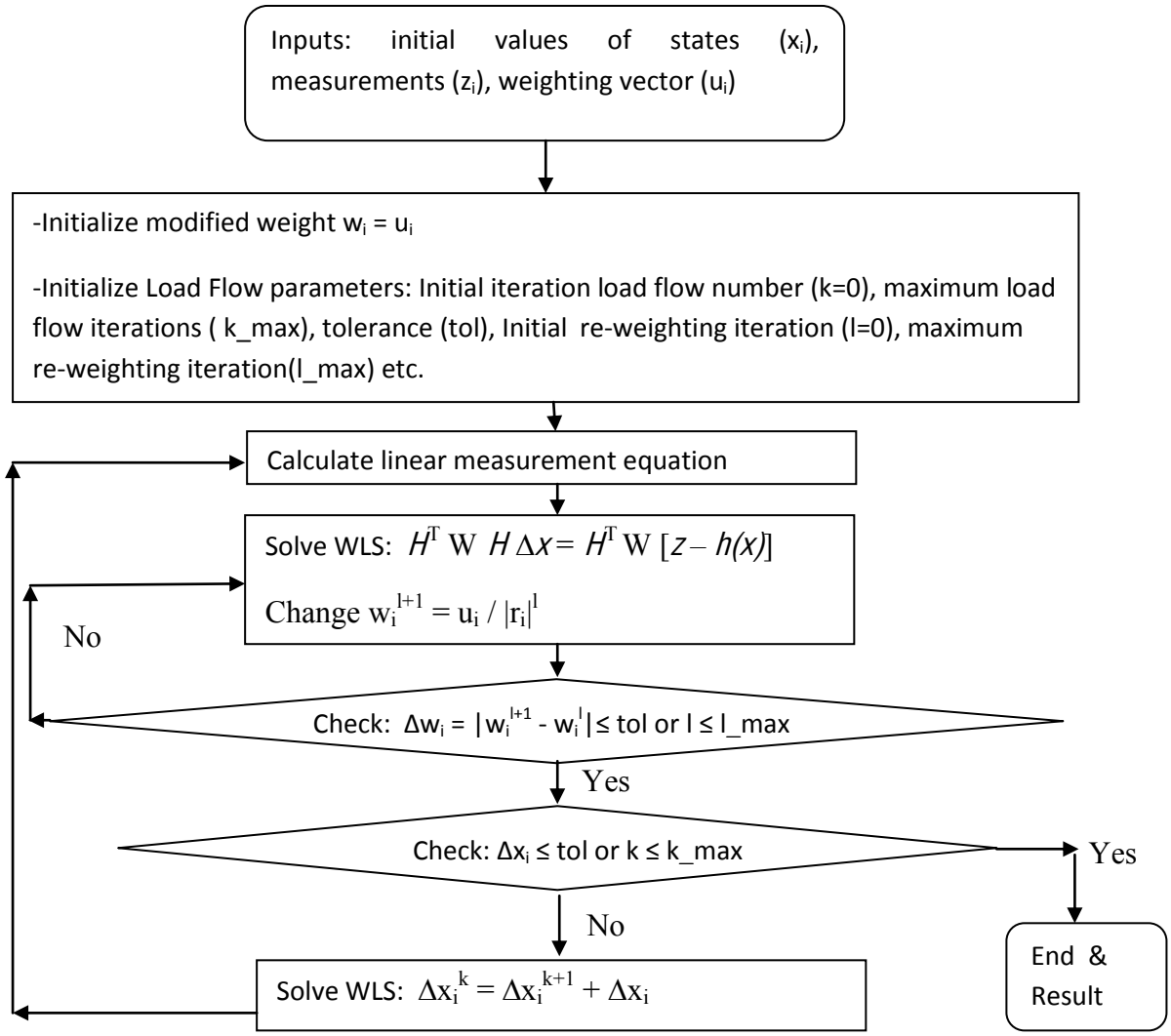

Figure 1: Flow Chart of DSSE

Results and Discussion: Initially, we consider a small circuit consisting of three buses and three lines. Bus or Node 1 is the reference bus where voltage angle is fixed at $\theta_1 = 0$. The Jacobian matrix therefore consists of five columns with five state variables and the number of measurement is equivalent to the number of rows.

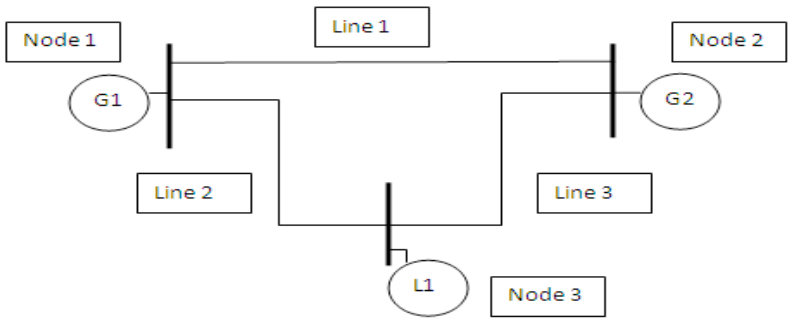

Figure 1: Case study of a 3 bus system

The DSSE tool that has been developed has been successful in performing WLS Estimation. The next step would be to modify WLS into WEM method. After accomplishing this step successfully, the method will then be checked for a larger system. Part of the research also includes checking the scalability of the method and the scope to utilize the data acquired from smart meters.

Conclusion: The proposed method is simple in the sense that it can be easily implemented in the existing WLS programme. The programme is particularly suitable for large scale problems, which enables it to estimate the large volumes of distribution level data. The estimator is also robust and is able to recover in the presence of bad data [2].

Reference:

1. O Chilard *et al*, *'Distribution State Estimation Based On Voltage Variables: Assessment of Results and Limitations*, 20th National Conference of Electricity Distribution, CIRED2009 Session 4, Paper 0524, 2009.

2. M R Irving and M J H Sterling, '*Robust State Estimation for Large Scale Power Systems'*, IEE conference on Power System Monitoring and Control, pp261-264, 1986.

3. A Abur and A G Exposito, Power System State Estimation: Theory and Implementation, Chapter 2, Marcel Dekker, 2004.

Novel Grain Refiner for Aluminium Alloys

M. Nowak and N. Hari Babu

Brunel Centre for Advanced Solidification Technology, Brunel University,

Uxbridge, Middlesex, UK

Magdalena.Nowak@brunel.ac.uk

Key words: Grain refinement, Nucleation and Growth, Al alloys

Introduction:

The grain refinement development is of scientific and practical significance in alloy casting as the fine and equiaxed grain structure is usually desirable. The grain refinement by inoculation brings many benefits in the casting process and has significant influence on improving mechanical properties [1-4]. The fine equiaxed grain structure imparts high yield strength, high toughness, good extrudability [2], uniform distribution of second phase and micro-porosity on a fine scale resulting in improved machinability, good surface finish and resistance to hot tearing.

The addition of Al-5Ti-B master-alloy to Al wrought alloys is a common practise [3] in industries for obtaining fine grain structure and for producing castings with reduced defects. However, Al-5Ti-B grain refiner is known to be ineffective for casting alloys particularly when Si concentration is above 7 weight (wt.) % the alloy [5].Therefore, our objective is to develop a grain refiner that can be effectively used for Al-Si casting alloys. Comparing Al-Ti and Al-Nb equilibrium phase diagram, it can be seen that both systems exhibit a peritectic reaction (Liquid + Al_3Ti → solid solution) between liquid aluminium and Al_3X solid phase (X = Ti and Nb). In addition, the crystal structure of Al_3Ti and Al_3Nb are both tetragonal with eight atoms per cell with lattice parameters a = 0.385 nm; c = 0.861 nm and a = 0.384 nm, c = 0.858 nm respectively [9]. These similarities indicate that niobium could exhibit grain refining characteristics. In this paper, we present development of efficient Nb-based novel grain refiner for Al and Al-Si casting alloys.

Experimental:

Commercial pure Al and practically used Al-13Si-0.1Mg-0.5Fe cast alloy (known as LM6) were melted in an electric furnace at the temperature range 750-800 ^{O}C and held for 2 hours. Newly developed Nb-based grain refiner has been added to the melt prior to casting the melt. We have conducted a wide range of casting experiments with range of holding times from <15 min to 4 h> and compositions <0.01-5 wt. %> to establish the right condition and chemical composition for developing the novel effective grain refiner. The standard test procedure, commonly known as TP-1 mould, was used to cast Al alloys with and without grain refiner addition. TP-1 mould offers the cooling rate of 3.5K/s, which is similar to that of large industrial casting conditions. Chemical electro-polishing ($HClO_4$+CH_3COOH) and Baker's anodizing have been used to reveal grain boundaries. A Zeiss polarized optical microscope with an Axio 4.3 image analysis system was used to measure the grain size using the linear intercept method. The macro-etching was performed with Keller's solution to have a visual comparison of the grain size.

Results and Discussion:

The effect of addition of Nb-based novel grain refiner to commercial pure Aluminium is shown in Fig. 1. The grain size is observed to reduce significantly with the addition of Nb-based chemicals. Fine grain structure brings several benefits (e.g, reduced chemical segregation, reduced porosity, absence of hot tearing) when large sized billets are manufactured as shown in Fig. 2(b). Large voids form as shown in Fig. 2(a), as a result of

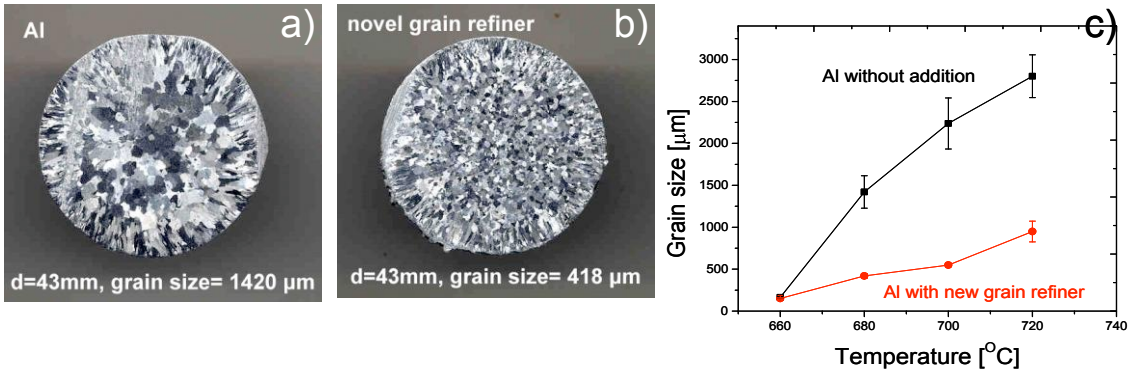

Figure 1 Surface of macro-etched TP-1 test mould specimens, revealing grain size for Aluminium (a) without and (b) with novel grain refiner addition. (c) The measured grain size as a function of casting temperature for Al with and without **the use of "novel grain refiner"** addition. Nb-based grain refiner is observed to refine Al grain size significantly, and is expected that this novel grain refiner would enhance further use of Al (lightweight) instead of steel in transport vehicles.

coarse grains, which prevent liquid feed to the solid, during solidification of Al liquid without grain refiner addition. These large defective ingots are not suitable for further shaping into components or sheets for structural applications. Fine grain structure results in not only reduced porosity but also results in much required uniform chemical composition across the Al alloy ingot. Figure 2(c) reveals the fine grain structures of TP-1 mould samples and their measured grain sizes are shown in Fig. 1(c).

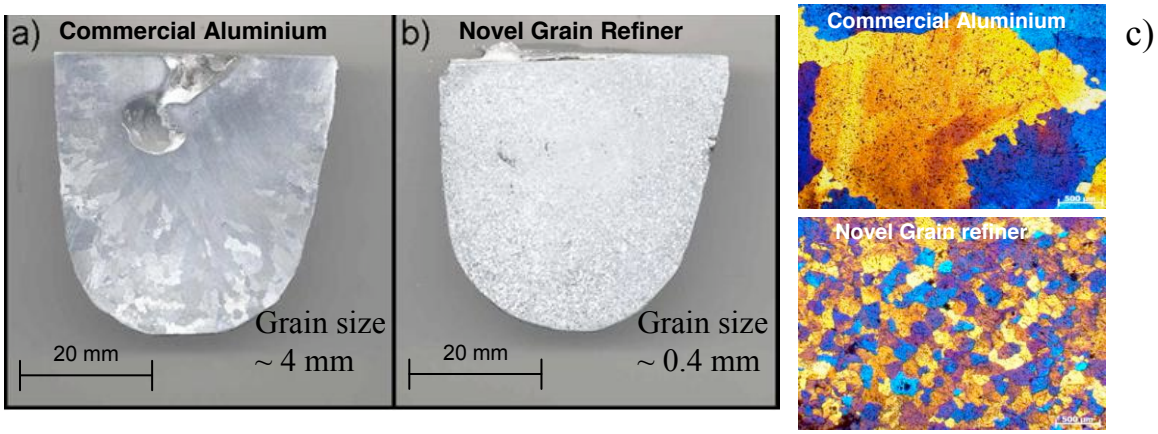

Figure 2 Photographs of macro-etched ingots (a) Aluminium (b) Al with novel grain refiner addition. A large shrinkage void, coarse and non-uniform grains can be seen in Fig (a) and highly uniform and fine grains can be seen in grain refined sample. (c) Microstructures of TP-1 mould samples (with and without grain refiner) produced by pouring liquid into TP-1mould at 680 ^{0}C.

The Al-Si alloys are classified as cast alloys and are extensively used in automotive applications. For these casting alloys, it is known that the Al-5Ti-B master-alloy is not an efficient grain refiner and can even have an adverse effect [6-8]. Our series of experiments in Al-Si binary alloys shows that the Nb-based grain refiner is highly

effective than Al-5Ti-B when Si content is > 6 wt. %. Experiments with LM6 casting alloy confirms that addition of novel grain refiner decreases the grain size effectively when compared to that of Al-5Ti-B addition, as shown in Fig 3 (a). Optical micrographs of colour etched surfaces are shown in Figures 3 (b) and 3 (c), where fine grains can be seen for Nb-based grain refiner added sample. The improved microstructural features in novel grain refined Al-Si casting alloys is expected to increase their mechanical properties and as a result fabrication of wide range of complex shaped Al-Si alloy castings with superior properties will be possible in near future. The exact chemical composition of the novel grain refiner and the method of producing the master alloy for grain refining process for both wrought and cast alloys are described in a patent application in association with Brunel Research Support and Development Office.

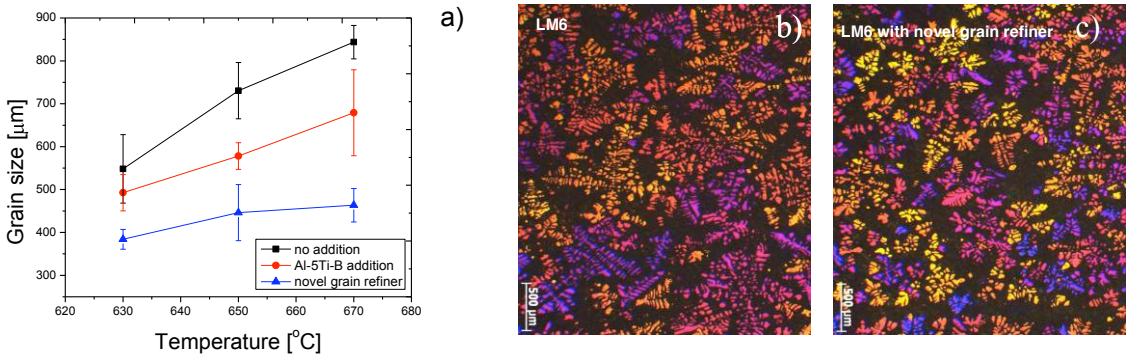

Figure 3 The grain size for Al-Si casting alloy as a function of casting temperature for LM6 alloy with Al-5i-B addition and with Nb based novel grain refiner addition. Polarized optical micrographs of anodized specimens revealing the grain structure for (b) LM6 without grain refiner addition and (c) with Nb based grain refiner addition. Nb-based grain refiner is observed to be more efficient than the Al-5Ti-B based grain refiner.

Conclusion:

We have presented the development of Nb-based novel grain refiner for Al alloys and measured the grain size for commercial pure Al and a casting Al-Si alloy. The experimental data proves that Nb-based grain refiner is responsible for the observed fine grain structure. Furthermore, the new Nb-based grain refiner is more effective in high silicon casting alloys. This novel grain refiner has the potential to improve mechanical properties significantly for both wrought and cast alloys, thus enhancing the wider use of Al in automotive applications in the place of steel. Al is 65% lighter than steel and widespread use of Al in transport sector can save enormous energy and reduce millions of tonnes of CO_2 emissions thus benefiting the planet's environment.

References:

[1] D.G. McCartney. *Int. Mater. Rev.* 34, 247 (1989).
[2] E.R Rooy. In: ASM International Handbook Committee, Metals handbook, Casting, vol. 15. Metals park, OH: ASM International; p. 743-70 (1989).
[3] D.A Granger. In: B.J Welch, editor. Light metals 1998. Warrendale, PA: TMS;. p. 941-52 (1998).
[4] J.D. Hunt, *Mat. Sci Eng.* 65, 75 (1984).
[5] M.A Easton, D.H. St John, *Metall.Mater.Trans.* 36A,1911(2005).
[6] D. Qiu, J.A. Taylor, M.X. Jang, P.M. Kelly, *Acta Mater.* 55, 1447 (2007).
[7] Y.C Lee, A.K. Dahle, D.H. St John J.E.C. Hutt, *Mat. Sci. Eng.* A259 43 (1999).
[8] S. A. Kori, B.S. Mutty, M. Chakraborty, *Mat. Sci. Eng.* A283, 94 (2000).
[9] F. Mondolf; *Aluminum Alloys: Structure and properties*, Butterworths, Boston, 1976.

Growth and tuning of many-layered graphene on the 4H-SiC (0001) - $\sqrt{3}$ x $\sqrt{3}$ R30° surface

Nikolai Issakov

Supervisor – Dr. Harris Makatsoris

Advanced Manufacturing & Enterprise Engineering

Key words: epitaxial growth; buffer; interface; truncated bulk; band gap; unpaired electrons.

Introduction

Hereby the results of systematic study aimed at the computational design carried out for graphene multilayer are presented. Multilayer means the sequence of few graphene mono-layers (MG) formed stepwise on the solid surface of precursor via intermediate layer (interface) in the course of either epitaxial growth (EG) or chemical vapour deposition (CVD). As a number of graphene sheets are running up to the 3D graphite crystal, the electronic properties of multilayer change layer-by-layer. Every constituting layer introduces the new characteristics changing the multilayer properties as a whole. The actuality of study is defined by using the multilayer as a molecular building block (MBB) for complicated nano-architecture, patterning, tailoring, etc., while graphene processing.

Methodology

The computational design exploring modelling, simulation and DFT first principle calculations by means of the CASTEP code (Payne et al, 1992; Seagall et al, 2002) was applied for processing of many-layered graphene construction. Proof of principle through the scanning probe microscopy nanolithography (SPML) was proposed.

Results and Discussion

Simulation for basal carbon layer by means of the local oxidation on the SiC surface is of crucial importance for the whole many-layered construction. It is determined by the proper choice of substrate with the ($\sqrt{3}$ x $\sqrt{3}$) R30° reconstruction and calculation for the geometrical commensuration between lattice of substrate and hexagonal graphene ring, when 4 graphene unit cells correspond to one unit cell of SiC (0001) substrate. Undertaken calculations have shown that the first carbon layer is devoid of the freestanding graphene characteristics. The buffer properties are strongly influenced by the unpaired electron behaviour and its displacement along with the Fermi level. The configurations of electronic structures are in good agreement with the previous *ab initio* studies (Varchon et al, 2007;

Mattausch, Pankratov, 2007), also with the experimental data about the more strong interactions of the first MG with the (0001) substrate. The carbon layer on the (0001) surface possesses the metallic properties, whereas the carbon layer on the $(000\bar{1})$ surface demonstrates the semiconductor properties (Hass et al, 2006; Rutter et al, 2007; Hiebel et al, 2008). The electronic characteristics of freestanding graphene were distinguished exclusively in the second layer over the buffer growing the (0001) - $(\sqrt{3} \times \sqrt{3})$ R30^{o} surface of substrate. The electronic structure proved to be *n*-doped.

As a majority of surface processes, the epitaxial events are hidden behind the sequence of reactions running simultaneously through the interface (Gates 1992). The generalized pathway $[Si^{4+}C^{4-} - H]^{(L)} + 2F_2^{(S)} = SiF_4\uparrow + [C - H]^{(L)}$ (1) is expanded into the number of intervening processes running through the interface resulted in local oxidation of substrate, removal of Si atoms and accumulation of carbon layer. Transition is schematically expressed as follows:

$$2[Si^{4+}C^{4-} - H]^{(L)} + [H^{+}(OH)^{-}]^{(S)} + F_2^{(S)} = 2Si^{4+}C^{4-(L)} + [H^{+} + (OH)^{-}]^{(S)} + 2HF^{(S)} \quad (2)$$

$$2(OH)^{-(S)} = O^{2-(L)} + H_2O^{(S)} + \text{Vacancy} \quad (3)$$

$$[Si^{4+}C^{4-} - O^{2-}]^{(L)} + H^{+} \rightarrow SiO_2 + (C - H)^{(L)} \quad (4)$$

$$SiO_2 + 4HF = SiF_4\uparrow + 2H_2O \quad (5)$$

The sequence (2)–(5) starts since dehydrogenation of the surface according to the reaction (2) after the 4H-SiC (0001) - $(\sqrt{3} \times \sqrt{3})$ R30° surface is covered by the F_2 aqueous solution. The additional supply of F_2 launches surface activation. As hydrogen is removed the self-organization catalytic processes under high current density, heating and vibration lead to the bonds breaking in the upper layers of substrate and reaction of local oxidation (Avouris et al, 1998). Since the aqueous HF solution is coexisting in interface with the $(OH)^{-}$ the latter is disintegrated as it follows from the reaction (3). This transition state caused by the mechanism of rearrangement is a driving force playing the crucial role for the local oxidation reaction (4). The O^{2-} is captured into substrate lattice to form SiO_2. The side effect of reaction is accompanied by vacancy in interfacial layer. Oxidation number of carbon is decreased. Its electrons are taken away by H^{+} to restore the electrochemical balance in interface. The proper site for the buffer is formed over the top of lattice where vacancies are occupied with the released carbon atoms. New-forming SiO_2 is removed from the surface by aqueous HF solution (5). SiF_4 should be sublimated because it is volatile. Carbon layer is passivated at expense of free hydrogen taking away the lost electrons from C atoms.

The second and subsequent layers are formed by using the organic halogen consisting of six carbon atoms already arranged into the hexagonal rings bound with the additional atom,

e.g. F, Cl, Br, J (Orlander, Larsen, 2002). Because the carbon bonds are weak enough to be easily broken under reasonable temperature and vibration, in contact with the buffer these molecules are decomposed. The substituent groups will detach from the carbon atoms as a volatilizing gas-phase and escape into ambient (Bronikowski, Manohara, 2008):

$$6[C-H]^{(L)} + C_6Cl_6 = 6[C-C-H]^{(L)} + 3Cl_2\uparrow \quad (6)$$

Conclusion

The properties of two dimensional graphene films constituting the many-layered constructions change stepwise as a number of sheets is running up to graphite crystal.

Electronic characteristics of every sheet are predominated by the several crucial factors:

(1) - SiC poly-type used as a substrate;

(2) - periodicity reconstruction of the substrate surfaces;

(3) - geometrical commensuration of the lattices forming the many-layered construction.

The first layer is factually devoid of the most definite graphene characteristics save some energy regularities around the Fermi level. The graphene relevance appears only in the subsequent layer growing the peculiar *n*-doped template where few electrons are transferred into the conductive band.

References:

Avouris Ph., Martel R., Hertel T., Sandstrom R. 1998, App;. Phys. A 66, S659-S667.

Bronikowski M. & Manohara H. NASA's Jet Propulsion Lab. (2008)

Gates, 1992. Catalytic chemistry. NY, Chichester Wiley.

Hass J, E. Millán-Otoya J E, First P N, and Conrad E H 2008 Phys. Rev. B 78, 205424.

Hiebel F., Mallet P., Varchon F., Magaud L., Veuillen J-Y. 2008, Phys. Rev. B 78, 153412.

Mattaush A., Pankratov O 2007 *Phys. Rev. Lett.* 9 076802.

Oshima C and Nagashima A 1997 J. Phys. Condens. Matter 9, 1-20.

Payne M. C., Teter M. P., Allan D. C., Arias T. A., Joannopoulus J. D., 1992 Rev. Mod. Phys. 64, 1945.

Rutter G M, Guisinger N P, Crain J N, Jarvis E A A, Stiles M D, Li T, First P N, Stroscio J A 2007 Phys. Rev. B 76 235416.

Segall M D, Lindan P J D, Probert M J, Pickard C J, Hasnip P J. Clark S J, Payne M C. 2002 J. Phys.: Condens. Matter 14 2717-44.

Tseng A. A. Notargiacomo A. Chen T.P. J. Vac. Sci. Technol. B 23 (3):877-894 (2005).

Varchon F, Feng R, Hass J, Li X, Nguyen B N, Naud C, Mallet P, Veuillen J-Y, Berger C, Conrad E H and Magaud L, 2007 Phys. Rev.Lett. 99 126805.

Day Three
Proceedings

A Novel High Gain Semi-Planar UWB Antenna

Thomas Peter[1], Rajagopal Nilavalan[2]
1,2. Electronic and Computer Engineering, School of Engineering and Design, Brunel University, Uxbridge, Middlesex, UK
Thomas.Peter @brunel.ac.uk

Keywords: gain, uwb, curved, polymer, semi-planar

Introduction

Much research has been done on ultra wideband (UWB) since the approval of its use in Europe. One of the key areas of research interest being how to improve gain of the UWB antenna which hovers between 0 dBi and 5dBi in earlier reported papers [1-4]. A recent paper has reported improvement of gain when the radiator of a flexible UWB antenna is bent or conformed [5]. Taking advantage of this findings, a semi-planar antenna was designed to produce the conformity or bend on a planar substrate to see if it can produce similar gain levels. Initial designs have demonstrated good results of gain thus opening an avenue for a new breed of microstrip or planar antennas with embossed radiator surface to achieve high gain and simultaneously minimize power requirements in wireless communication systems.

In this paper, a coplanar wave guide (CPW)-fed Semi-Planar Monopole UWB Antenna for Wireless Communications using CST2010 [6] is designed and simulated. Comparative narrow band antennas are also designed to test 'proof of concept' and portability.

Methodology/Approach

The proposed CPW-fed Semi-Planar Monopole UWB antenna here is first designed using a planar radiating copper surface on a polymer and later an embossed radiating copper surface on a polymer. The gains of both the antennas will be compared to show the gain improvement achieved by embossing the radiator. The embossing is done to produce a curved surface onto to a planar plane to replicate the curved surface of the flexible transparent polymer antenna when bent [5]. Narrow band antennas will be similarly designed and optimized. Their gains will be studied to see whether a similar improvement to that of UWB antennas can be achieved.

Results and discussion

Initial findings on the UWB antennas show that an additional 1 to 3 dBi gain can be achieved by embossing the radiator of the antenna. Parametric studies for example, like varying the height of the emboss would be carried out to see what possible maximum gain can be achieved. A similar gain improvement for the narrow band antennas could confirm the portability of the concept. Positive results could help provide a solution for power-hungry wireless mobile devices.

Conclusion

The simulation study shows that efficiency improvements observed by bending a flexible polymer antenna can be reproduced on a semi-planar antenna. This is to be verified with experimental results later. If experimental results confirm the findings of the simulations, this would introduce a new breed of antennas that are power efficient for mobile and other wireless communication devices. This power efficient antennas directly contribute to cost savings and indirectly to the green radio technology initiatives of the UK government.

References:

[1] Seok H. Choi, Jong K. Park, Sun K. Kim, and Jae Y. Park, "A new ultra-wideband antenna for UWB applications," Microwave Opt. Technol. Lett., Vol. 40, No. 5, March 5 2004.

[2] Amjad A. Omar, Maximilian C. Scardelletti, Nihad Dib, Raed Shubair, " A Curvature CPW-fed Ultra-Wideband Monopole Antenna on Liquid Crystal Polymer Substrate Using Flexible Characteristic" International Journal of Electronics, vol. 96, Issue 4 pp. 397 – 407, 2009 ,

[3] Su Won Bae, Hyung Kuk Yoon, Woo Suk Kang, Young Joong Yoon, Cheon-Hee Lee, "A Flexible Monopole Antenna with Band-notch Function for UWB Systems", Proceedings of the Asia-Pacific Microwave Conference 2007.

[4] Hyok Jae Song; Tsung Yuan Hsu; Sievenpiper, D.F.; Hui Pin Hsu; Schaffner, J.; Yasan, E., "A Method for Improving the Efficiency of Transparent Film Antennas," *Antennas and Wireless Propagation Letters, IEEE* , vol.7, pp.753-756, 2008

[5] T. Peter and R. Nilavalan, "Study on the performance deterioration of flexible UWB antennas," Antennas and Propagation Conference Loughborough (LAPC'09), pp. 669-672, 2009.

[6] CST Microwave Studio 2010, 1998-2006, CST GmbH

SED Research Student Conference 2010
Brunel University
21st - 23rd June 2010

The effects of radiation damage on the spectral resolution of the Chandrayaan-1 X-ray Spectrometer

T. E. Walker [1], D. R. Smith [1], C. J. Howe [2], B. J. Kellett [2], P. Sreekumar [3], M. Grande [4]

1. Centre for Sensors and Instrumentation, School of Engineering and Design, Brunel University, Uxbridge, Middlesex, UB8 3PH, UK
Thomas.Walker@brunel.ac.uk
2. Space Science and Technology Department, Rutherford Appleton Laboratory, Didcot, Oxon OX11 0QX, UK
3. Indian Space Research Organisation, Bangalore, India
4. Institute of Mathematical and Physical Sciences, University of Wales, Aberystwyth, Ceredigion SY23 3BZ, UK

Keywords (3): Swept-charge device, X-ray spectroscopy, radiation damage

Introduction

The Chandrayaan-1 X-ray Spectrometer (C1XS) was launched onboard the Indian Space Research Organisation (ISRO) Chandrayaan-1 lunar mission in October 2008, and put into a ~100 km circular polar orbit around the Moon on the 12th November 2008. The primary purpose of this instrument was to map the lunar surface over the energy range of 1 – 10 keV, to find the distribution of elements such as Mg, Al, Si, K, Ca, Ti and Fe. The instrument consisted of 24 swept-charge device silicon X-ray detectors providing a total collecting area of ~24 cm^2, corresponding to a 14° field of view (FWHM), with the ability to measure X-rays from 0.8 – 20 keV.

During the 10 months the spacecraft was located in orbit around the Moon a number of solar flare X-ray events were detected, along with calibration data from X-ray sources housed inside the movable door of the instrument. Collection of such calibration data is important for monitoring the impact of space weather, in particular radiation damage, on the operational performance of the detectors. This research presents a study of the degradation in spectral resolution of the measured X-ray calibration lines, comparing those recorded at intervals during the mission lifetime with ground based calibration data collected prior to the launch of the instrument.

Methodology/Approach

In order to measure any degradation in spectral resolution, the calibration data of each detector from a specific time period must first be added and converted from raw data in bins to a full ADC scale spectrum. An example of raw data from a single detector can be seen in the plot below. The data were collected over a 10 minute period.

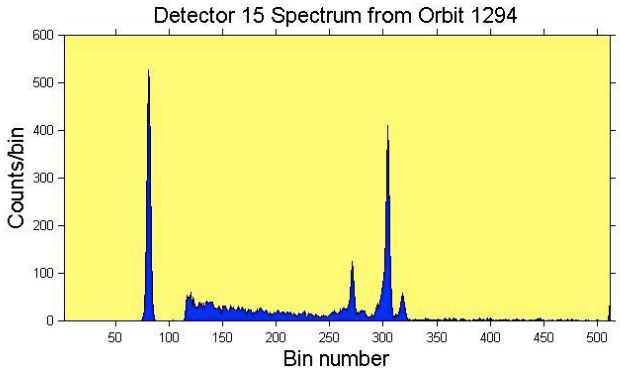

The plot shows a noise peak around bin 80 and several detected peaks between bins 250 and 350. The peaks are being produced by ^{55}Fe sources located on the inside of the instrument door.

This raw data must be converted to ADC channels before being converted to an energy scale. The reason for this is the spectrum is formed by grouping adjacent A/D conversion levels to give 512 energy bins. The number of ADC conversion levels that make up each bin is given in the following table.

Width	Bin Numbers
4	0 to 249
8	250 to 387
16	388 to 510
24	511

The bins are divided by their respective width to give an x-axis scale in ADC channels from 0 – 4095 as shown in the following plot.

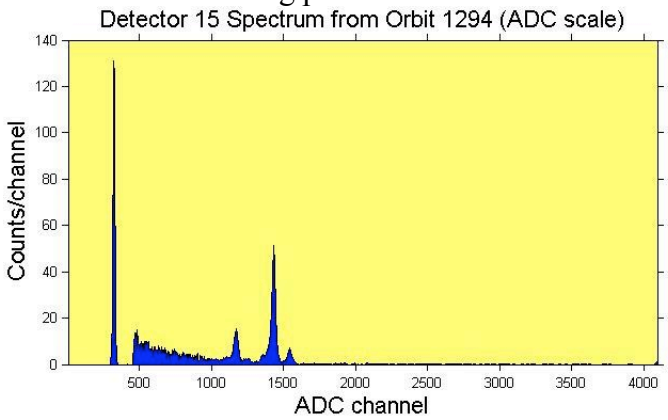

From a full ADC channel spectrum, an energy scale can be calculated using the position of the noise peak and the position of the known X-ray lines to calculate the gain of the detector in eV/channel.

The peaks are fitted with Gaussian functions to locate the peak channel in each case. At this stage it is possible to look at the change in energy resolution of a single detector throughout the duration of the mission by fitting the Manganese Kα peak in energy space and measuring the FWHM of the line for each calibration data set. If radiation damage has occurred to the device, a broadening of the FWHM should be seen in the on orbit data compared with the ground calibration data.

To measure over the instrument as a whole, the separate detector spectra need to be co-added into a master energy scale of all 24 detectors, accounting for the different detector gain values.

Results and discussion

The following plot shows the spectrum of detector 15 after it has been converted to an energy scale.

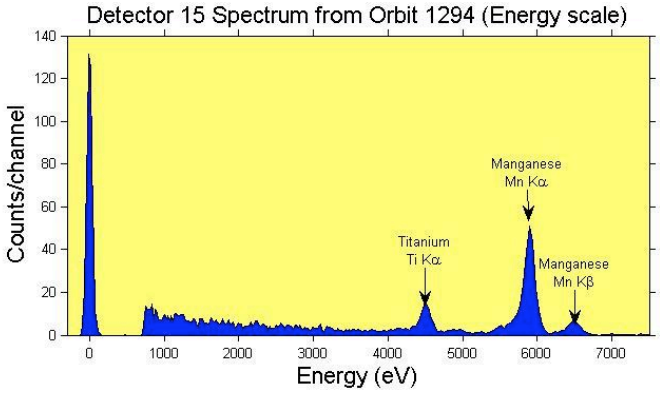

At the current stage of research, calibration data from all detectors for orbit 1294 have been converted to their individual energy scales and from this data, a master spectrum will be created to measure the on orbit changes in FWHM of the Mn Kα peak across the whole focal plane to assess the impact of radiation damage.

Conclusion

From the data obtained so far, and due to the low activity of the Sun during the time of the mission, it appears that the C1XS instrument was subject to little radiation damage and overall performed exceptionally well.

The calculated detector gains from orbit 1294 displayed in the following plot are in good agreement with measurements taken before the mission.

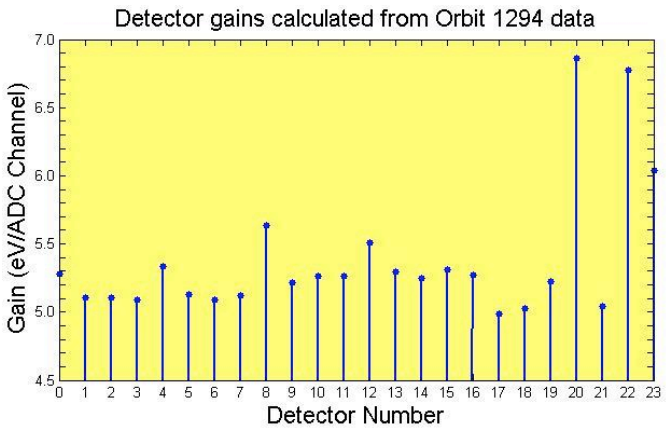

The next step of the research is to convert ground calibration spectra to energy scale in order to compare with the data taken in orbit 1294. The FWHM of the Mn Kα line in both sets of data will then be measured to determine the radiation damage.

It is important to understand the radiation damage of the instrument as a whole when analysing the science data, as the scientific performance will change dependant on the amount of damage done. In particular, the Mg and Al lines at 1254 eV and 1487 eV respectively, are important for lunar science studies and are the first lines to be blurred together following radiation damage.

References

1. D. R. Smith, J. Gow, "The effect of protons on the performance of swept-charge devices", *Nuc. Inst. Meth.*, vol. A604, (2009), pp. 177-79.

2. D. R. Smith, J. Gow, A. D. Holland, "Proton Irradiation of Swept-Charge Devices for the Chandrayaan-1 X-ray Spectrometer (C1XS)", *Nuc. Inst. Meth.*, vol. A583, (2007), pp. 270-77.

3. M. Grande, et al., "The C1XS X-ray Spectrometer on Chandrayaan-1", *Planetary and Space Science*, vol. 57, (2009), pp. 717-24.

4. C. J. Howe, et al., "Chandrayaan-1 X-ray Spectrometer (C1XS) – Instrument design and technical details", *Planetary and Space Science*, vol. 57, (2009), pp. 735-43.

5. I. A. Crawford, et al., "The scientific rationale for the C1XS X-ray spectrometer on India's Chandrayaan-1 mission to the moon", *Planetary and Space Science*, vol. 57, (2009), pp. 725-734.

SED Research Student Conference
Brunel University
2[1st]-23[rd] June 2010

Representing Unstructured User Data for Inclusive Design

Farnaz Nickpour [1], Hua Dong [2]
1. Inclusive Design Research Group, School of Engineering and Design,
Brunel University, Uxbridge, Middlesex, UK
2. Human Centred Design Institute, School of Engineering and Design,
Brunel University, Uxbridge, Middlesex, UK
farnaz.nickpour@brunel.ac.uk

Keywords (4): Inclusive Design, Unstructured Data, User Data, Designers

1. Introduction

Inclusive design is an approach to the design of mainstream products and services that are 'accessible to and usable by as many people as reasonably possible, without the need for adaptation or specialist design' [1]. User data needs to be properly communicated to designers when setting up user-centred design specifications. In many cases, first hand field data need to be accurately and effectively communicated to designers. Such data is mostly unstructured primary data in pictorial, audio, visual or textual formats collected by researchers and need structure and organisation. Unstructured data are an important source of input in various stages of the design process specifically in the 'discover' and 'develop' stages, described in the Double Diamond model [2]. Challenges will arise in the process of structuring such data.

This paper reflects on the opportunities and limitations in the process of representing unstructured user data for designers. A real world design case study is discussed where primary data were collected through observation, video ethnography, interview and questionnaire in hospitals. The researchers applied a database construction tool to create a data structure that could embody the rich primary information collected from various hospital stakeholders (i.e. patients, nurses and visitors).

2. Methodology

In order to create a data structure to embody rich primary unstructured data, it is possible to either employ an already existing database construction tool or create a new database tool. However, the potentials and limitations of existing database construction tools in representing unstructured user data needed to be explored and studied before creating a totally new tool, therefore, an already existing relevant database tool was used in the study. The Cambridge Engineering Selector (CES) Constructor was employed to represent the unstructured data collected in a real world design study. A real world design project was selected where firstly, a group of researchers from various backgrounds collected primary data about diverse hospital stakeholders (i.e. patients, nurses, porters, and visitors) through observation, video ethnography, interview and questionnaire. These primary unstructured data were then presented to several design consultancies who were commissioned to address specific design briefs regarding patients' dignity in the hospital environment.

3. Results and discussion

The authors started processing the hospital data report in order to explore potentials for embodying it into the CES constructor. A number of opportunities and challenges were observed throughout this process. These issues are briefly discussed below.

3.1 Strengths & Opportunities

The data available in the report was large in volume, lacked structure and was difficult to browse. Some parts of the information provided lacked relevance; however, the designers had to skim through the whole report to find the relevant and useful bits of information. By categorizing the information and creating tables, sub-categories and forms, it was easy to identify the relevant data.

Following the structural logic of the CES software, the authors were encouraged to think analytically and to develop a 'data model' by breaking down the chunks of unstructured data into separated sections. This could support developing an information system which would make the data more explicit, accessible and hence usable.

One major benefit of using the CES structure was the opportunity to classify quotes and images from various stakeholders under various categories at the same time, i.e. the issues each addressed, the stakeholder, the hospital. It was also possible to link the relevant categories; for example linking the quote from a patient regarding lack of hygiene to a photograph from the ward visualizing the same issue.

3.2 Challenges & Limitations

By putting unstructured data into a structured format, it is inevitable to limit the analysis of the data to the logic and mental model of the analyzer (here the researcher who populated the CES software). Given the original unstructured report, various researchers would have come with various mental models in terms of how to classify, analyse and structure the data. Therefore the database could look and work totally different based on each developer's way of interpretation.

In this case, the concern was that the researchers structuring the data may not necessarily share the same mental model with designers who the database was aimed at. It is also worth considering the differences among various designers in terms of approach to working with data and interpreting it.

One limitation was the interface design of the CES software. The CES has been designed and developed by engineers and is mainly aimed at engineering design students, therefore, it has a typical engineering-minded interface. The interface follows a mental logic which is not necessarily compatible with designers' way of processing the data. The current structure also has certain limitations as it is dependent on what data have been collected and is very project-specific.

The other issue is designers' tendency to have access to the original data as well as processed and structured information; designers appreciated structured data in reality but they also wanted to have raw data as a backup.

4. Conclusion & further work

It is argued that despite major benefits of structuring the unstructured user information (in both visual and textual formats), certain qualities of such rich data are lost in the process of sorting and interpretation. An ideal tool is suggested to enable the designer to see the big picture through structuring the information as well as providing access to the raw data.

References

[1] BSI. (2005), Design Management Systems Part 6: Managing Inclusive Design Guide. British Standards Institute
[2] Design Council, (2005), The Double Diamond Model. Available at: http://tiny.cc/fTQcJ. Date viewed: 01.03.2010

SED Research Student Conference
Brunel University
21-23rd June 2010

Novel Game-Theoretic Cross-Layer Scheduling for Single-Cell OFDMA Systems with Heterogeneous QoS and Partial CSIT[1]

Charilaos Zarakovitis, Qiang Ni
Electronic & Computer Engineering, School of Engineering & Design
Brunel University, Uxbridge, Middlesex, UK
Charilaos.Zarakovitis@brunel.ac.uk

Keywords: cross-layer design, Nash bargaining solution, resource allocation

Introduction

This paper proposes a novel game-theoretic cross-layer design for orthogonal frequency division multiple access (OFDMA) wireless networks, which operates optimal subcarrier, power and rate allocation. Based on the Nash bargaining solution (NBS) and coalitions, the proposed scheme not only maximizes the system's effective data rate but also supports proportional fairness among the users by considering the heterogeneity of their requirements, as well as the rate outage due to imperfect channel state information (CSI) available at the transmitter (CSIT). Our simulation results confirm that the proposed scheme achieves an optimum trade-off between effective data rate and proportional fairness, while it guarantees the quality of service (QoS) requirements, and outperforms existing solutions [1-3] in terms of power consumption, resilience to CSIT errors and stability.

Methodology/Approach

An intelligent medium access control layer (MACL) accounts the data outage, described by the target outage probability P_{out}, caused by the imperfect channel realization $\hat{h}_{ij}$ of user $j \in K$ on subcarrier $i \in N_F$ at the physical layer (PHYL), as well as the various QoS requirements Q_j from the upper layers' applications. Following appropriate adaptation of the PHYL's and the queuing model's parameters, we use cooperative game theory and through a proper bargaining rule $S_{NBS} | \Phi \to \Im^K$ we design a fair and efficient QoS guaranteed resource allocation scheme based on each user's utility function f_j, with $U = \{ f_j(\psi) \,|\, \psi \in \Psi \}$ defined on a subset $\Im^K$ of termed Ψ. The intuitive idea is that, after the minimal requirements u^0 are satisfied for all users, the remaining resources are allocated proportionally to the users according to their channel conditions and classes $\Phi = \left[U, u^0 \,|\, U \subset \Im^K \right]$. After performing dexterous maximization of the optimization objective, subject to realistic system's parameters, we implement our model by utilizing the derived joint optimal dynamic subcarrier allocation (DSA) and adaptive power allocation (APA) policy, fostered by a rapid global convergence iteration process.

[1] This work is jointly funded by the UK Engineering and Physical Sciences Research Council (EPSRC) and Motorola Ltd under Grant No 07000486 and EP/G070350/1.

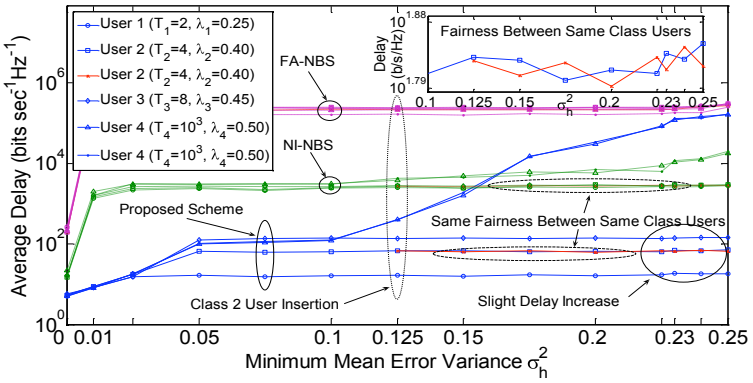

Figure 1: Average Delay vs. CSIT imperfectness (σ_h^2) in a system of P_{out}=0.01, N_F=6 and total available power to the BS (P_{TOTAL}) 10dB.

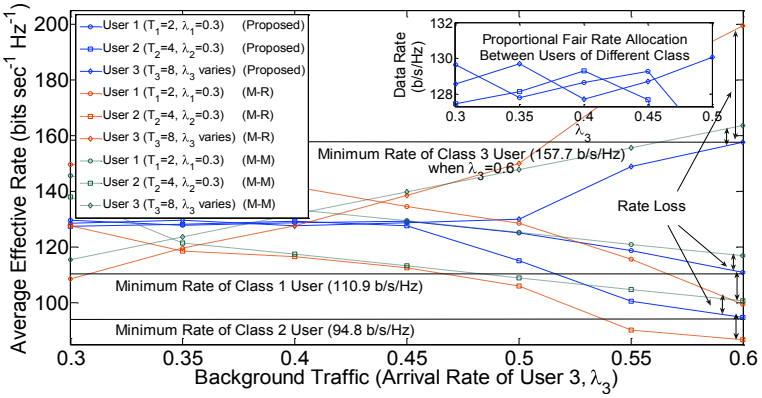

Figure 2: Data Rate vs. background traffic loading (λ_3) in a system of $\sigma_h^2 = 0.05$, P_{TOTAL}=-11dB, P_{out}=0.01, N_F=6.

Results and discussion

Performance comparison with existing approaches show that our scheme offers higher resource management efficiency along with superior service stability even when the channel imperfectness and background traffic load are medium to significantly high i.e. Figures 1 and 2.

Conclusion

In this paper has been briefly described, a novel NBS-based cross-layer OFDMA design framework for both delay-sensitive and delay-insensitive users under QoS heterogeneity, packet outage, CSIT imperfection and fairness criteria. The proposed scheme establishes an excellent settlement between effective throughput and equity by enhancing system's data rate, ensuring fairness provision and guaranteeing all the prescribed QoS requirements of the heterogeneous users. The extended version of this paper has been accepted by the IEEE ICC'10 conference [4], and its journal version is planned to be submitted to the IEEE Transaction on Communications.

References

[1] E. Hahne. "Round-Robin Scheduling for Max-Min Fairness in Data Networks," IEEE Journal on Selected Areas in Communications, Vol. 9, No. 7, Sept. 1991, pp 1024- 1039.

[2] H. Yin and H. Liu, "An efficient multiuser loading algorithm for OFDM-based broadband wireless systems", IEEE Globecom 2000, Vol.1, pp. 103-107, 2000.

[3] Z. Han, Z. Ji, and K. J. R. Liu, "Fair multiuser channel allocation for OFDMA networks using nash bargaining solutions and coalitions," *IEEE Trans. Commun.*, vol. 53 no.8, pp. 1306–1376, Aug 2005.

[4] C. C. Zarakovitis, Q. Ni, D. E. Skordoulis "A Novel Game-Theoretic Cross-Layer Design for OFDMA Broadband Wireless Networks", IEEE ICC'10 proceedings, Cape Town, South Africa, accepted in Jan. 2010.

SED Research Student Conference
Brunel University
21-23rd June 2010

The Use of Sustainable Materials and Designs to achieve Affordable Housing in Developing Countries. (A case study of Nigeria).

Eboziegbe Patrick Aigbomian
Mechanical Engineering, School of Engineering and Design, Brunel University, Uxbridge, Middlesex, UK
Email - eboziegbe.aigbomian@brunel.ac.uk

Keywords: Sustainable; Affordable; Housing; Materials; Wall panels
The primary conference subject area: Performance of Sustainable Housing for developing Countries

INTRODUCTION

Many countries face the problems brought about by the increasing pressure of urbanisation as the pace of their economic development increases. In the last two decades, Nigeria has witnessed an incredible increase in the rate of urbanization. Early Fifties census showed that there were about 56 cities in the country and about 10.6% of the total population lived in these cities [1]. This rose dramatically to 19.1% in 1963 and 24.5% in 1985. From the last head count in 2006, the national population is now estimated to be about 120 million with the urban population constituting about 30%. Given the expected increase in urban population, the magnitude of housing problem in the country is enormous. According to the National Rolling Plan (NRP), the national housing requirement is between 500,000 and 600,000 units considering the prevailing occupancy ratio of between three and four persons per room [2,4]. If this estimated annual requirement was to be provided at an average of N500, 000 per unit which is rather conservative, the costs would be enormous and indeed unrealisable. The cost of providing housing alone would be between N250 Trillion and N300 Trillion which is excluding the cost of infrastructural development [3]. With extraordinary rise in population, number and size of Nigeria cities over the past few years, there is acute shortage of dwelling units which has resulted in overcrowding, high rents, poor urban living conditions, and low infrastructure services and indeed high crime rates.

Fig A shows a cross section of buildings in Nigeria sorely built on cement which at the moment is not only an expensive material with the present economic situation of the country but also a heavyweight material that adds to the load bearing capacity of the entire building envelope. Studies shows that Nigeria will need about 8.5million metric tonnes yearly in order to meet up to the present demands of housing. While cement companies in the country are only able to produce about 2-3million metric tonnes. This however accounts for the galloping cost of cement every year which is the main factor that has led to the high

construction cost in Nigeria amongst other reasons. While Nigeria does not produce enough cement domestically to meet demand, imports have been restricted and subject to a process of quota allocation which has led to sharp increases in the price of cement. According to recent survey, Nigeria is the world largest importer of cement even with restriction with about 70.5% dependence on importation. The chances of the local industry rising to the task remain very slim as only four out of the seven of the cement companies in the country are still limping along at various levels of capacity utilisation.

The primary aim of this research is therefore to achieve a low-load bearing capacity material for buildings with the use of lightweight materials (wood and bamboo sourced locally) as most buildings in Nigeria are built with heavyweight materials e.g. concrete and block. Thus this research also aims at reducing energy consumption, improving thermal conductivity and reducing heat absorption of wall panels whilst creating a built environment that meets people's needs across all levels of income; provides affordable and healthy homes. Assumptions will be tested through accurate modelling and use of tools such as BREAM and LEED (modified).

Designs will be made of local materials and building methods as well as local building conditions and lifestyles to achieve a high standard of wall panel to be used for construction.

Fig.A [5,6,7]

Design Concept and Theoretical Results

With average temperature of Nigeria ranging from 23 – 32 degrees Celsius and up to 42 - 48 degrees Celsius in some areas, the concept design of the wall panel is focused mainly

on the climatic condition of Nigeria. As a result, considerations have been made to designing a single panel in 3 phases namely Reflection, Absorption and Penetration. Figs 1, 2 and 3 shows a proposed panel with outer plane as phase 1 (Reflection), phase 2 (conduction layer) and phase 3 inside coating which helps to stop penetration. When sun light hits the surface of the panel as some amount of heat goes through the material, a certain amount is also absorbed. The material in the conduction layer helps to convert/store this heat while the final layer helps to trap any amount of temperature still travelling through this material.

Based on theoretical/calculated results, we propose a concept of wall panels and materials which is appropriate for developing countries. The appropriate conditions refers to both having a lightweight material with good thermal environmental properties that the utilization of the concepts will produce a lesser load bearing material. The basic principle of the proposed sandwich wall-panel design is based on three mechanisms of heat transfer, namely

1. Reflective surface to act against direct solar radiation.
2. Wall shaft to conduct convective cooling
3. Thermal insulation to avoid heat transfer through the material.

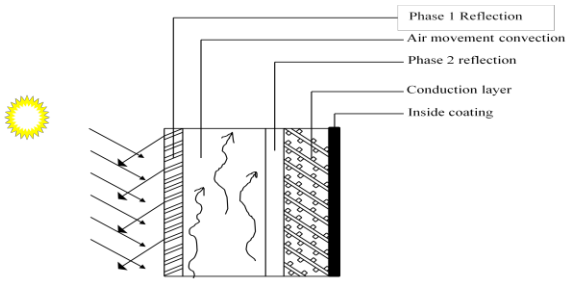

Fig 1

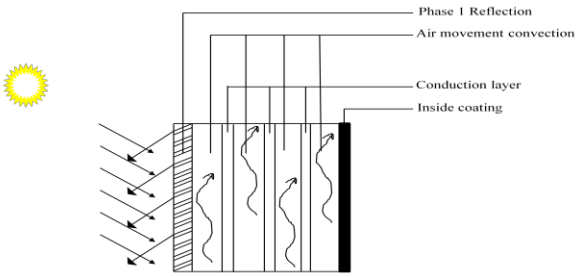

Fig 2

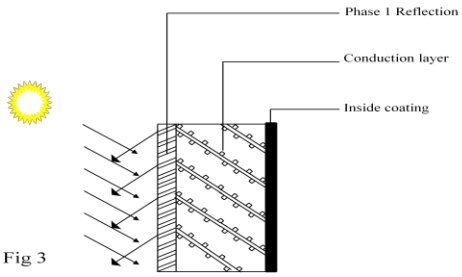

Fig 3

Existing calculation for hollow blocks which is the primary construction material in Nigeria shows a U-Value of 2.09 W/m^2K and a thermal Resistance of 0.48 m^2K/W. Comparing these values with the values of sandwich panel in Fig 3, made with glass, polyurethane foam and wood we discover that the material provides more thermal resistance than the hollow blocks.

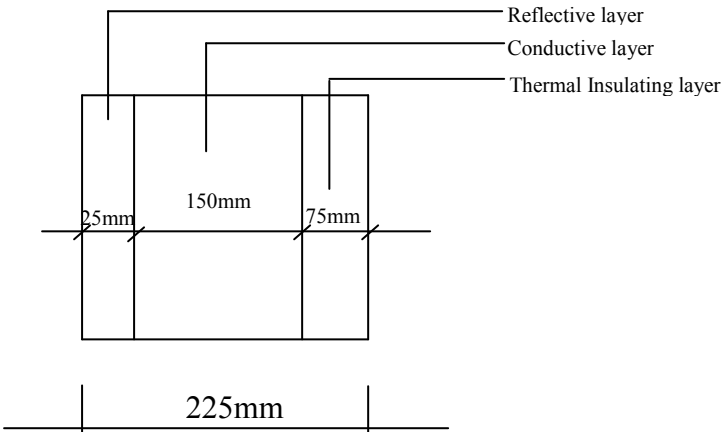

Proposed Measurement of sandwich wall panel in fig 3.

Theoretically,

Reflective area made of coated glass = 25mm

Conductive area made of polyurethane = 150mm

Insulating area made of wood = 75mm

Rg = 25mm (0.025m) / 0.8 (thermal conductivity of Glass) – Assumption

= 0.031 m²K/W

Rp = 150mm (0.15m) / 0.023 (thermal conductivity of Polyurethane)

= 6.523 m²K/W

Rw = 75mm (0.075m) / 0.17 (thermal conductivity of hard wood)

= 0.294 m²K/W

Total thermal resistance of Material = 0.031+6.523+0.294

= 6.848 m²K/W

U-value of sandwich panel 1/6.848

= 0.146 W/m²K.

CONCLUSIONS

From calculation of the U-Value of the proposed sandwich panel, an inappropriate use of building materials will reduce the quality of environment and raise negative implication such as higher energy consumption. Conclusively, heavyweight building materials are inappropriate for buildings due to its load bearing nature and its high heat capacity that could change the outdoor thermal environment. While designing wall panels for tropical countries, concentration needs to be paid to design concept due to the nature of sun path in the tropics and in addition, lightweight sandwich wall panel with low heat capacity, low load bearing capacity, high thermal insulation and high reflective outer surface is appropriate due to the tropical extreme heating condition.

REFERENCES

1. CBN (1990-1998) Annual Report and Statement of Accounts, Central Bank of Nigeria; Abuja.
2. Federal Republic of Nigeria 2006 Population Census Available from http://www.nigerianstat.gov.ng/Connections/Pop2006.pdf. (Accessed on 15/01/2009).
3. Oduwaye. A.O (1998): Beyond Structural Adjustment Programme: Strategic Options for increasing Housing Stock in Nigeria
4. Joseph Segun Ajanlekoko: Sustainable Housing Development in Nigeria – The financial implication. International Conference on Spatial Information for Sustainable Development Nairobi, Kenya.
5. Goshen Beach Estate, Lekki Lagos. Available from http://images.google.co.uk/imgres?imgurl=http://static.panoramio.com/photos/original/15276157.jpg&imgrefurl=http://www.panoramio.com/photo/15276157&usg=__AfWgD2_NZI5f381WvMh_3UQQbUM=&h=1372&w=2058&sz=1175&hl=en&start=11&um=1&itbs=1&tbnid=wdLu_kowSowukM:&tbnh=100&tbnw=150&prev=/images%3Fq%3Destate%2Bin%2Blagos%26um%3D1%26hl%3Den%26tbs%3Disch:1. Accessed on 15th of March, 2010
6. Nigeria Concrete Home Construction - Posted by Carl Engelken on April 24, 2009 at 12:53pm. Available from http://www.buildingsystems.com/profiles/blogs/nigeria-concrete-home. Accessed on 15th of March, 2010.
7. Residential housing Units – Real Estates. Available from http://www.lagos-nigeria-real-estate-advisor.com/images/banana-island-suite-of-flat.gif. Accessed on 20th March, 2010

SED Research Student Conference
Brunel University
21-23rd June 2010

Long Range Ultrasonic Testing Using Chirp and Broadband Excitation Techniques

Keith Thornicroft[1,2], Alex Haig[2], Cristinel Mares[1], Phil Catton[2]
1. Mechanical Engineering, School of Engineering and Design, Brunel University, Uxbridge, Middlesex, UK. keith.thornicroft@twi.co.uk
2. NDT Technology Group, TWI Ltd., Granta Park, Great Abington, Cambridge, CB21 6AL.

Keywords (4): Long range ultrasonics, Chirp, Linear frequency modulation, Broadband

Introduction

Long range ultrasonic testing (LRUT) is a relatively new development within the non-destructive testing sector. Traditionally, conventional ultrasonic testing (UT) methods are operated at high frequencies and are capable of detecting small flaws within a range of millimetres whereas long range ultrasonic inspection is carried out at lower frequencies and is capable of highlighting structural detail and discontinuities tens of metres from a test position [1]. Conventional ultrasonic testing relies on the transmission of bulk waves, the velocities of which are independent of frequency and can be predicted easily if the properties of the material under test are known. The dynamics of waves involved in LRUT, however, are dependent upon frequency making the analysis of received data from a specimen complex [2]. It is usual practice to choose a wide selection of test frequencies in order to gather information on the behaviour and condition the specimen. This 'frequency sweep' method of testing is lengthy and produces a large amount of data for processing. The efficiency of such a test could be raised by modulating the frequency content of the signal transmitted. This process is effectively a pulse compression and for this study a linear chirp signal is considered. A broadband signal approach has been used widely in RADAR pulse generation as a method of solving the problem of power limitation with respect to spatial resolution [3] but its potential has not been fully investigated for the generation of a variety of elastic wave modes in solid media.

Methodology/Approach

The test piece used for the initial tests was a steel pipe with an internal bore of 200mm, 4.1m long and a wall thickness of 8.179 mm with no defects. The array of transducers was positioned 2.5m from one end of the pipe, with 24 equally separated elements encircling the circumference. A compressive load of about 100N on all 24 transducers was ensured by pneumatic pressure. Within the array the transducers were orientated so that displacements would be in the theta direction, exciting torsional wave modes. The pulser/receiver used for the tests was the Teletest® Mk.3 unit which has the ability to accept modified excitation parameters such as the chirp waveform.

The first step in this investigation was to modify the existing waveform used by commercial LRUT equipment to accommodate the chirp feature. This was achieved by developing and validating the excitation signal using MATlab. A linear sinusoidal chirp was generated with a Hann window applied. The signal had a frequency bandwidth between 20 kHz and 80 kHz. A set

of comparison tests sequentially swept between this frequency bandwidth could then be carried out based upon normal test conditions; this is a lengthy process and could be significantly reduced by using a single chirp test. The data collected was then used as a baseline for subsequent chirp tests.

Results

Figure 1 displays the input signal generated in MATlab. All of the parameters used in generating this waveform can be modified to suit a range of tests. This particular waveform has been truncated from the pure sinusoidal form using a Hann window. A Fast Fourier Transform (FFT) was performed on the input signal in order to determine the frequency content and it appears that the FFT magnitude values concur with the waveform displayed in the time domain (*figure 1)*. The A scans produced from the chirp tests show that the frequency content within the reflected features still retains a linear frequency modulation *(see figure 2)*.

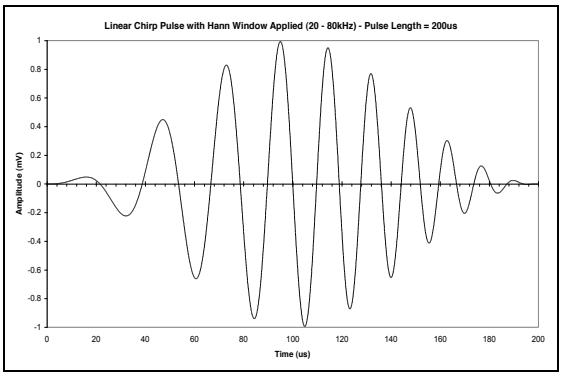

Figure 1: The input signal clearly showing the change in frequency over the pulse duration (200**µs).**

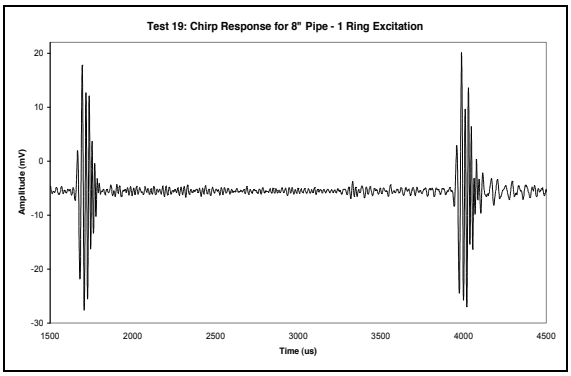

Figure 2: The received signal from a chirp test on the specimen. The reflection on the left represents the near end T(0,1) reflection and the right-hand feature is the far end T(0,1) reflection.

Conclusion and Further Work

An analysis of the received signals shown in figure 2 indicates that the signal has retained the frequency modulation feature. However the measured amplitudes in the 25 - 30 kHz region of the pulse are distorted due to the resonant properties of the transducers used. Although the arrival times for the reflections appear at the predicted times the frequency content of each reflection will lead to a phase velocity and therefore a particular wave mode. This can be achieved through wavelet analysis or a short-time Fourier transform in order to locate local arrival time behaviour. This in turn will display the frequency dependant nature of the specimen and should correlate well with analytical predictions. If this behaviour can be predicted and a number of modes can be identified within one reflection then the time taken to carry out a test will be reduced considerably.

References

[1] Rose, J. L., "An Introduction to Ultrasonic Guided Waves", *4th Middle East NDT Conference and Exhibition,* Kingdom of Bahrain, December 2007.

[2] Rose, J. L., "Dispersion Curves in Guided Wave Testing", *Materials Evaluation,* January 2003, pp. 20 - 22.

[3] Pollakowski, M., Ermert, H., von Bernus, L. and Schmeidl, T., "The Optimum Bandwidth of Chirp Signals in Ultrasonic Applications," *Ultrasonics*, Vol. 31, No. 6, 1993, pp. 417 – 420.

SED Research Student Conference
Brunel University
21-23rd June 2010

Inspection of Defects in Storage Tanks using Ultrasonic Guided Wave Inspection

Balraj Ghataore[1, 3], Rajagopal Nilavalan[2], Ray Kirby[1], Phil Catton[3], Devashish Fuloria[3]
1. Mechanical Engineering, School of Engineering and Design, Brunel University, Uxbridge, Middlesex, UB8 3PH, UK
2. Electronic and Computer Engineering, School of Engineering and Design, Brunel University, Uxbridge, Middlesex, UB8 3PH, UK
3. NDT Technology Group, TWI Ltd, Granta Park, Great Abington, Cambridge, CB21 6AL, UK

Keywords (3): Ultrasonic Guided Waves, Storage Tank Inspection, Non-destructive Testing

Introduction

Failure of storage tanks can have catastrophic consequences as the leakage of potential hazardous substances pose a risk to human health and damage to the environment. Storage tanks therefore need to be non-destructively inspected to ensure that the tank is defect free. Currently used Non-Destructive Testing (NDT) techniques provide good results, however to carry out such tests require the tank to be emptied of potential hazardous chemicals. This leads to large time periods where the tank is out of service which results in an associated financial cost to the operating company.

Ultrasonic guided waves for the non-destructive testing (NDT) of elongated geometries with simple cross sections, such as pipes, rods and rectangular beams have been extensively researched [3]. The physics of guided waves are particularly useful for Long Range Ultrasonic Testing (LRUT) as they exhibit very low attenuation and therefore can travel greater distances than conventional, high frequency ultrasonic bulk waves. Guided waves can be used to detect changes in cross sectional area which is very useful to assess the level of corrosion and cracks [3]. The applications of guided waves have not been fully explored and this research aims to explore the possibility of the use of guided waves in non-prismatic structures that do not have a continuous cross section.

Guided waves have the ability to propagate through the floor of the tank without the tank being emptied as guided waves can travel through structures that are partially inaccessible. As such, there is a possibility that guided waves could be used to inspect the floor from the outside of the tank preventing any downtime and the resultant financial implications.

Methodology/Approach

The tank can be simplified as a large cylinder (walls of the tank) attached to circular plate (floor). Therefore to begin to understand the inspection of a tank floor, a circular plate of a similar geometry is considered.

Fig 1: Scaled down model of Storage Tank produced for experimental purposes.

Using piezoelectric transducers at apposing ends of the diameter of the tank, it is possible to inspect the whole floor of the tank and the weld which crosses the floor. It is thought that transducers in a 'pitch and catch' formation (Transmitter and Receiver are at opposite sides of the plate) would work best compared to a single transducer location. Before the transducers are attached to the tank, an approximate 150mm by 70mm area on the rim (Shown in Fig 1) is surface treated by using increasing grades of emery paper and acetone to ensure a smooth and reliable contact surface. The transducers are then attached to the rim whilst ensuring that the excited wave and the reflected wave from the outer edge of the circular plate are superimposed. This is done by placing the transducers a distance of $\lambda/4$ away from the outer edge of the rim. λ (wavelength) can be calculated from the equation below where C is the phase velocity of the wave (which can be found on a dispersion curve) and f is the frequency that phase velocity C occurs.

$$C = \lambda f$$

Results and discussion

Experiments are underway and are yet to yield conclusive results. However, similar approaches have been used in other applications to good affect. Potential areas of improvement and further work have been identified, such as using Macro fibre composites (MFC) transducers and Electromagnetic Acoustic Transducers (EMAT).

Conclusion

Guided waves can travel across the diameter of a circular plate and there is promise that guided wave technology can be applied to non-prismatic and complex structures.

References

[1] Krautkramer, J. & Krautkramer, H., 1969. *Ultrasonic Testing of Materials*. 1st Ed. Springer-Verlag

[2] Cawley, P. & Castaings, M., *The Generation, Propagation, and Detection of Lamb Waves in Plates using Air-Coupled Ultrasonic Transducers.* Journal of the Acoustical Society of America, 100(05), pp3070-3077.

[3] Rose, J. L., *An Introduction to Ultrasonic Guided Waves*. In Penn State University, 4th Middle East NDT Conference and Exhibition. Kingdom of Bahrain. December 2007, Penn State University, USA.

SED Research Student Conference
Brunel University
21-23rd June 2010

Parameter Investigation of Rheo-Extrusion Using AZ91D Alloy

CASSINATH Zen, XIA Ming-xu, FAN Zhongyun
BCAST, Brunel University, Uxbridge, Middlesex, UB83PH, UK
Zen.Cassinath@brunel.ac.uk

Keywords: Semi-solid shaping, Rheo-extrusion, Counter rotating twin screw extruder

Introduction

Rheo Extrusion is a novel technology developed at BCAST and marks significant progress made in the methods of semi solid processing and final net shaping to produce extruded bars/rods with a highly refined microstructure [1].

This technology, based on a counter rotating twin screw extruder, is being studied as a possible supplementary process for conventional extrusion, which saves both, cost and energy consumption by combining slurry making and extrusion into one step. Rheo-extruded AZ91D bars were continuously produced at a semisolid temperature. Microstructural analysis reveals that the extrudates had a uniformly fine microstructure in both transitional and longitude directions. Low extrusion temperature effectively suppressed the formation of the continuous eutectic and intermetallic phases. The detailed microstructural observation suggests a high temperature deformation character with twining and grain boundary migration occurring.

The rheoextruder consists of two counter rotating screws in a heated barrel that deliver shear to a melt. Due to the nature of the flow within the barrel a differential pressure is built up which causes the melt to be pumped out of the barrel and through an extrusion die where it solidifies.

This Extended abstract presents the results of the initial settings investigated in order to optimise this relatively newly founded process. Based on previous studies [2], parameters such as pouring temperature, barrel temperature and RPM have been varied to measure the effect on over all grain size and porosity in cross sections of samples taken from bars.

Methodology

Commercial AZ91D alloy with a nominal composition of Mg-9 wt pct Al-1 wt pct Zn-0.3 wt pct Mn was used in this study. The alloy was melted at 680^{o}C and held at 650^{o}C for 30 minutes for homogenization. Different extrusion conditions were explored to produce rheo-extrudates with a required microstructure. The melting, transforming and extrusion were fully protected under the mixture atmosphere of N_2 and 0.5 wt pct SF_6.

At least three metallurgical samples for each condition were cut from the different lengths of the extrudates in order to investigate the uniformity along the extrusion direction. The specimens were grinded with SiC abrasive papers and polished with alumina suspension. A Zeiss optical microscope, Zeiss Axioskop2 (Zeiss Gmbh, Gottingen, Germany), equipped with a polarized light system was used for the optical microscopy. Both the transitional and longitudinal sections were investigated. To

evaluate the grain size and deformation twining samples were colour etched with picric acid. The linear intersect method was applied for the grain size measurement under the standard of ASTM E112-96.

Results and Discussion

Micrographs of the studied samples revealed that a low shearing speed produced minor developed dendrites and coarser grains and higher chamber temperature gave more chance to growth of grains. A semisolid pouring temperature reveals more porosity and developed dendrites, it is seen that higher pouring temperature can cause coarser grain size but reduce porosity as well. It was observed that porosity was controlled by the viscosity of the slurry. In conjunction to this, shearing speed has a direct coalition to viscosity, affects the slurry temperature near the outlet and is directly linked with the output. The general findings of the parameter investigation have been outlined in figure 1.

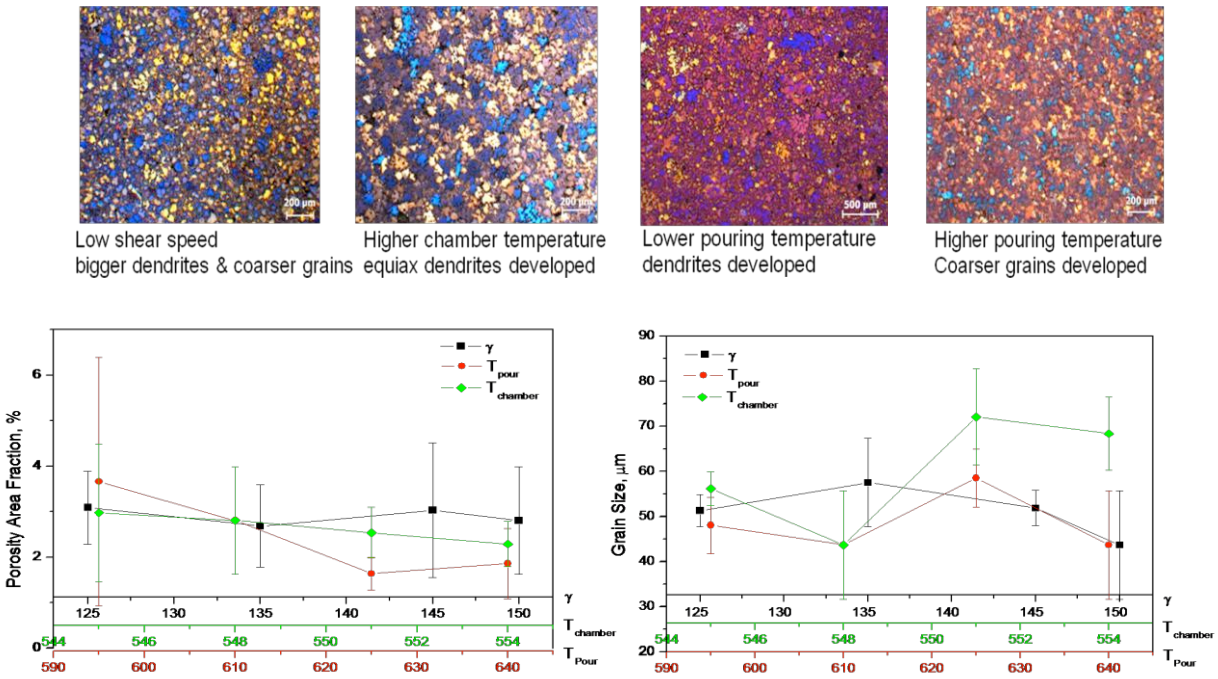

Fig.1 Findings of parameter investigation

Furthermore it was noticed that chamber temperature of the barrel affects pumping force as increasing chamber temperature reduces pumping force. Flight depth was observed to have a negative effect on pumping force even though increasing flight depth increases output. It was also observed that barrel length had no impact on the output, however, increasing barrel length can increase pumping force; and that increasing pitch length can increase both output and pumping force.

In order to achieve homogeneous deformation by conventional extrusion methods an extrusion billet needs to be well cast with an as fine and uniform as possible microstructure and homogenized for a long time. It is a cooling and reheating process with tremendous energy, time and manpower consumption costs. Moreover, solid state deformation depends on the deformability of the alloy. Even if the alloy is deformable, large plastic deformation still requires a number of process steps and large loads. Normal semisolid extrusion saves on the extrusion force but the slurry

making costs a fortune. The rheo-extrusion process uses a temperature interval during the solidification, which reduces not only the energy consumption for the billet production and homogenization, but also the extrusion force. It can push alloys to have a higher deformability and more complex profiles. The advantages of rheo-extrusion are summarised as:

- *Homogeneous deformation during the extrusion,*
- *Uniformly fine microstructure,*
- *Higher deformability of the processed alloys,*
- *High tolerance and complex profiles of the products,*
- *Compact processing procedure*
- *Energy, time and manpower savings*

Conclusions

A new rheo-extrusion technology based on a counter rotating twin screw extruder was introduced in this study. Commercial AZ91D alloy was pressed by using a prototype twin screw extruder. A continuous extruded bar was obtained with a smooth surface. The morphology of the extrudates was extremely fine and uniform along both transitional and longitudinal directions. The detailed observation reveals that the processed alloy was subjected to a high temperature deformation with typical twining across the grains. Furthermore, the low processing temperature, compared to the other semisolid processes, suppressed the formation of the eutectic and intermetallic phases, which are discontinuously distributed along the grain boundaries. The demonstration of AZ91D rheo-extrusion provides a supplement of a shortened extrusion process for alloys.

References

[1]. K.A. ROBERTS, Z. FAN, Development of Twin-Screw Rheo-Extrusion Proccess

[2]. FROST H, ASHBY M, Deformation mechanism maps [M]. Oxford: Pergamon Press, 1983.

SED Research Student Conference
Brunel University
21-23rd June 2010

Cracking of large hydrocarbon molecules using non-thermal plasma

I. Aleknaviciute[1], J. Cosgrove[2], T. G. Karayiannis[1] and M. W. Collins[1]

1. School of Engineering and Design, Brunel University, Uxbridge, Middlesex, UK
2. Professional Scientific LTD, ETTC Biospace, University of Edinburg, Edinburg

irma.aleknaviciute@brunel.ac.uk

Keywords: heavy hydrocarbons, hydrocarbon cracking, non-thermal plasma.

Introduction

Crude oil is a mixture of hydrocarbon compounds ranging from the smallest with only one carbon atom to the largest containing 300 and more carbon atoms [1]. Every refinery is uniquely designed to process given crude into selected products, with an increasing demand for high value petroleum products such as gasoline [2]. However, only a relatively small fraction of fuel in the gasoline range (3-12 carbon atoms) is contained within the crude oil [3]. To increase the yields of gasoline and other light fuels, large hydrocarbon molecules are broken down to smaller ones by thermal or catalytic cracking. The energy requirement for carbon to carbon (C-C) bond breakage in hydrocarbons is always lower than that for the carbon to hydrogen bonds, therefore cracking proceeds in the C-C bonds first. At moderate temperatures, cracking proceeds at the weakest hydrocarbon bond, which in the long chain is the C-C bond at the centre of the molecule. Thermal cracking occurs at high temperatures and may proceed with the same probability at all C-C bonds, hence reducing the control of product selectivity. Compounds resistant to cracking can block the active sites of the catalyst, and coke deposition may cause catalyst deactivation; both resulting in impaired catalyst efficiency and the need for regeneration [4]. Both thermal and catalytic cracking processes are very energy intensive and produce a considerable amount of air emissions such as SOx, CO, hydrocarbons, NO_2, aldehydes and ammonia, where catalytic cracking is one of the largest sources of air emissions in the refinery [3, 5].

Plasma is a term used to describe an ionized gas, consisting of positively and negatively charged particles with approximately equal charge densities [6]. Non-thermal plasmas are more selective and energy efficient than thermal plasmas, hence minimisation of electrical energy cost can be achieved with high productivities of the process. Non-thermal plasma systems can provide extremely high concentrations of energetic and chemically active species, keeping bulk temperatures as low as room temperature; ionization and chemical reactions are directly determined by electron temperature [7]. Cracking of hydrocarbon molecules can be achieved by plasma ionization of the hydrocarbon molecules by an impact of an energetic electron. The energy necessary to break a C-C bond at moderate temperatures in a large hydrocarbon molecule differs slightly depending on the bond position within the molecule [3], hence the ability of non-thermal plasma to keep low bulk temperature could allow higher selectivity over the position of the bond breakage. Non-thermal plasmas have

been experimentally shown to be viable for liquid hydrocarbon cracking [8]; however, in this study a rather complex plasma system was used and problems may occur to up-scale it. To this day, there is still very limited information and experimental results presented in the literature for the use of plasma in hydrocarbon cracking.

In the present study we will apply non-thermal plasma, namely corona discharge, to crack large hydrocarbon molecules in the liquid state into smaller ones. Corona discharge is formed on sharp points, edges or thin wires where the electric field is sufficiently large [9]. Hexadecane (containing 16 carbons) has been chosen as a model compound in this study because of its intermediate molecular weight and relative abundance in crude oil; it will be subjected to corona discharge plasma with the aim to break the molecule into smaller hydrocarbons. Our main objectives are to determine the parameters of the electron gas (valence electrons completely detached from their ions) to increase selectivity and control over plasma induced chemical reactions such as ionization in hydrocarbons, and gain deeper understanding and control of plasma effects on molecular bonds. The parameters that will be investigated in this study are: (i) the strength of the electric field and the energy consumption, (ii) the use of pulses, (iii) the temperature of the working media, (iv) the residence time of the reaction, (v) the inter-electrode distance and (vi) different configurations of the pin electrode.

Methodology

Hexadecane in a liquid state will be subjected to corona discharge in a pin-to-plate electrode configuration and the products will be characterised by Gas Chromatography Mass Spectrometer (GC-MS). Hence, the experimental facility can be divided into two major parts: plasma chamber and product analysis system. The plasma chamber consists of two 316 stainless steel disks, a stainless steel multiple pin electrode, borosilicate glass cylinder, C103 copper disk with integrated cartridge heater, in house built PID temperature control system, high voltage power supply (Matsusada, max output = 30kV, 5mA), vacuum pump (Edwards), pressure gauge and data logging system for temperature and pressure; see figures 1 and 2. The bottom stainless steel disk acts as a plate electrode and has an integrated well to position a measured amount of liquid hexadecane (refer to figure 1).

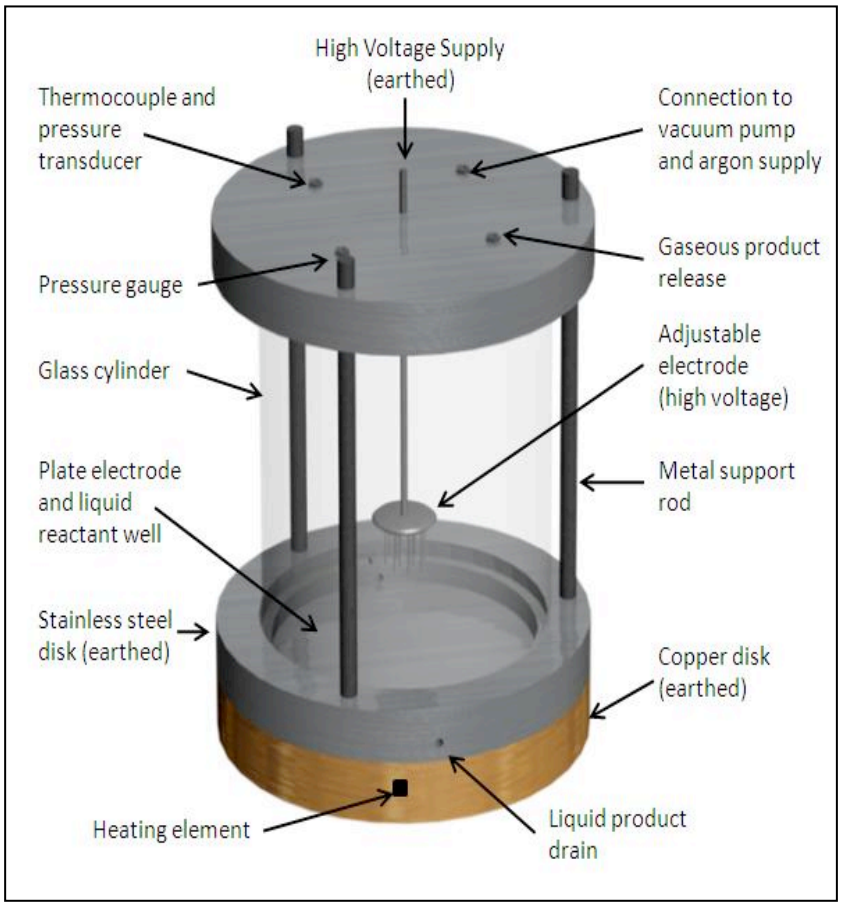

Figure 1: Plasma Chamber reactor design

Argon will be used as a working gas; high voltage direct current power will be supplied to the pin electrode initiating electrical break down of the argon gas and hence generating active plasma species such as electrons and ions. Cracking of hydrocarbon molecules will be achieved by plasma ionization of the hydrocarbon molecules by an impact of an energetic electron.

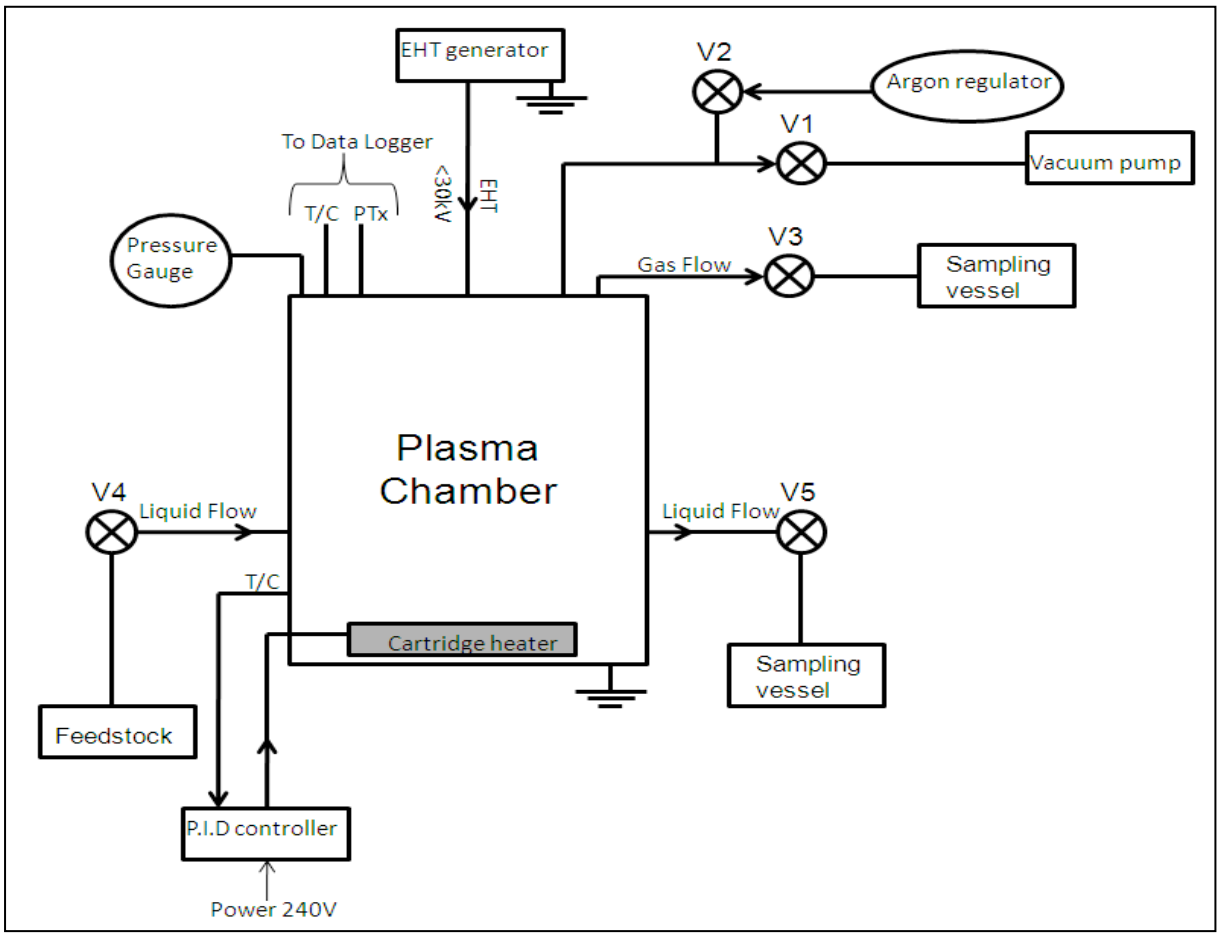

Figure 2: Corona discharge reactor schematic: V1-V6 - valves; T/C – thermocouple; PTx – pressure transducer. See Figure 1 for detailed 3D view of the plasma chamber.

Gaseous and liquid samples will be collected after each experiment and characterized by the GC-MS instrument comprised of Hewlet Packard series 5890 Gas Chromatography instrument and Trio-1 Mass Spectrometer. Gaseous products do not need any treatment and will be analysed by the GC-MS directly. Liquid products will need dilution with dichloromethane prior to the analysis, to avoid contamination. Standards manufactured by Supelco (C7-C40 saturated alkanes, 1000µg/mL) will be run prior to each liquid batch of samples; this will allow the determination of an accurate range of carbon bandings in the hydrocarbon mixture. MassLab software installed on the computer will be used to control GC-MS run parameters and record the run chromatogram, which can be saved, accessed and analysed after the run.

Conclusion

Both thermal and catalytic cracking processes in crude oil refineries of large molecules to generate smaller hydrocarbons are highly energy consuming processes with a considerable impact on the environment, lacking in the selectivity of final products. Non-thermal plasmas offer significant intensification of traditional chemical processes, essential increases in their efficiency and often successful stimulation of chemical reactions impossible in conventional chemistry [7]. Cracking of large hydrocarbon molecules can be achieved by plasma ionization of the hydrocarbon molecules by an impact of an energetic electron. This technology could provide an energy efficient, more selective and better controlled method for heavy hydrocarbon cracking. Our main objective is to determine the parameters of the electron gas to increase selectivity and control over plasma induced chemical reactions in hydrocarbons and gain deeper understanding and control of plasma effects on molecular bonds.

References

[1] Jones D. S. J., Pujado P. R. (2006), Handbook of petroleum processing. Netherlands: Springer.

[2] Rana M. S., Sa´mano V., Ancheyta J., Diaz J. A. I. (2007), A review of recent advances on process technologies for upgrading of heavy oils and residua, Fuel, vol. 86, p. 1216.

[3] DOE (2007), Energy and Environmental Profile of the U.S. Petroleum Refining Industry. Prepared by Energetics, Inc. Columbia, Maryland

[4] Simanzhenkov V., Idem R. (2003), Crude oil chemistry. Marcel Dekker, Inc., p. 40-41

[5] DOE (1998), Energy and Environmental Profile of the U.S. Petroleum Refining Industry. Prepared by Energetics, Inc. Columbia, Maryland

[6] Gurnett D. A., Bhattacharjee A. (2005), Introduction to plasma physics. Cambridge: Cambridge University Press, p. 1-3.

[7] Fridman A. (2008), Plasma Chemistry. Cambridge: Cambridge University Press.

[8] Kong P. C., Nelson L. O., Detering B. A. (2005), Non-thermal plasma systems and methods for natural gas and heavy hydrocarbon co-conversion. U. S. Patent 6,896,854 B2.

[9] Antano D. S., Staack D. A., Fridman A., Farak B. (2009), Atmospheric pressure DC corona: operating regimes and applications. Plasma Sources Sci. Technol., vol. 18, p. 1.

Occurrence, Fate, and Removal of Emerging Contaminants from Wastewater Plants

Hussein Janna-PhD student (†), Mark D. Scrimshaw (†), A.J. Chaudhary (†)

† Institute for the Environment, Brunel University, West London, Kingston Lane, Uxbridge, UB8 3PH

Abstract

Emerging contaminants frequently enter fresh water systems through sewage treatment works (STW). Benzotriazoles are one of these emerging contaminants and they are widely used as anti-corrosive agents. The aim of this paper is to determine the occurrence and fate of benzotriazole in wastewaters and rivers in the UK.

The results demonstrated that all selected compounds were present in the sewage treatment works. Although these compounds are not fully removed during wastewater treatment, the nitrifying activated sludge process was more effective at eliminating these compounds than the trickling filter process. In addition to that, advanced treatment may remove these compounds by up to 99%. These compounds are not degraded and they are likely to display cumulative concentration in the river. Studies on occurrence, toxicity and removal are needed of these contaminants.

Introduction

Many researchers around the world are investigating the occurrence of trace levels of some emerging contaminants in water related with wastewater treatment plants effluents (1, 2). The issue began to receive more attention by environmental scientists in the late 1990s when these pollutants were linked to toxicological effects in fish (3). Other chemicals are present at higher concentration and although effects have not been observed, they may still be cause for concern due to volume of use and persistence.

Benzotriazoles are one of these emerging contaminants and they have major applications, being added to many formulations as anti corrosive additives, such as cooling and hydraulic fluids, in antifreeze products, in aircraft de-icer and anti-icing fluids, brake fluids, metal-cutting fluids, and dishwasher detergents for silver protection. Thus, benzotriazoles reach municipal wastewater treatment plants via household wastewater, indirect discharge from industry, or surface runoff. Benzotriazoles have relevance in terms of occurrence and removal.

The overall aim of this paper is to determine the occurrence and fate of benzotriazoles in wastewaters and rivers in the UK, comparing two types of biological wastewater treatment processes (trickling filters and nitrifying activated sludge) and comparing three different types of advanced treatment processes (ozone, granular activated carbon and chlorine dioxide).

Materials and Methods

Sampling Sites.

Two sewage treatment works were selected for the study, both discharging into the river Erewash a tributary of the River Trent near Nottingham, UK. One was a trickling filter (TF) plant, and the other site was a nitrifying activated sludge (N/AS) works. All samples were (200ml). In addition to sampling the whole process in these two sites, the final effluents of six other sewage treatment works and 16 points along Erewash river were sampled in order to investigate the fate of these compounds in the river.

Reagents, Chemicals and Solid-Phase Extraction (SPE)

The purity of all benzotriazoles was more than 98%. Solid-phase extraction (SPE), Oasis HLB (500mg/6cm3) cartridges were obtained from Waters (Watford, UK). The analytical method for benzotriazoles followed that used by Voutsa et al. 2006 (4). Samples were acidified with nitric acid to lower the pH to less than 3. Cartridges were preconditioned with methanol, followed by 18MΩ water (Milli-Q, Millipore). After extraction, the cartridges were rinsed with 5mL of reagent water and the dried with a stream of air. Cartridges were then eluted with 5 ml mixture of dichloromethane/methanol (97:3; v/v). Elutes were collected and evaporated on a miVac concentrator. Samples were re-dissolved in methanol / water (50:50; v/v) prior to quantification by liquid chromatography tandem mass spectrometry.

Results and Discussion

A) Occurrence in wastewater:

All the selected compounds were found in the influent of the two sewage treatment plants. The concentrations of benzotriazoles found at different treatment stages during the sampling period are summarized in table 1. This shows concentrations in ng/l after the settling stage, after the nitrifying activated sludge(N/ASP) or trickling filter (TF) , and after the Sand filter (final effluent) stage. It can be seen that abundant chemicals was tolytriazole, of which the concentration ranged from 575 to 2515 ng/l in the settled sewage which represent the well mixture of the sample avoiding in that the bias that might be happen in the crude samples. Benzotriazole (BT) and tolytriazole (TT) have recently been found in municipal effluents in Switzerland, as well as in receiving waters, at µg/L concentrations (5).

Table 1: Mean concentrations of the compounds in two different wastewater treatment plants.

Compound	Nitrifying Activated Sludge			Trickling filter		
	settled Sewage	Sand Feed	final effluent	settled Sewage	Sand Feed	final effluent
Benzotriazole	1610	1078	799	876	630	605
Tolyltriazole	2303	1205	801	1464	918	879

B) Tertiary Treatment

Figure 1 shows the concentrations of benzotriazole and tolytriazole as observed at a pilot plant facility located at the N/AS works. In the first treatment process, an ozone system was found to be efficient to remove benzotriazole and tolytriazole with 77% and 83% respectively. A granular activated carbon (GAC) system demonstrated more efficient removal for benzotraizole and tolytraizole with 92% and 99% respectively. The third type process which was a chlorine dioxide dosing exhibited removal efficiency similar to ozone for benzotriazole and tolytriazole with 81% and 86% respectively.

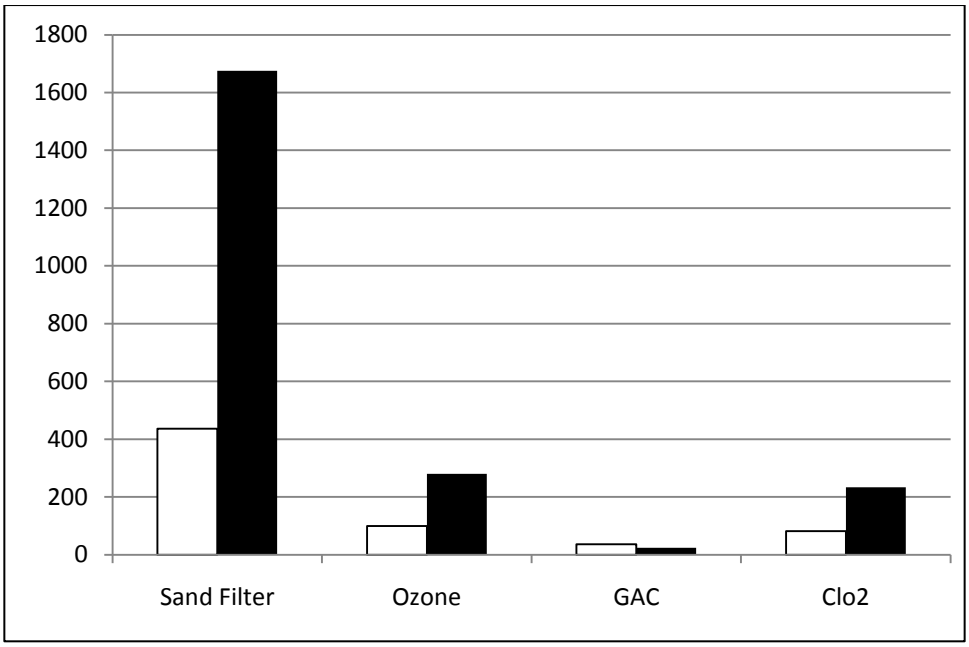

Fig. 1 Removal of BT and TT in wastewater using various tertiary treatment processes. ☐ benzotriazole ng/l, ■ tolytriazole ng/l

C) Occurrence in river.

Figure 2 shows the trend of the concentrations of BT and TT along the River Erewash. It is apparent that concentrations increase due to further inputs from sewage treatment works downstream. Compounds are not degraded in the river and remain in solution, not partitioning to sediment. In addition, low dilution of effluents in UK rivers, especially in dry weather, may increase the concentrations of these compounds in the rivers to be greater than 200ng/l for BT and 400 ng/l for TT which we have shown in modelling exercises (data not shown).

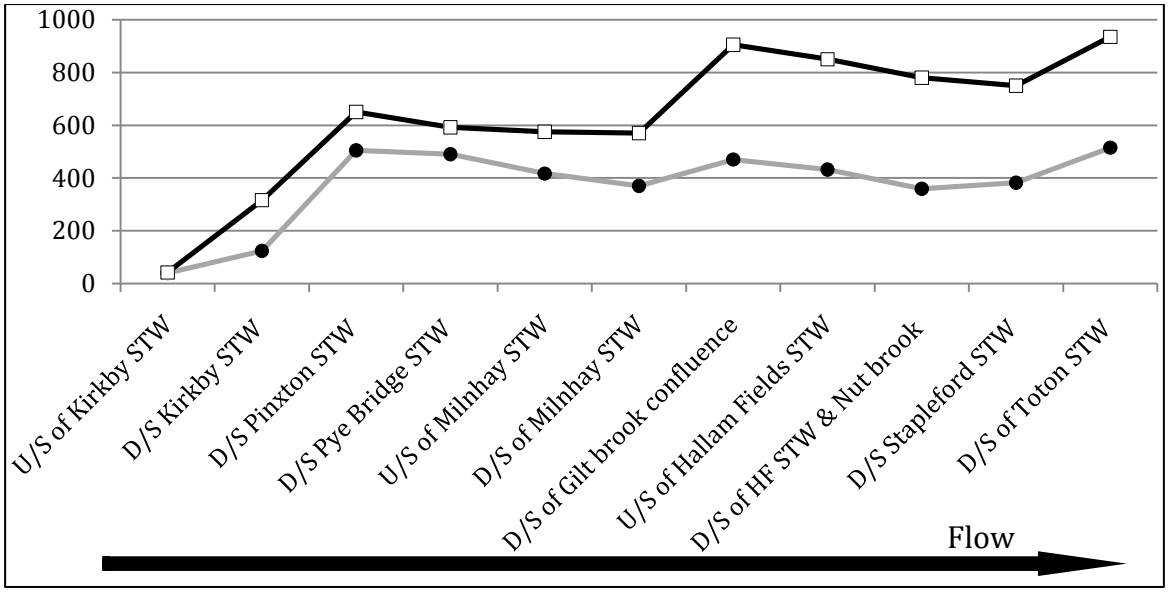

Fig. 2 Trend of BT and TT in ng/l along the River Erewash. ●BT ng/l, □TT ng/l

Conclusions

According to the above results, it is clear that benzotriazoles are ubiquitous in sewage treatment influents, effluents and river waters. Although these compounds are not fully removed, the nitrifying activated sludge was more effective at eliminating these compounds than the trickling filter by biological treatment processes. Furthermore, advanced treatment may remove up to 99%; however, these processes are not yet used in UK sewage treatment works. Finally, river concentrations are around 200-1000ng/l based on modelling and measured data.

References

(1) Halling-Sorensen, B., Nielsen, S.N., Lanzky, P.F., Ingerslev, F.,Lutzhoft, H.C.H., Jorgensen, S.E., 1998. Occurrence, fate and effect of pharmaceutical substances in the environment—a review. Chemosphere 36 (2), 357–393.

(2) Ternes, T.A., Kreckel, P., Mueller, J., 1999a. Behaviour and occurrence of estrogens in municipal sewage treatment plants—II. Aerobic batch experiments with activated sludge. Sci. Total Environ. 225, 91–99.

(3) Jobling, S., Noylan, M., Tyler, C.R., Brighty, G., Sumpter, J.P., 1998. Widespread sexual disruption in wild fish. Environ. Sci.Technol. 32, 2498–2506.

(4) Voutsa, D., Hartmann, P., Schaffner, C. and Giger, W. (2006). Benzotriazoles, alkylphenols and bisphenol a in municipal wastewaters and in the Glatt River, Switzerland. Environ. Sci. Pollut. Res., 13, 333-341.

(5) Giger, W., Schaffner, C. and Kohler, H.P.E. (2006). Benzotriazole and tolyltriazole as aquatic contaminants. 1. Input and occurrence in rivers and lakes. Environ. Sci. Technol., 40, 7186-7192.